Theoretical Investigation of Laser-Produced Hot, Dense Plasmas

（ レーザー生成高温・高密度プラズマに関する理論的研究 ）

Hiroyuki Furukawa

（ 古 河 裕 之 ）

January 1991

（ 1991年 1月 ）

Theoretical Investigation of Laser-Produced Hot, Dense Plasmas

（ レーザー生成高温・高密度プラズマに関する理論的研究 ）

Hiroyuki Furukawa

（ 古 河 裕 之 ）

January 1991

（ 1991年 1月 ）

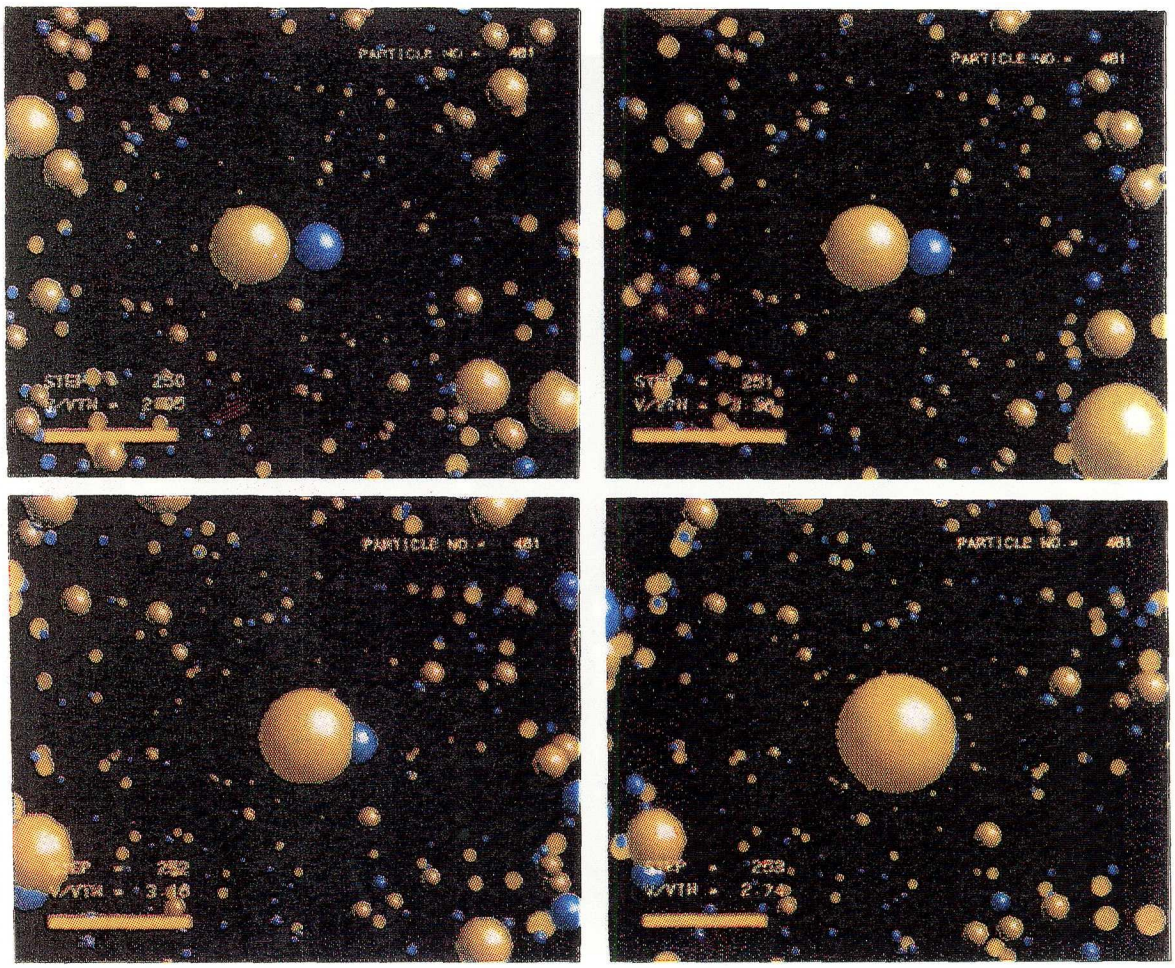

強結合プラズマのミクロ粒子シミュレーション。黄色はイオン、青色は電子。

内容梗概

本論文は著者が大阪大学大学院工学研究科博士課程前期２年間、及び後期３年間において行なった、レーザー生成高温高密度プラズマに関する理論的研究の成果をまとめたものである。

最近の慣性核融合実験の進歩により、高密度圧縮モードにより燃料となる重水素の密度は固体密度の約６００倍、高温圧縮モードにより温度は約一億度に達する高温高密度プラズマが実現できるようになった。これまで実験結果を定量的に評価する場合に、理想プラズマ近似を基に評価してきた。理想プラズマ近似によるプラズマ物理学の分野は比較的確立されており、高温低密度領域では十分精度の良い結果を与える。しかし上記のような高密度領域には適用できず、高密度プラズマに関しては基本的性質についても未知なものが多い。理想プラズマでは、粒子間のクーロン相互作用が粒子の熱運動に比べ無視できるが、高温高密度プラズマでは近接の粒子間におけるクーロン相互作用が、その物性に非常に重要である。また通常の固体と違い、温度が数千万度から数億度という高温状態にあるので、通常の固体物理学の結果をそのまま引用することはできない。著者は、粒子シミュレーション及び統計力学的理論モデルの二つの手法により、高温高密度プラズマの基本的性質について研究を行なった。

本論文は、７章より構成されている。

第１章は緒論であり、慣性核融合における高温高密度プラズマの基本的性質についての研究の重要性を述べ、各種物理モデルが適用される温度密度などの範囲を明かにする。

第２章では、本研究において新たに開発した３次元高温高密度プラズマ粒子コード "SCOPE" について、その構成、基本式及び計算上の工夫などについて述べる。電子及びイオンからなる２成分プラズマで、近接の粒子間におけるクーロン相互作用を正確に取り入れ、量子効果を近似的に取り入れたコードは、これが初めてである。

第３章では、"SCOPE" を応用した研究として高密度効果による炭素水素混合プラズマの制動輻射エネルギー損失の減少について述べる。輻射の強度が十分小さい極限では、制動輻射損失は動径分布関数と関係付けられる。シミュレーションにより動径分布関数を計算し、制動輻射損失の評価を行なった。その結果、プラズマ振動数と同程度の振動数での制動輻射は理想プラズマの場合に比べ、約７５％程度に減少することを示した。

第４章では、"SCOPE" を応用した研究として高温高密度プラズマ中の自己拡散及び電気伝導度について述べる。自己拡散係数は速度自己相関関数、電気伝導度は電流密度

自己相関関数と揺動散逸定理により関係付けられている。シミュレーションにより速度自己相関関数と電流密度自己相関関数を計算し、自己拡散係数と電気伝導度を評価した。また、自己拡散係数と電気伝導度に関しては、そのクーロン結合係数 Γ に対する依存性を求めた。

第５章では、密度汎関数法をもとにした原子モデルについて述べる。このモデルでは、２体相関関数と Poisson 方程式と Schrödinger 方程式を連立させて電子状態を決定する。本章では、電子ー電子間の分布の計算に Fermi 縮退の効果を導入するなどの改良を行ない、より正確な原子モデルを作った。

第６章では、原子モデルを応用して高密度プラズマ中の荷電粒子の阻止能を評価した。荷電粒子の阻止能はプラズマの誘電応答関数から求めた。高密度プラズマの誘電応答関数は、局所場補正理論により計算した。著者は、従来の局所場補正理論において無視されていた電子ーイオン間の局所場補正関数を原子モデルを用いて計算し、荷電粒子の阻止能の評価を行なった。その結果、従来の局所場補正理論によるそれより約５％程度阻止能が向上することを示した。

第７章は結論であり、以上の研究で得られた結果をまとめ、本論文の総括とした。

Table of Contents

I. INTRODUCTION

High density compression of six hundred times of solid density has been recently achieved with the use of a deuterated polystyrene shell[1]. Figure 1.1 shows the number density and temperature diagram of laser fusion hydrogen plasmas. As shown in Fig 1.1, in such a laser-produced hot, dense plasma, plasma density and temperature cover very wide domains. There exists a domain in which the Coulomb coupling constant for ions, $\Gamma=Z^2e^2/ak_BT\sim1\sim10$, and the electron degeneracy parameter, $\theta=k_BT/\varepsilon_F\sim 0.1\sim10$. Here, a is the ion sphere radius, $(3/4\pi n_i)^{1/3}$, ε_F is the Fermi energy, $\hbar^2(3\pi^2 n_e)^{2/3}/2m$, n_i and n_e are number densities of ions and electrons, k_BT is plasma thermal energy, k_B is the Boltzmann constant and $\hbar$ is Plank constant divided by 2π. Such a domain is called a two-component, i.e., electrons and ions, strongly coupled plasma[2]. In the present paper, two different approaches, particle simulation and analytical modeling, are employed to investigate some basic properties of a two-component strongly coupled plasma.

The knowledge of the interparticle correlations is required to evaluate the heat transport by radiation, self-diffusion, electric conductivity, stopping power, and etc. of two-component strongly coupled plasmas. For the estimation of such physical values quantitatively, it is desirable to simulate numerically many charged particle system for a long time with enough statistical accuracy. It is, however, very expensive to calculate all forces between particles. Therefore, 3-dimensional two-component Particle-Particle Particle-Mesh (PPPM) Code "SCOPE" has been developed[3,4]. In "SCOPE", the short-range forces are computed by using a direct particle-particle summation over the spatially localized

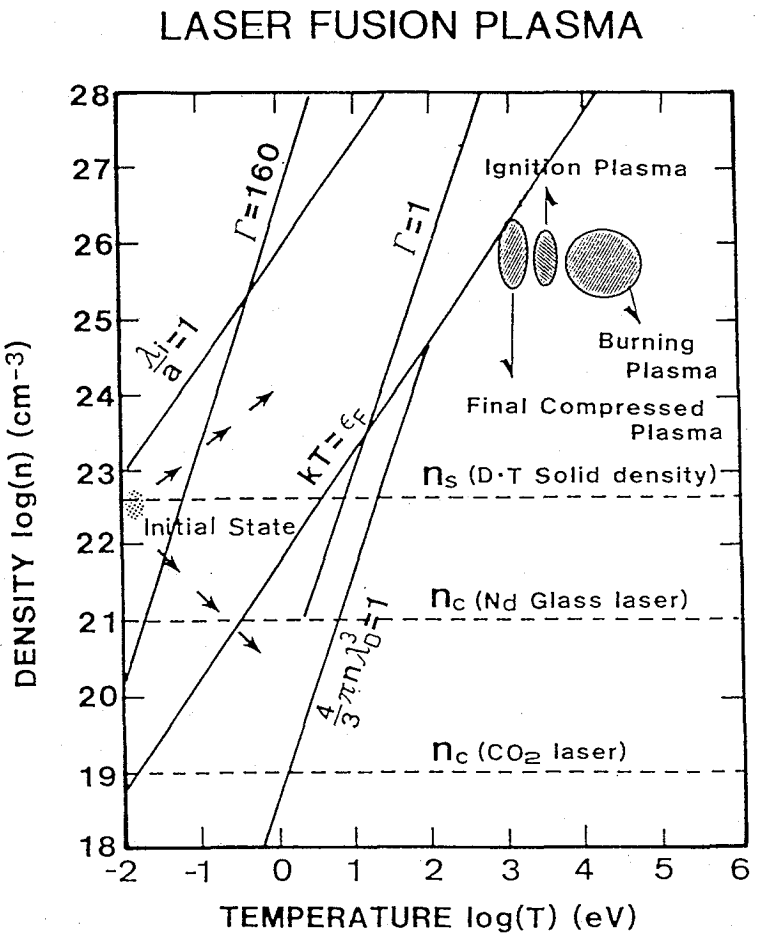

Fig. 1.1 The number density and temperature diagram of laser fusion hydrogen plasma.

forces and long-range forces are calculated by the Particle-In-Cell (PIC) method[5]. Quantum diffraction and symmetry effects are taken into account in the short-range forces through the effective pair potentials[6]. The PPPM method was used for molecular dynamics simulations[7]. This scheme is the first to apply the PPPM method for the two-component strongly coupled plasmas. The details of the code is discussed in Chap. II.

The heat transport by radiation is one of the important problems in laser fusion plasmas. The electron shielding and ion-ion correlation reduce the X-ray emission and absorption coefficients of free-free transitions in such a plasma[3,8-10]. Developed has been the formulation of the bremsstrahlung emission coefficients from a binary ionic mixture plasma based on the formulation made by H. Totsuji[8,9] and that made by R. Kawakami et al[10]. In this formula, the pair distribution functions are related to the bremsstrahlung emission coefficients. And estimated are the reduction in bremsstrahlung emission from a binary ionic mixture plasma using the pair distribution functions obtained by simulation with "SCOPE". The reduction in bremsstrahlung emission is described in Chap. III.

In laser-produced hot, dense plasmas, it is expected that the self-diffusion coefficients are smaller than those in the ideal plasma. To estimate the self-diffusion coefficients quantitatively, the knowledge of the time dependent interparticle correlations is required. The self-diffusion coefficients are related to the velocity auto-correlation functions (V.A.F.)[11,12]. Calculated are the velocity auto-correlation functions of the two-component nondegenerate plasmas by the simulations, and estimated are the self-diffusion coefficients as a function of the Coulomb

coupling constant for ions Γ. In the same way, the electric conductivities are related to the auto-correlation functions of the total microscopic electric current [11,12]. Calculated are the auto-correlation functions of the total microscopic electric current of the two-component nondegenerate plasmas by the simulations, and estimated are the electric conductivities. The self-diffusion coefficients and the electric conductivities are mentioned in Chap. IV.

For very highly compressed plasmas, for example, the plasma of six hundred times of solid density which has been recently made with the use of a deuterated polystyrene shell target[1] at ILE, the thermal de Broglie wavelength defined by $\lambda\!\!\!^{-}_e=\hbar/(2\pi m_e k_B T)^{1/2}$ and the electron sphere radius defined by $a_e=(3/4\pi n_e)^{1/3}$ are comparable. "SCOPE" cannot be applied to such very highly compressed plasmas because in "SCOPE" the quantum effects are taken into account approximately. It is very important for laser fusion to calculate various thermodynamics functions of plasmas in such a region. In order to investigate such very highly compressed plasmas, the quantum effects should be taken into account through the Schrödinger equation, and many body effects are also important because of high density. To calculate the pair distribution functions, and the effective potential acting on an electron and an ion, an atomic model has been developed within the framework of density functional theory (DFT)[13,14]. And found are the unnegligible difference of the pair distribution functions from other theoretical models[2,10]. The atomic model is described in Chap. V.

Recently the various physical values can be observed by using the charged particles which are made by fusion reaction experimentally. The energy spectra of the charged particles which are produced by fusion

reaction has to be estimated correctly in order to obtain the correct physical values which characterize the highly compressed fusion plasmas experimentally. The charged particles made by fusion reaction lose the energy by collisions. The ratio of the lost energy to the range moving in the plasma is called stopping power. It is very important to estimate the stopping power correctly for the estimation of the self-heating of the plasma by the charged particles and the estimation of the product of the mass density ρ and the core radius R[15,16]. The stopping power can be calculated using the dielectric function $\varepsilon(k,\omega)$. The dielectric function $\varepsilon(k,\omega)$ of such a highly compressed plasma can be calculated using the local field correction theory[2]. In Ref. 2 the electron-ion local field correction function $G_{ei}(k,\omega)$ is assumed to be zero because it is very difficult to calculate electron-ion local field correction function in their frame work. In this paper the static electron-ion local field correction function $G_{ei}(k)$ is estimated with the aid of the atomic model. The stopping power is described in Chap. VI.

In Chap. VII, conclusions and summaries are presented.

REFERENCES OF CHAPTER I

1). S. Nakai, Bull. Am. Phys. Soc, **34,** 2040 (1989).

2). S. Ichimaru, S. Mitake, S. Tanaka and Xin-Zhong Yan, Phys. Rev. A, **32,** 1768 (1985).

3). H. Furukawa and K. Nishihara, Phys. Rev. A, **42,** 3532 (1990).

4). K. Nishihara, H. Furukawa, M. Kawaguchi and Y. Abe, Japanese Supercomputing (Springer-Verlag, New York, 1988), P59.

5). C. K. Birdsall and A. B. Langdon, Plasma Physics via Computer Simulation (McGraw-Hill, New York, 1985).

6). C. Deutsch, Phys. Lett. **60A,** 317 (1977).

7). J. W. Eastwood, R. W. Hockney and D. N. Lawrence, Comput. Phys. Commun. **19,** 215 (1980).

8). H. Totsuji, Phys. Rev. A, **32,** 3005 (1985).

9). H. Totsuji, Memoirs of the School of Engineering, Okayama University, **21,** 45 (1986).

10). R. Kawakami, K. Mima, H. Totsuji and Y. Yokoyama, Phys. Rev. A, **38,** 3618 (1988).

11). L. Sjögren, J. P. Hansen and E. L. Pollock, Phys. Rev. A, **24,** 1544 (1981).

12). J. P. Hansen and I. R. McDonald, Phys. Rev. A, **23,** 2041 (1981).

13). F. Perrot, Phys. Rev. A **25,** 489 (1982).

14). M. W. C. Dharma-wardana and F. Perrot, Phys. Rev. A **26,** 2096 (1982).

15). Y. Setsuhara, H. Azechi, N. Miyanaga, H. Furukawa, R. Ishizaki, K. Nishihara, M. Katayama, A. Nishiguchi, K. Mima, and S. Nakai, Laser and Particle Beams, **8,** 609 (1990).

16). Y. Setsuhara, H. Azechi, N. Miyanaga, H. Furukawa, K. Nishihara, A. Nishiguchi, K. Mima, and S. Nakai, to be submitted.

II. 3-Dimensional Two-Component Particle-Particle Particle-Mesh Code "SCOPE"

In order to simulate the two-component strongly coupled plasmas, 3-dimensional Particle-Particle Particle-Mesh (PPPM) Code "SCOPE" has been developed (Ref. 1). In "SCOPE", the short-range forces are calculated by using a direct Particle-Particle (P-P) summation over the spatially localized forces and the long-range forces by Particle-Mesh (P-M) method. Quantum diffraction and symmetry effects are taken into account through the effective pair potential by an approximated way (Ref. 2). In "SCOPE", the Poisson equation has been solved by the 4-th order finite difference method and third order spline weighting method. To obtain accuracy within error $\leq 1\%$, the distance x is required $15\,\Delta$ in the conventional P-M (Cloud In Cell) method, but only $3\,\Delta$ is required in the newly developed P-M method. For the close interactions, especially electron-ion interactions, the small time increment $\Delta t'$ is estimated as satisfies the condition $\Delta t' << \tau$, where τ is the interaction time. Initial positions are determined by the Metropolis method (Ref. 3) and initial velocity distribution function is Maxwellian.

II - 1. BASIC EQUATIONS AND OUTLINE OF "SCOPE"

The plasmas considered in "SCOPE" consist of many point plus charges (plus ions) and many point minus charges (electrons) which subject to Newton equation of motion. The basic equations are as follows.

$$\frac{d\mathbf{r}_i}{dt} = \mathbf{v}_i \quad , \quad (2.1)$$

$$m_i \frac{d\mathbf{v}_i}{dt} = \mathbf{F}_i \quad , \quad (2.2)$$

$$\mathbf{F}_i = \sum_{j \neq i} \mathbf{F}_{i,j} \quad , \quad (2.3)$$

where $\mathbf{r}_i$, $\mathbf{v}_i$ and m_i are position, velocity and mass of the i-th particle.

As Eq. (2.3) shows, the force on the i-th particle is defined by the summation over the forces among all particles except i-th particle. But it is too expensive to calculate Eq. (2.3) about all particles in the plasmas. In "SCOPE" the force on the i-th particle is calculated from the summation of the short-range forces and the long-range forces as follows,

$$\mathbf{F}_i = \mathbf{F}_i^{sr} + \mathbf{F}_i^{lr} \quad . \quad (2.4)$$

Namely, the short-range forces are calculated by using a direct Particle-Particle (P-P) summation over the spatially localized forces and the long-range forces by Particle-Mesh (P-M) method. Quantum effects are taken into account in the short-range forces. In the next section, I describe how to evaluate the short-range forces which include the quantum effects.

II - 2. SHORT-RANGE FORCES INCLUDE QUANTUM EFFECTS

In order to introduce quantum effects and treat nondegenerate strongly coupled plasmas by classical mechanics[4], effective pair potentials, which account for quantum diffraction and symmetry effects in an approximate way, are used. Effective pair potentials may be derived by using the quantum-mechanical Slater sum

$$W(\{\mathbf{r}\}) = \sum_n \psi_n^* \exp(-\beta E_n)\,\psi_n \quad , \qquad (2.5)$$

in a form reminiscent of the classical Boltzmann factor[5], i.e., as

$$W(\{\mathbf{r}\}) = \exp\left(-\beta \sum_{i<j} \upsilon_{ij}(r)\right) \quad . \qquad (2.6)$$

In Eq. (2.5) Ψ_n and E_n are the eigenfunctions and eigenvalues of the full Hamiltonian of the system, {**r**} denotes the set of all positions of electrons and ions, and $\upsilon_{ij}(r)$ represents the effective pair potential between i-th and j-th particles. At sufficiently high temperature, the contribution of bound state to electrons-nuclei Slater sum can be neglected. If, moreover, the scattering states are limited to s waves, the following very simple effective pair potentials can be derived[2]

$$\upsilon_{ij}(r) = \frac{q_i q_j}{r}\left\{1 - \exp\left(-\frac{r}{\lambda\!\!\!^{-}_{ij}}\right)\right\} \quad , \qquad (2.7)$$

where $\lambda\!\!\!^{-}_{ij}$ is the thermal de Broglie wavelength, i.e.,

$$\lambda_{ij} = \frac{\hbar}{\sqrt{2\pi m_{ij} k_B T}} \quad , \qquad (2.8)$$

and m_{ij} is the reduced mass of an i-j pair. In the classical (high-temperature) limit, $\upsilon_{ij}(r)$ reduces to be bare Coulomb potential, as λ_{ij} reduces to zero.

To take account of symmetry effects (i.e., the Pauli principle) for electrons, a term must be added to the effective pair potential. It has been shown[6] that in the high temperature limit

$$\begin{aligned} \upsilon_{e,e}(r) &= \upsilon^{(d)}(r) + \upsilon^{(s)}(r) \\ &= \frac{e^2}{r}\left\{1 - \exp\left(-\frac{r}{\lambda_{ee}}\right)\right\} \\ &\quad + k_B T \ln 2 \exp\left(-\frac{r^2}{\pi \lambda_{ee}^{\,2} \ln 2}\right) \end{aligned} \quad , \qquad (2.9)$$

where the first term $\upsilon^{(d)}(r)$ arises from quantum diffraction effects, while the second term $\upsilon^{(s)}(r)$ take care of symmetry. The forces arising from quantum diffraction effects and symmetry effects are defined as,

$$\begin{aligned} f^{(d)}(r) &= -\frac{\partial}{\partial r}\upsilon^{(d)}(r) \\ &= \frac{e^2}{r^2} - \frac{e^2}{r}\left(\frac{1}{r} + \frac{1}{\lambda_{ee}}\right)\exp\left(-\frac{r}{\lambda_{ee}}\right) \end{aligned} \quad , \qquad (2.10)$$

$$\begin{aligned} f^{(s)}(r) &= -\frac{\partial}{\partial r}\upsilon^{(s)}(r) \\ &= \frac{2k_B T}{\pi \lambda_{ee}^{\,2}} r \exp\left(-\frac{r^2}{\pi \lambda_{ee}^{\,2} \ln 2}\right) \end{aligned} \quad . \qquad (2.11)$$

The direct particle-particle interaction force between the i-th and j-th particles with the charge q_i and q_j is given by

$$\mathbf{F}_{ij} = \frac{q_i q_j}{r^3}\mathbf{r}_{ij} - \frac{q_i q_j}{r^2}\mathbf{r}_{ij}\left(\frac{1}{r} + \frac{1}{\lambda_{ij}}\right)\exp\left(-\frac{r}{\lambda_{ij}}\right) + \delta_{ie}\delta_{je}\frac{2k_B T}{\pi\lambda_{ee}^{\,2}}\mathbf{r}_{ij}\exp\left(-\frac{r^2}{\pi\lambda_{ee}^{\,2}\ln 2}\right) \quad , \quad (2.12)$$

where δ is Kronecker's delta.

II - 3. PARTICLE-MESH METHOD AND LONG-RANGE FORCES

The long-range forces are calculated by introducing 3-dimensional meshes through the Poisson equation as follows.

1). The charge density $\rho_{l,m,n}$ at the grid point (l,m,n) is calculated from the positions of the particles.

2). By using the charge density $\rho_{l,m,n}$ at the grid point (l,m,n), the finite difference Poisson equation is solved about the static electric potential $\phi_{l,m,n}$ at the grid point (l,m,n), for example, with the aid of Fast Fourier Transform for a periodic boundary condition system.

3). The electric force $\mathbf{F}_{l,m,n}$ at the grid point (l,m,n) is calculated from $\phi_{l,m,n}$.

4). The long-range force on the i-th particle $\mathbf{F}_i^{lr}$ is calculated from the electric force $\mathbf{F}_{l,m,n}$ at the grid point (l,m,n).

The method mentioned above is called Particle-Mesh (P-M) method, and is usually used to simulate the ideal plasmas. The conventional P-M method has an enough precision to simulate the ideal plasmas, but does not have an enough precision to simulate two-component strongly coupled plasmas. The new P-M method which has an enough precision to simulate two-component strongly coupled plasmas has been developed. In the following sub section, the two types of P-M methods are described and compared.

II - 3 - 1. THE CONVENTIONAL P-M METHOD

In the conventional P-M method, the charge density $\rho_{l,m,n}$ at the grid points (l,m,n) is obtained by the Cloud-In-Cell (CIC) method[7,8]. By introducing the finite size particle, whose size is same as a mesh size, I assign the charge of a particle to the nearest 8 grid points with linear area weighting method. By using the charge density $\rho_{l,m,n}$ at the grid point (l,m,n), I solve the second order finite difference Poisson equation,

$$\frac{1}{\Delta^2}\{6\phi_{l,m,n} - (\phi_{l+1,m,n} + \phi_{l-1,m,n} + \phi_{l,m+1,n} + \phi_{l,m-1,n} + \phi_{l,m,n+1} + \phi_{l,m,n-1})\} = 4\pi\rho_{l,m,n} \quad , \quad (2.13)$$

for example, with the aid of Fast Fourier Transform for a periodic boundary condition system. The electric field of a grid point is obtained from the relation which has a second order precision

$$\mathbf{E}_{l,m,n} = \left\{ -\frac{(\phi_{l+1,m,n} - \phi_{l-1,m,n})}{2\Delta} \cdot -\frac{(\phi_{l,m+1,n} - \phi_{l,m-1,n})}{2\Delta} \cdot -\frac{(\phi_{l,m,n+1} - \phi_{l,m,n-1})}{2\Delta} \right\} \quad . \quad (2.14)$$

The long-range force on the i-th particle is calculated from the electric field of the nearest 8 grid points with the linear area weighting method.

II - 3 - 2. NEWLY DEVELOPED P-M METHOD

In the newly developed P-M method, I assign the charge of a particle to the nearest 8 grid points and neighbor 56 grid points with the third order spline function

$$S_3(x - x_{\pm o}) = \mp\frac{1}{2}\tilde{x}^2(\tilde{x} \pm 2) + \frac{2}{3}$$

$$S_3(x - x_{\pm 1}) = \pm\frac{1}{6}(\tilde{x} \pm 2)^3$$

$$\tilde{x} = x - x_{\pm 1} \qquad . \quad (2.15)$$

By using the charge density $\rho_{l,m,n}$ at the grid point (l,m,n), the fourth order finite difference Poisson equation

$$\begin{aligned} -\nabla^2\phi_{l,m,n} = \frac{1}{12\Delta^2}\{&\phi_{l+2,m,n} - 16\phi_{l+1,m,n} + 30\phi_{l,m,n} - 16\phi_{l-1,m,n} + \phi_{l-2,m,n} \\ &+ \phi_{l,m+2,n} - 16\phi_{l,m+1,n} + 30\phi_{l,m,n} - 16\phi_{l,m-1,n} + \phi_{l,m-2,n} \\ &+ \phi_{l,m,n+2} - 16\phi_{l,m,n+1} + 30\phi_{l,m,n} - 16\phi_{l,m,n-1} + \phi_{l,m,n-2}\} \\ = 4\pi\rho_{l,m,n} \end{aligned}$$

, (2.16)

is solved for example, with the aid of Fast Fourier Transform for a periodic boundary condition system. I obtain the electric field of a grid point, from the relation which has the fourth order precision

$$-\frac{\partial\phi_{l,m,n}}{\partial x} = \frac{1}{12\Delta}(\phi_{l+2,m,n} - 8\phi_{l+1,m,n} + 8\phi_{l-1,m,n} + \phi_{l-2,m,n}) = E_{x\,l,m,n}$$

. (2.17)

The long-range force on the i-th particle is calculated from the electric field of the nearest 8 grid points and neighbor 56 grid points with the third order spline function.

II - 3 - 3. COMPARISON BETWEEN NEW DEVELOPED P-M METHOD AND CONVENTIONAL P-M METHOD

The improvement of accuracy of the long-range forces by using newly developed P-M method is described as follows. Figure 2.1 shows the error of the calculation of the long-range forces from the bare Coulomb forces as a function of the distance from the observation point to the test particle. In Fig.

2.1, CIC means the conventional P-M method, P4 means that the charge density is obtained by CIC but the Poisson equation is solved by the fourth order difference, S3P2 means that the charge density is obtained by the third order spline function but the Poisson equation is solved by the second order difference and S3P4 means the newly developed P-M method. The horizontal axis represents the distance normalized by the mesh size Δ, and the vertical axis represents the error of the calculation of the long-range force from the bare Coulomb forces. In the case using the charge density obtained by CIC the error oscillates as the function of x, but in the case using the charge density obtained by S3 the error decreases smoothly as the function of x. On the other hand, the absolute value of the error is dependent on the accuracy of transforming the Poisson equation to a finite difference equation. To obtain accuracy within error $\leq$ 1%, the distance x is required 15 Δ in the conventional P-M, but only 3 Δ is required in the newly developed P-M method.

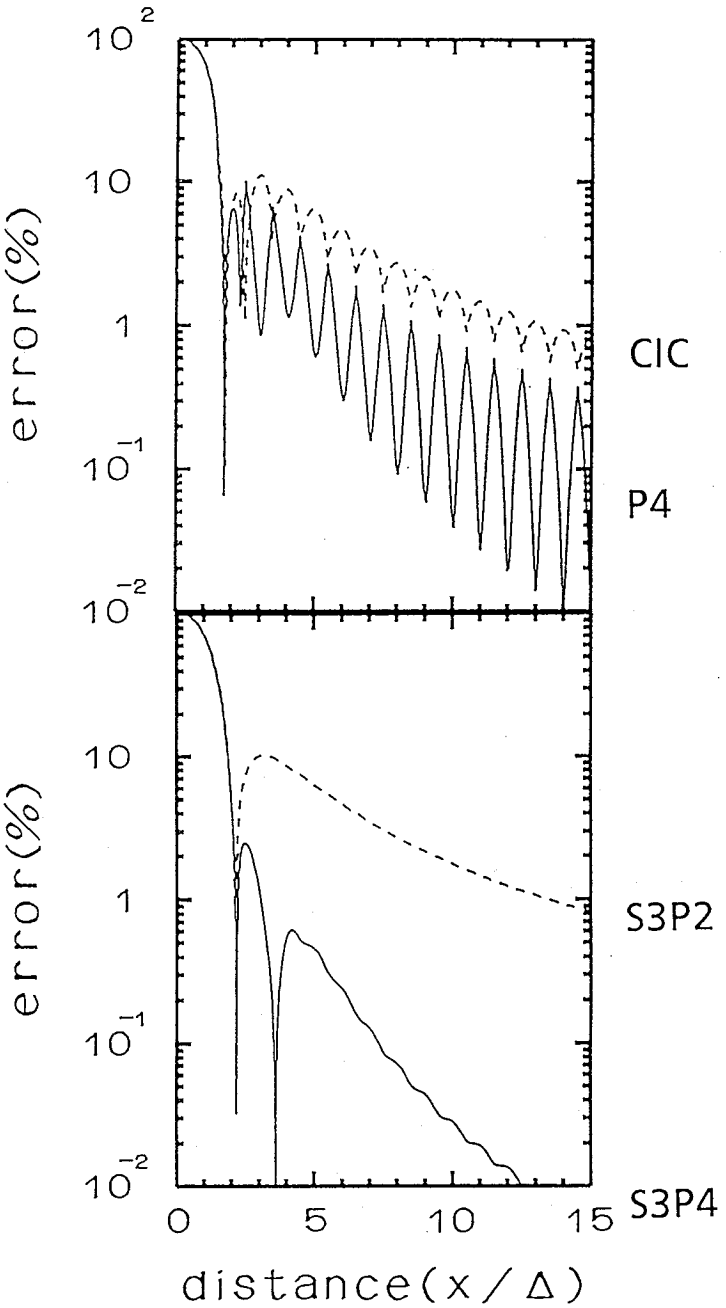

Fig 2.1 The error of the calculation of the long-range forces from the bare Coulomb forces as a function of the distance from the observation point to the test particle.
The horizontal axis represents the distance normalized by the mesh size Δ, and the vertical axis represents the error of the calculation of the long-range force from the bare Coulomb forces.

II - 4. CONNECTION OF P-P AND P-M METHOD

In "SCOPE" the size of 3-dimensional meshes is a few electron Debye lengths, defined by

$$\lambda_{De} = \sqrt{\frac{k_B T_e}{4\pi e^2 n_e}} \quad , \quad (2.18)$$

where e, T_e and n_e are electron charge, temperature and number density respectively. Figure 2.2 illustrates 2-dimensional meshes and particle positions by open and closed circles. If the i-th particle locates at the position shown in Fig. 2.2, the direct particle-particle forces are calculated by summing over the forces from the particles within a obliquely lined region and a hatched region, and the long-range forces are calculated beyond a hatched region[1,7]. It should be noted that when the long-range forces are calculated, the long-range forces contributed from the oblique lined region and the hatched region are excluded because the forces contributed from the oblique lined region and the hatched region are calculated by P-P method. To exclude the long-range forces contributed from the obliquely lined region and the hatched region, the following equation is used.

$$\mathbf{E} = \frac{4\pi}{LMN} \sum_{l,m',n'} \rho_{l,m',n'}$$

$$\times \sum_{k_l,k_m,k_n} \frac{\sin\{2\theta_l(l-l')+2\theta_m(m-m')+2\theta_n(n-n')\}}{\sin^2\theta_l\left(1+\frac{1}{3}\sin^2\theta_l\right)+\sin^2\theta_m\left(1+\frac{1}{3}\sin^2\theta_m\right)+\sin^2\theta_n\left(1+\frac{1}{3}\sin^2\theta_n\right)}$$

$$\times\left[\sin^2\theta_l\left(1+\frac{2}{3}\sin^2\theta_l\right),\ \sin^2\theta_m\left(1+\frac{2}{3}\sin^2\theta_m\right),\ \sin^2\theta_n\left(1+\frac{2}{3}\sin^2\theta_n\right)\right]$$

$$\theta_l = \frac{\pi k_l}{L} \quad , \quad \theta_m = \frac{\pi k_m}{M} \quad , \quad \theta_n = \frac{\pi k_n}{N} \quad . \quad (2.19)$$

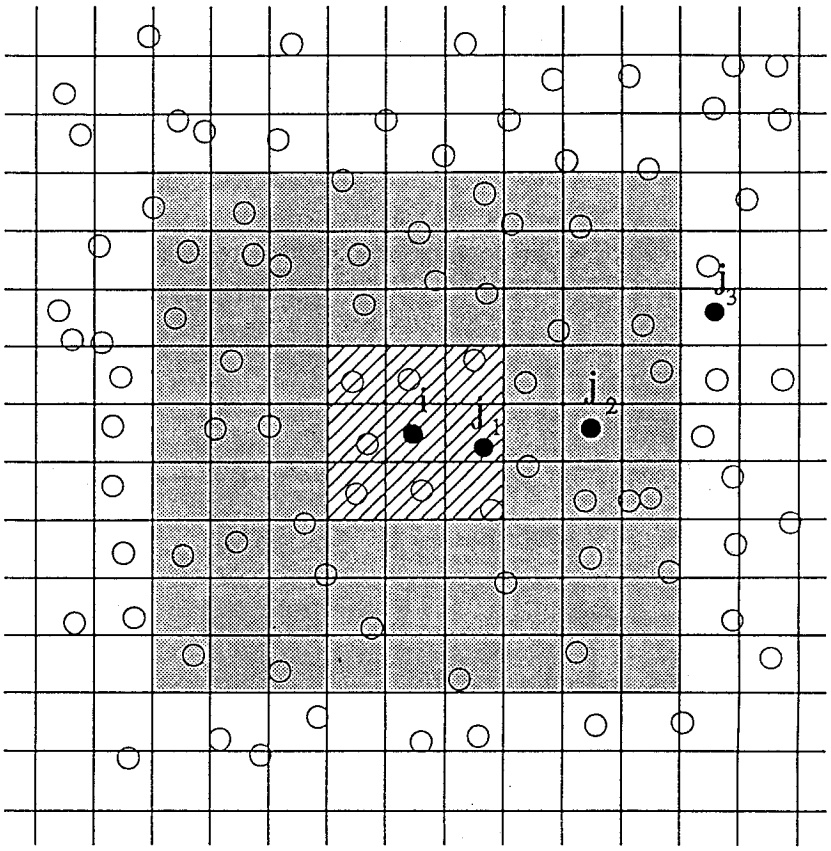

Fig 2.2 Schematic diagram of 2-dimensional meshes band particle positions with the open and closed circles.

II - 5. INITIAL POSITIONS AND VELOCITIES IN "SCOPE"

Initial positions of electrons and ions are determined by the Metropolis method[3]. In our Metropolis code, the electron-ion pair interaction potential is defined as the summation of a repulsive soft-core potential and an attractive Coulomb potential,

$$\upsilon_{ei}(r) = \varepsilon k_B T \left(\frac{\sigma}{r}\right)^n - \frac{q_i e}{r} \quad , \quad (2.20)$$

where σ is the soft-core radius, n and ε are constants. The electron-electron and ion-ion pair interaction potentials are bare Coulomb potentials. Figure 2.3 (a) shows the electron-ion pair interaction potential normalized by the plasma temperature, where Z=6, Γ=1, σ=0.2a, ε=0.1 and n=3. The horizontal axis represents the distance normalized by the ion sphere radius a. At r~0.1a the υ(r) has the minimum value. Figure 2.3 (b) shows the ion-ion and electron-ion pair distribution functions. At r~0.1a the electron-ion pair distribution function has the peak value. The ion number N_i which used in this calculation is 100 and the electron number N_e is 600.

Initial velocities of electrons and ions are determined as follows. First, the following function as the velocity

$$F(v) = 4\pi \int_0^v v^2 \exp\left(-\frac{v^2}{2v_T{}^2}\right) dv \quad , \quad (2.21)$$

is defined and the following equation

$$F(v_{max}) \frac{i}{N_v} = F(v_i) \quad , \quad (2.22)$$

is solved about v_i. Where the N_v is the number of the particles making Maxwellian. And in order to decrease the differences of the velocity distribution function from Maxwellian, the velocity of the i-th particle is corrected as follows.

$$v_i \rightarrow v_i \{1 + \alpha(\gamma_i - 0.5)\} \quad . \quad (2.23)$$

Where α is a constant and γ_i is the random number from 0 to 1. Figure 2.4 shows the velocity distribution functions of ions and electrons. The ion number N_i which used in this calculation is 800, the electron number N_e is 4800, α=0.5 and $v_{max}=3v_T$. The horizontal axis represents the velocity normalized by the thermal velocity and the vertical axis represents the distribution function of the absolute value of velocity. The dashed line represents Maxwellian. The direction of velocity is determined by 20 unit vectors. They go from the center of a regular icosahedron to the center of the faces of that.

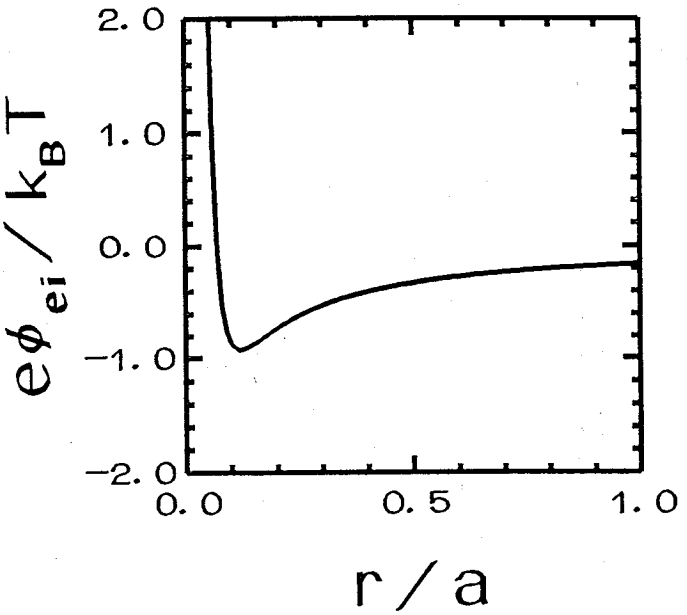

Fig 2.3 (a) The electron-ion pair interaction potential normalized by the plasma temperature, where Z=6, Γ=1, σ=0.2a, ε=0.1 and n=3. The horizontal axis represents the distance normalized by the ion sphere radius a.

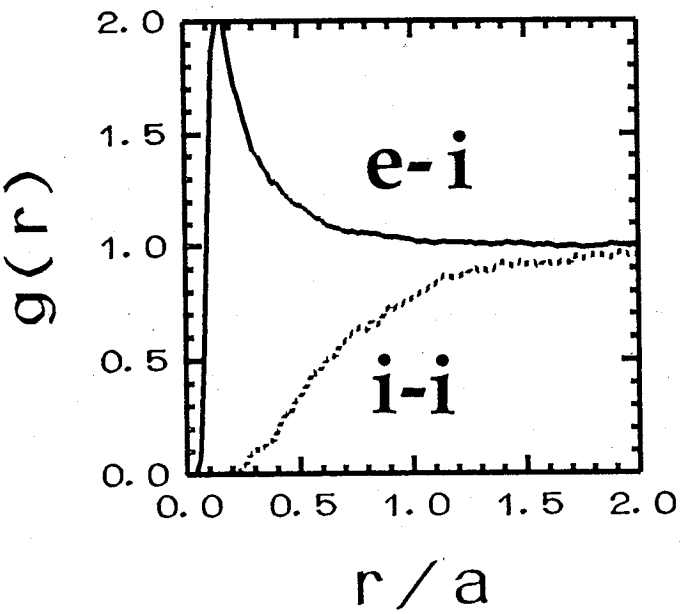

Fig 2.3 (b) The ion-ion and electron-ion pair distribution functions. The horizontal axis represents the distance normalized by the ion sphere radius a.

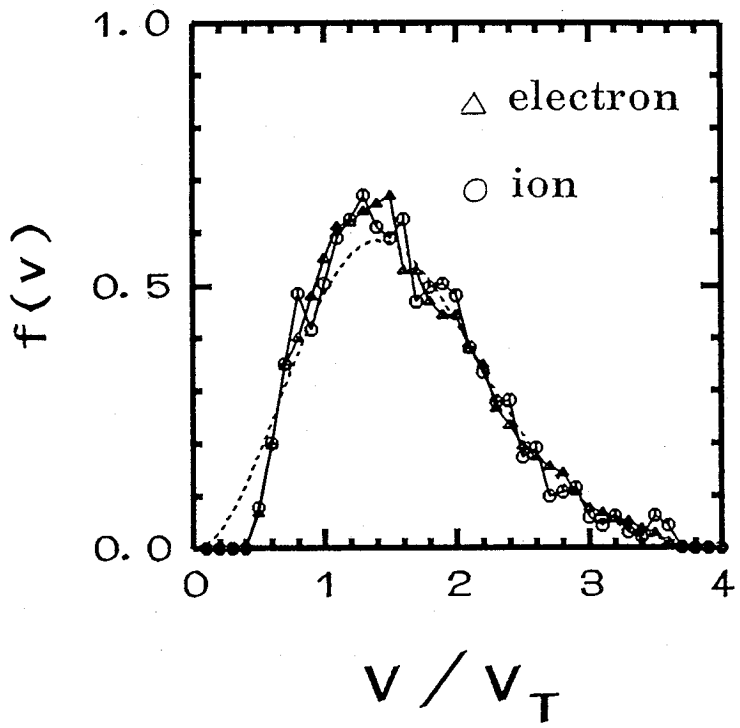

Fig 2.4 The velocity distribution functions of ions and electrons. The ion number N_i which used this calculation is 800 , the electron number N_e is 4800, a=0.5 and $v_{max}=3v_T$. The horizontal axis represents the velocity normalized by the thermal velocity and vertical axis represents the distribution function of the absolute value of velocity.

II - 6. INTEGRAL OF EQUATION OF MOTION

The equations of motion are integrated for all particles with respect to the normalized time increment of $\Delta t\omega_{pe}=0.05$. In order to simulate two-component strongly coupled plasmas with sufficient accuracy, for electron-ion interactions which have very small impact parameter or fast relative velocity, such events are selected and sufficiently small time increment are used, for example $\Delta t'=\Delta t/6000$. The normalized interaction time of an electron-ion pair can be estimated as follows.

$$\tilde{\tau}=\frac{\omega_{pe}}{\frac{d\theta}{dt}}=\frac{\sqrt{3}\,Z^{1/2}}{\Gamma^{3/2}}\,\frac{\tilde{r}^{3}\,\tilde{v}_{\theta}^{\,3}}{\left[1+\left\{\frac{2\tilde{v}_{\theta}\tilde{r}^{2}}{\Gamma Z^{1/3}}\left(\frac{Z^{5/3}}{\Gamma}\frac{\tilde{v}^{2}}{2}-\frac{1}{\tilde{r}}\right)+1\right\}^{1/2}\sin\vartheta\right]^{2}}$$

$$\tilde{r}=r/a_e\ ,\quad \tilde{v}=v/v_T \qquad .\ (2.24)$$

For example when Z=1, Γ=0.63, $\tilde{v}_{\theta}$=0.2 and $\tilde{r}$=0.2, t ~ 2.2×10^{-4}. The small time increment $\Delta t'$ is determined as satisfies the condition of $\Delta t'<<\tau$.

II - 7. SUMMARY

In order to simulate the two-component strongly coupled plasmas, 3-dimensional Particle-Particle Particle-Mesh (PPPM) Code "SCOPE" has been developed[1]. In "SCOPE", the short-range forces are calculated by using a direct Particle-Particle (P-P) summation over the spatially localized forces and the long-range forces by Particle-Mesh (P-M) method. Quantum diffraction and symmetry effects are taken into account through the effective pair potential by an approximated way[2]. In "SCOPE", the Poisson equation has been solved by the 4-th order finite difference method and third order spline weighting method. By introducing the 4-th order finite difference and the third order spline weighting, the number of meshes required to obtain the accuracy within a error $\leq$ 1%, is reduced $(1/5)^3$ of the conventional P-M method. For the close interactions, especially electron-ion interactions, the small time increment $\Delta t'$ is estimated as satisfies the condition $\Delta t' << \tau$, where τ is the interaction time. Initial positions are determined by the Metropolis method and initial velocity distribution function is Maxwellian.

REFERENCES OF CHAPTER II

1). H. Furukawa and K. Nishihara, Phys. Rev. A, **42,** 3532 (1990).

2). C. Deutsch, Phys. Lett. **60A,** 317 (1977).

3). 田中實、山本良一、計算物理学と計算化学、pp15-21、海文堂。

4). J. P. Hansen and I. R. McDonald, Phys. Rev. A, **23,** 2041 (1981).

5). T. Dunn and A. A. Broyles, Phys Rev. **157,** 156 (1967).

6). C. Deutsch, M. M. Gombert and H. Minoo, Phys. Lett. **66A,** 381 (1978).

7). K. Nishihara, H. Furukawa, M. Kawaguchi and Y. Abe, Japanese Supercomputing (Springer-Verlag, New York, 1988), P59.

8). C. K. Birdsall and A. B. Langdon, Plasma Physics via Computer Simulation (McGraw-Hill, New York, 1985).

III. Application of "SCOPE" to Laser-Produced Hot, Dense Plasmas I

~ Reduction in bremsstrahlung emission from hot, dense binary-ionic-mixture plasmas ~

With the use of "SCOPE", ion-ion and electron-ion pair distribution functions are observed for two-component strongly coupled plasmas and compared with statistical models (Ref. 1, 2) in detail. The reduction in bremsstrahlung emission from a binary-ionic-mixture plasma is calculated from the pair distribution functions obtained by the simulation. It is found that the reduction in bremsstrahlung emission from a binary ionic mixture plasma is approximated by that for a fictitious single ion species plasma (Ref. 3) with a certain ion charge even for the two-component plasma (Ref. 4).

III - 1. INTRODUCTION

The heat transport by radiation is one of the important problems in laser fusion plasmas. In a laser-produced hot, dense plasma, plasma density and temperature cover very wide domains, and there exists a domain in which the Coulomb coupling constant for ions, $\Gamma=Z^2e^2/ak_BT\sim1$, and the electron degeneracy parameter, $\theta=k_BT/\varepsilon_F \sim 1\sim10$. Here a is the ion sphere radius, $(3/4\pi n_i)^{1/3}$, ε_F is the Fermi energy, $\hbar^2(3\pi^2 n_e)^{2/3}/2m$, n_i and n_e are the number densities of ions and electrons, k_BT is the plasma thermal energy, k_B is the Boltzmann constant and $\hbar$ is Plank constant divided by 2π. Such a domain is called a two-component, i.e., electrons and ions, strongly coupled plasma[1]. The electron shielding and ion-ion correlation reduce the X-ray emission and absorption coefficients due to free-free transitions[2-5].

The knowledge of the interparticle correlations is required to calculate the effects of the electron shielding and ion-ion correlation on the bremsstrahlung. In this chapter the ion-ion and electron-ion pair distribution functions are obtained directly with the use of "SCOPE".

Developed is the formulation of the bremsstrahlung emission coefficients from such a binary ionic mixture plasma based on the formulation made by H. Totsuji[3,5] and that made by R. Kawakami et al[2]. In this formula, the pair distribution functions are related to the bremsstrahlung emission coefficients.

The pair distribution functions obtained by simulations are compared in detail with theories[1,2]. The symmetry effects[6] in the effective pair potentials on the pair distribution functions are also

discussed for a hot, dense plasma. Estimated is the reduction in bremsstrahlung emission from a single ion species plasma and a binary ionic mixture plasma. It is shown that the reduction for a binary ionic mixture plasma can be approximated by that for a fictitious single ion species plasma[3] even for a two-component plasma.

III - 2. Formulation of bremsstrahlung emission from a binary-ionic-mixture plasma

The cross section for dipole emission of photon is given by[7]

$$d\sigma_{k,p'} = \frac{(2\pi)^2}{\omega^3}\frac{m}{\hbar p}\left|\mathbf{e}\cdot\left[\frac{d^2\mathbf{d}}{dt^2}\right]_{f,i}\right|^2 \delta(E_i - E_f - \hbar\omega) \times \frac{d\mathbf{k}}{(2\pi)^3}\frac{d\mathbf{p}'}{(2\pi)^3} \quad , \quad (3.1)$$

where **e** and **k** are the polarization and the wavenumber of the emitted photon respectively, $\omega=(k^2c^2+\omega_{pe}^2)^{1/2}$ and $(d^2\mathbf{d}/dt^2)_{f,i}$ is the matrix element of the time derivate of the electric dipole moment **d** between the initial state ($E_i=(\hbar p)^2/2m$ and asymptotic wave number **p**) and the final state ($E_f=(\hbar p')^2/2m$ and asymptotic wave number **p'**) of electrons.

H. Totsuji[5] has introduced the formulation of bremsstrahlung emission coefficients from a one-component strongly coupled plasma which consists of only one species of ions, and R. Kawakami et al[2] have introduced that from a two-component strongly coupled plasma which consists of electrons and only one species of ions. The formulation is extended to the case of a binary ionic mixture plasma[4], which consists of electrons and two species of ions of the charges Z_1e and Z_2e and their numbers are N_1 and N_2. When the electron position is **r**(t),

$$\frac{d^2\mathbf{d}}{dt^2} = e\frac{d^2\mathbf{r}}{dt^2} = \frac{e^2}{m}\left\{\sum_{j=1}^{N_1}\nabla U_1(|\mathbf{r}-\mathbf{R}_j|) + \sum_{k=1}^{N_2}\nabla U_2(|\mathbf{r}-\mathbf{R}_k|)\right\} \quad , \quad (3.2)$$

and the matrix element is given as follows,

$$\left(\frac{d^2\mathbf{d}}{dt^2}\right)_{f,i} = \frac{e^2}{m}\int \varphi_f^*(r)\left[\frac{\partial}{\partial \mathbf{r}}\left\{\sum_{j=1}^{N_1} U_1(|\mathbf{r}-\mathbf{R}_j|) + \sum_{k=1}^{N_2} U_2(|\mathbf{r}-\mathbf{R}_k|)\right\}\right]\varphi_i(r)\,d\mathbf{r} \quad , \qquad (3.3)$$

where U_1 and U_2 are the ion potentials shielded by electrons, the suffixes 1 and 2 denote the ions of the charges Z_1e and Z_2e, and $\mathbf{R}_j$ and $\mathbf{R}_k$ are ion positions.

In the Born approximation I can replace $\varphi_i(r)$ by $\exp(i\hbar\mathbf{p}\cdot\mathbf{r})$ and $\varphi_f^*(r)$ to $\exp(-i\hbar\mathbf{p}'\cdot\mathbf{r})$ in Eq. (3.3), and by changing the values $\mathbf{r} - \mathbf{R}_j = \mathbf{r}_1$ and $\mathbf{r} - \mathbf{R}_k = \mathbf{r}_2$, Eq. (3.3) can be rewritten as

$$\left(\frac{d^2\mathbf{d}}{dt^2}\right)_{f,i} = \frac{e^2}{m}\left[\sum_{j=1}^{N_1}\int e^{iq\cdot R_j} e^{iq\cdot r}\cdot\left\{\frac{\partial}{\partial \mathbf{r}_1}U_1(r_1)\right\}d\mathbf{r}_1 + \sum_{k=1}^{N_2}\int e^{iq\cdot R_k} e^{iq\cdot r_2}\left\{\frac{\partial}{\partial \mathbf{r}_2}U_2(r_2)\right\}d\mathbf{r}_2\right] \quad , \qquad (3.4)$$

where $\hbar\mathbf{q}=\hbar\mathbf{p}-\hbar\mathbf{p}'$ is the change of the electron momentum in the collision. If assumed is that the potential $U_1(r)$ and $U_2(r)$ are dependent only on the species of ions, namely independent on the particle number j and k, Eq. (3.4) can be written as

$$\left(\frac{d^2\mathbf{d}}{dt^2}\right)_{f,i} = \frac{e^2}{m}\left[\left\{\sum_{j=1}^{N_1} e^{iq\cdot R_j}\right\}(-iq)\int U_1(r_1)\,e^{iq\cdot r_1}\,d\mathbf{r}_1 + \left\{\sum_{k=1}^{N_2} e^{iq\cdot R_k}\right\}(-iq)\int U_2(r_2)\,e^{iq\cdot r_2}\,d\mathbf{r}_2\right] \quad . \qquad (3.5)$$

With the use of Eq. (3.5), the term $|\ \mathbf{e}\ (d^2\mathbf{d}/dt^2)_{f,i}\ |^2$ can be written as follows.

$$\left| \mathbf{e} \cdot \left[\frac{d^2\mathbf{d}}{dt^2} \right]_{f,i} \right|^2 = \frac{e^4}{m^2 q^2} \left[\left\{ \sum_{j=1}^{N_1} e^{-i\mathbf{q}\cdot\mathbf{R}_j} \right\} \left\{ \sum_{j=1}^{N_1} e^{i\mathbf{q}\cdot\mathbf{R}_j} \right\} q^2 U_1(q) q^2 U_1(-q) \right.$$
$$+ \left\{ \sum_{j=1}^{N_1} e^{-i\mathbf{q}\cdot\mathbf{R}_j} \right\} \left\{ \sum_{k=1}^{N_2} e^{i\mathbf{q}\cdot\mathbf{R}_k} \right\} q^2 U_1(q) q^2 U_2(-q)$$
$$+ \left\{ \sum_{k=1}^{N_2} e^{-i\mathbf{q}\cdot\mathbf{R}_k} \right\} \left\{ \sum_{j=1}^{N_1} e^{i\mathbf{q}\cdot\mathbf{R}_j} \right\} q^2 U_2(q) q^2 U_1(-q)$$
$$\left. + \left\{ \sum_{k=1}^{N_2} e^{-i\mathbf{q}\cdot\mathbf{R}_k} \right\} \left\{ \sum_{k=1}^{N_2} e^{i\mathbf{q}\cdot\mathbf{R}_k} \right\} q^2 U_2(q)\, q^2 U_2(-q) \right] \quad , \quad (3.6)$$

where $U_\alpha(q)$ is the Fourier Transform of $U_\alpha(r)$,

$$U_\alpha(q) = \int U_\alpha(r)\, e^{-i\mathbf{q}\cdot\mathbf{r}}\, d\mathbf{r} \quad . \quad (3.7)$$

With the use of Eq. (3.6), the cross-section averaged over the ion distribution, the polarization and the propagation direction of photon is calculated as[8]

$$\overline{d\sigma_{k,p}} = \frac{\delta(E_i - E_f - \hbar\omega)\sqrt{\omega^2 - \omega_{pe}^2}\, d\omega\, d\mathbf{p}}{3\pi^2 m c^3 \hbar p\, \omega^2} \sum_{\alpha=1}^{2} \sum_{\beta=1}^{2} Z_\alpha Z_\beta e^6 \sqrt{n_\alpha n_\beta}\, \frac{1}{q^2} S_{\alpha\beta}(q)\, P_\alpha(q) P_\beta(-q)$$

, (3.8)

$S_{\alpha\beta}(q)$ is the ion structure factor defined by[3]

$$S_{\alpha\beta}(q) = \left\langle \rho_\alpha(q)\, \rho_\beta(-q) \right\rangle / \sqrt{N_\alpha N_\beta} \quad , \quad (3.9)$$

where

$$\rho_\alpha(q) = \sum_{j=1}^{N_\alpha} \exp(-i\mathbf{q}\cdot\mathbf{R}_j) \quad , \quad (3.10)$$

and $P_\alpha(q)$ is the electron shielding factor[2],

$$P_\alpha(q) = \frac{q^2}{4\pi Z_\alpha e}\, U_\alpha(q) \quad . \quad (3.11)$$

The ion structure factor $S_{\alpha\beta}(q)$ is related to the pair distribution function $g_{\alpha\beta}(r)$ as[3]

$$S_{\alpha\beta}(q) = \delta_{\alpha\beta} + n_\alpha \int \{ g_{\alpha\beta}(r) - 1 \} e^{-iq \cdot r} \, d\mathbf{r} \quad , \quad (3.12)$$

and the electron shielding factor $P_\alpha(q)$ is related to the pair distribution function $g_{e\alpha}(r)$ as

$$P_\alpha(q) = 1 - \frac{n_e}{Z_\alpha} \int \{ g_{e\alpha}(r) - 1 \} e^{-iq \cdot r} \, d\mathbf{r} \quad . \quad (3.13)$$

The emission coefficient $E(\omega)d\omega$ (energy emitted per unit time, volume, solid angle and polarization) is given by

$$E(\omega)\, d\omega = \iint \hbar\omega \, \frac{\hbar p}{m} \, \overline{d\sigma_{k,\,p'}} \, f(p) \{ 1 - f(p') \} \frac{2}{(2\pi)^3} \, d\mathbf{p} \quad , \quad (3.14)$$

where f(p) is the distribution function of electrons with momentum $\hbar p$,

$$f(p) = \frac{1}{1 + \exp \dfrac{(\hbar p)^2 / 2m - \mu}{k_B T}} \quad , \quad (3.15)$$

and μ is the chemical potential. Carrying out the integration of Eq. (3.14) with respect to p and p' got is

$$E(\omega)d\omega = \frac{2e^6 k_B T \sqrt{\omega^2 - \omega_{pe}{}^2} \, d\omega}{3\pi^3 \hbar^3 c^3 \omega \{ \exp(\hbar\omega / k_B T) - 1 \}} \times \sum_{\alpha=1}^{2} \sum_{\beta=1}^{2} Z_\alpha Z_\beta \sqrt{n_\alpha n_\beta} \int_0^\infty dq \, S_{\alpha\beta}(q) P_\alpha(q) P_\beta(-q) F(q) / q \quad , \quad (3.16)$$

where

$$F(q) = \ln \frac{1 + \exp\left[\frac{\mu}{k_B T} - \frac{\hbar^2}{2m k_B T} \left(\frac{q}{2} - \frac{m\omega}{\hbar q} \right)^2 \right]}{1 + \exp\left[\frac{\mu}{k_B T} - \frac{\hbar^2}{2m k_B T} \left(\frac{q}{2} + \frac{m\omega}{\hbar q} \right)^2 \right]} . \quad (3.17)$$

It is clear from Eqs. (3.12) and (3.13) that the ion-ion correlation effects on the reduction of bremsstrahlung emission coefficients are included in $S_{\alpha\beta}(q)$, while the electron shielding effects are included in $P_\alpha(q)$ and $P_\beta(q)$. If the pair distribution functions, $g_{\alpha\beta}(r)$, $g_{e\alpha}(r)$ and $g_{e\beta}(r)$ are given, the bremsstrahlung emission coefficients can be calculated.

As in Ref. 2, in order to show the strongly coupled effects on the reduction of the bremsstrahlung emission coefficients, the ratio $R(\omega)$ is also introduced by

$$R(\omega) = \frac{E\left(S_{\alpha\beta}(q).P_\alpha(q).P_\beta(-q)\right)}{E\left(S_{\alpha\beta}(q)=\delta_{\alpha\beta}.P_\alpha(q)=P_\beta(-q)=1\right)}$$

$$= \frac{\sum_{\alpha=1}^{2}\sum_{\beta=1}^{2} Z_\alpha Z_\beta \sqrt{n_\alpha n_\beta} \int_0^\infty dq S_{\alpha\beta}(q) P_\alpha(q) P_\beta(-q) F(q)/q}{\sum_{\alpha=1}^{2}\sum_{\beta=1}^{2} Z_\alpha Z_\beta \sqrt{n_\alpha n_\beta}\, \delta_{\alpha\beta} \int_0^\infty dq F(q)/q} . \quad (3.18)$$

Furthermore, the following ratios,

$$R_1(\omega) = \frac{E\left(S_{\alpha\beta}(q).P_\alpha(q)=P_\beta(-q)=1\right)}{E\left(S_{\alpha\beta}(q)=\delta_{\alpha\beta}.P_\alpha(q)=P_\beta(-q)=1\right)} = \frac{\sum_{\alpha=1}^{2}\sum_{\beta=1}^{2} Z_\alpha Z_\beta \sqrt{n_\alpha n_\beta} \int_0^\infty dq S_{\alpha\beta}(q) F(q)/q}{\sum_{\alpha=1}^{2}\sum_{\beta=1}^{2} Z_\alpha Z_\beta \sqrt{n_\alpha n_\beta}\, \delta_{\alpha\beta} \int_0^\infty dq F(q)/q}$$

, (3.19)

are introduced to express the ion-ion correlation effects separately.

III - 3. PAIR DISTRIBUTION FUNCTIONS

The pair distribution function g(r) represents the probability to find a particle at a distance r from the origin where a test particle locates. In an ideal plasma there is less correlation among the particles, thus the probability is independent of the distance, i.e. g(r)=1. However in a strongly coupled plasma, the repulsive force between ions and the attractive force between ion and electron affect the pair distribution functions.

If random phase approximation (R.P.A.) is applicable, the pair distribution functions are calculated analytically. If the plasma consists of fully ionized hydrogen, the pair distribution functions, $g_{ii}(r)$ and $g_{ei}(r)$ are described as[9]

$$g_{ii}(r) = 1 - \frac{k_i^{\,2}}{4\pi n_i} \exp\left(-\sqrt{2}k_i r\right) \quad , \quad (3.20)$$

$$g_{ei}(r) = 1 + \frac{k_e^{\,2}}{4\pi n_e} \exp\left(-k_e r\right) \quad , \quad (3.21)$$

where n_i is the ion number density, $k_e=\lambda_{De}^{-1}$ and

$$k_i = \sqrt{\frac{4\pi n_i e^2}{k_B T_i}} \quad . \quad (3.22)$$

If R.P.A. theory is not applicable, the pair distribution functions can be calculated analytically from the hypernetted chain approximation (HNC) theory[1] and the finite temperature Thomas-Fermi (T-F) model[2]. The ion-ion pair distribution function $g_{ii}(r)$ is obtained from the HNC equation,

$$g_{ii}(r) = \exp\left\{ -\frac{\phi_{ii}(r)}{k_B T} + h(r) - c(r) \right\} \quad , \quad (3.23)$$

where h(r) is the pair correlation function,

$$h(r) = g_{ii}(r) - 1 \quad , \quad (3.24)$$

with HNC equation, I use the Ornstein-Zernike relation,

$$h(r) = c(r) + n_i \int c(|\mathbf{r} - \mathbf{r}'|)\, h(r')\, d\mathbf{r}' \quad , \quad (3.25)$$

where $\phi_{ii}(r)$ is the ion-ion interaction potential shielded by electrons[1],

$$\phi_{ii}(r) = \frac{(Z^* e)^2}{2\pi^2} \int d\mathbf{k}\, \frac{1}{k^2 \varepsilon_e(k)} \exp(i\mathbf{k}\cdot\mathbf{r}) \quad , \quad (3.26)$$

and c(r) is the direct correlation function. Z^* is the effective ionization state which will be determined later and $\varepsilon_e(k)$ is the electronic dielectric function[1]. It should be noted that no ion-ion correlation effect is taken into account in the calculation of $\varepsilon_e(k)$. Namely, in the calculation of the ion-ion pair distribution function in the frame of the equations mentioned above, electron shielding is treated only as a linear-response shielding.

The electron-ion pair distribution function $g_{ei}(r)$ is obtained from

$$g_{ei}(r) = n_e(r) \,/\, Z^* n_i \quad , \quad (3.27)$$

where $n_e(r)$ is the electron number density around a test ion, which is calculated from the following equations[2].

$$-\nabla^2 U(r) = 4\pi e\,[\, Z\,\delta(r) - n_e(r) + Z^* n_i \,] \quad , \quad (3.28)$$

$$n_e(r) = \int \frac{2\, d\mathbf{p}}{(2\pi)^3} f_T(p) \quad , \quad (3.29)$$

and

$$f_T(p) = \frac{1}{1 + \exp \dfrac{(\hbar p)^2 / 2m - e\,U(r) - \mu}{k_B T}} \quad . \quad (3.30)$$

Here U(r) is the Thomas-Fermi potential. In the frame of T-F model, the bound electron number density is calculated from

$$n_{be}(r) = \int_{E<0} \frac{2\,d\mathbf{p}}{(2\pi)^3} f_T(p) \quad , \quad (3.31)$$

where

$$E = \frac{(\hbar p)^2}{2m} - eU(r) \quad . \quad (3.32)$$

Thus the effective ionization state Z^* is given by

$$Z^* = Z - N_{be} \quad , \quad (3.33)$$

where

$$N_{be} = \int_0^\infty 4\pi r^2 n_{be}(r)\,dr \quad . \quad (3.34)$$

Since $Z^* n_i$ is equal to the average free electron number density,

$$Z^* n_i = \int \frac{2\,d\mathbf{p}}{(2\pi)^3} f(p) \quad , \quad (3.35)$$

which determines the chemical potential, where f(p) is defined by Eq. (3.15). It should be also noted that in the calculation of the electron-ion pair distribution function in the frame of Eqs. (3.27)-(3.35), the ion-ion correlation is neglected, i.e, $g_{ii}(r)=1$.

The pair distribution functions are observed by simulations with electron-electron symmetry effects. Simulations have been performed as follows. Integrated are the equations of motion for all particles by

normalized time increment of $\Delta t\omega_{pe}=0.05$ for maximum time $t_{max}\omega_{pe}=60$. I recognize that simulation plasmas are sufficiently quiet at the time of $t\omega_{pe}=60$ because of good initial positions and velocities. Simulation parameters are summarized in Table 3.1. Note that the mass ratio of proton to electron has been chosen the value of 100, and that of carbon to electron has been chosen the value of 600. But the pair distribution functions are almost unaffected by the ratios because these are static properties.

After the time of $t\omega_{pe}=60$, the pair distribution functions are observed at every two time steps and averaged over the time interval of $t\omega_{pe}=60\sim120$.

In the first case, which corresponds to a weakly coupled plasma, the physical parameters are the atomic number Z=1, the Coulomb coupling constant for ions $\Gamma=0.0278$ and the plasma temperature T=1keV. The ion-ion pair distribution function and the electron-ion pair distribution function are shown in Fig. 3.1, in which the solid line represents the results obtained by simulation and the dashed line represents the results of R.P.A. theory. The distance r is normalized by the ion-sphere radius a. They are in good agreement except for $r\lesssim0.2a$. The reason why there is a little difference between simulation and R.P.A. theory for $r\lesssim0.2a$ is that in R.P.A. theory the short-range correlation effects between particles are not included. However, in this case, the difference is not significant on any physical quantities.

In the second case, which corresponds to a two-component strongly coupled plasma, the physical parameters are the atomic number Z=6, the Coulomb coupling constant for ions $\Gamma=1$, and the plasma

Table 3.1

Details of simulations. N_e and N_i are the numbers of electrons and ions used in simulations. Δ is the size of one mesh in space. Δt is the time step in the numerical integration.

	case (1)	case (2)
Z	1	6
Γ	0.0278	1.0
θ	19.145	5.808
$n_i(cm^{-3})$	$1.7X10^{24}$	$1.7X10^{24}$
T(keV)	1.0	1.0
N_e	1600	4800
N_i	1600	800
Mesh	4X4X4	4X4X4
Δ/λ_{De}	1.361	2.645
$n_e \Delta^3$	25.0	75.0
$n_i \Delta^3$	25.0	12.5
$\Delta t\omega_{pe}$	0.05	0.05
m_i / m_e	100.0	600.0

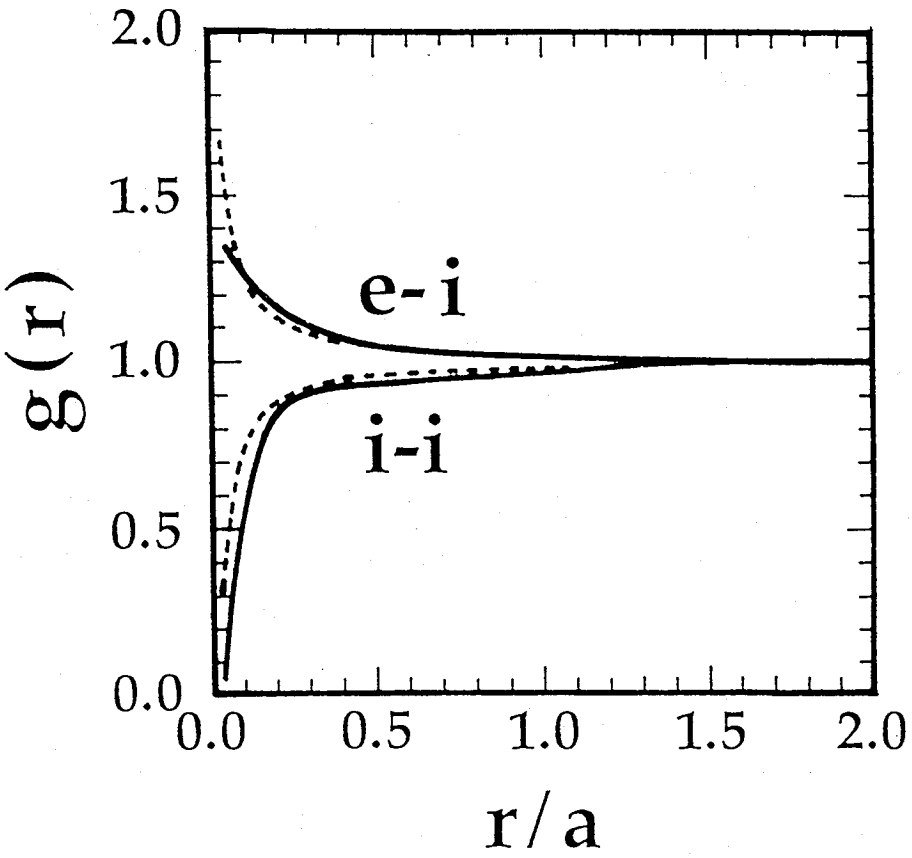

Fig. 3.1 The ion-ion and electron-ion pair distribution functions for the case of Z=1, Γ=0.0278 and T=1keV. The solid line represents the results obtained by simulation and the dashed line represents the results calculated by R. P. A. theory. The distance r is normalized by the ion-sphere radius a.

temperature T=1keV. Figure 3.2 shows the electron-ion pair distribution function, in which the solid line represents the results obtained by simulation and the dashed line represents the results calculated from Eqs. (3.27)~(3.35). The result from Eqs. (3.27)-(3.35) is greater than that by simulation for $r \lesssim 0.2a$. Many electrons are needed to shield the test particle charge Ze since when the electron-ion distribution function is calculated from Eqs. (3.27)~(3.35), the ion-ion pair distribution function is set $g_{ii}(r)=1$, i.e., no three-body correlation effects are included. And another reason of the difference is that no quantum effects are included in Eqs. (3.27)~(3.35). In the second case, the plasma is not fully ionized. The bound electron-ion pair distribution function is observed by simulation with symmetry effects. The electrons trapped by the nearest ion are defined as the bound electrons. Figure 3.3 shows the electron-ion pair distribution functions, in which the solid line represents total electron distribution function, the dashed line represents bound electron distribution function and the solid-dashed line represents free electron distribution function. The effective ionization state is estimated by

$$Z^* = Z - N_{be} \quad , \quad (3.36)$$

$$N_{be} = 4\pi n_e \int r^2 g_{be-i}(r)\, dr \quad . \quad (3.37)$$

Here $g_{be-i}(r)$ is the bound electron-ion pair distribution function obtained by the simulation. For this plasma Z^* is estimated to be 5.67. The value of $Z^*=5.67$ is under-estimated slightly because the potential lowering by neighborhood ions is not included in the definition of the bound electrons. But probably for this plasma, its effects can be small. In the frame of Eqs. (3.27)-(3.35), Z^* is estimated to be about 5.21 for the plasma Z=6, $\Gamma=1$ and T=1keV. The ion charge $Z^*=5.21$ is under-estimation because the ion-ion correlation effects and the quantum

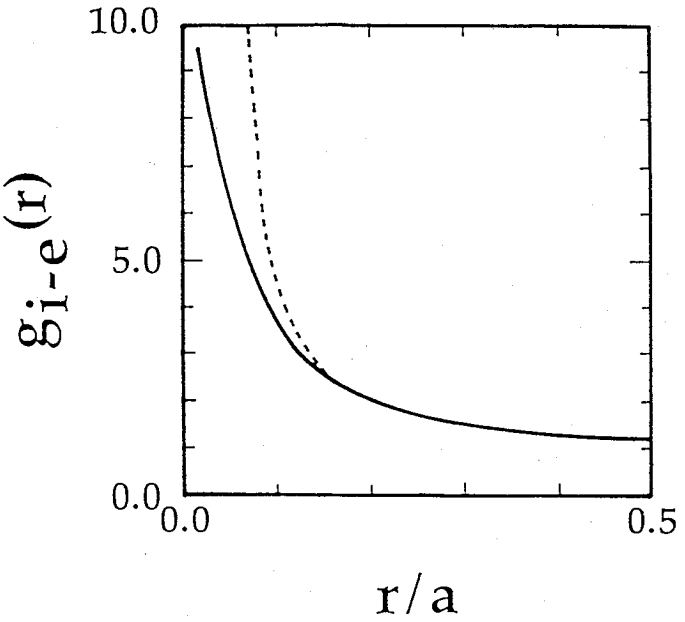

Fig. 3.2 The electron-ion pair distribution functions for the case of Z=6, Γ=1 and T=1keV. The solid line represents the results obtained by simulation and the dashed line represents the results calculated by finite temperature T-F model. The distance r is normalized by the ion-sphere radius a.

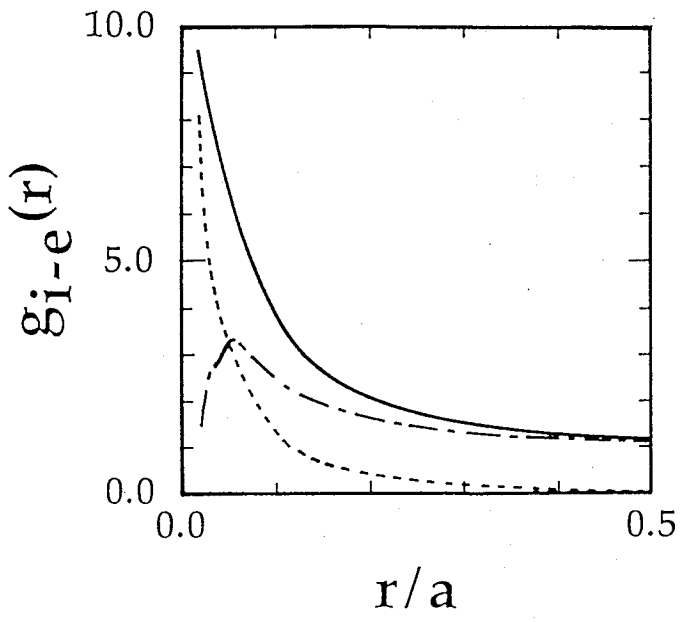

Fig. 3.3 The electron-ion pair distribution functions for the case of Z=6, Γ=1 and T=1keV. The solid line represents that of the total electrons, the dashed line represents that of the bound electrons and the solid dashed line represents that of the bound electrons. The distance r is normalized by the ion-sphere radius a.

effects are not included in Eqs. (3.27)-(3.35). Figure 3.4 shows the bound electron-ion pair distribution functions, in which the solid line represents the results obtained by simulation and the dashed line represents the results calculated from Eqs. (3.27)-(3.35). Many bound electrons are needed to shield the test particle charge Ze compared with the simulation because no ion-ion correlation effects are included in Eqs. (3.27)-(3.35), as mentioned above.

The difference of the effective ionization state and that of the electron shielding effects in the calculation of the ion-ion pair distribution function between the simulation and the Eqs. (3.23)-(3.26) affect ion-ion pair distribution function. Figure 3.5 shows the ion-ion pair distribution functions, in which the solid line represents the ion-ion pair distribution function obtained by the simulation, the dashed line represents that obtained from Eqs. (3.23)-(3.26), and the solid-dashed line represents that obtained from Eqs. (3.23)-(3.26) by replacing Z^* by Z. The simulation result decreases the fastest of the three as the distance r decreases, and approaches to unity the fastest of the three as the distance r increases. The result obtained from Eqs. (3.23)~(3.26) by replacing Z^* to Z is closer to that of the simulation than that obtained from Eqs. (3.23)~(3.26) by no replacing. This fact shows that in the calculation of $g_{ii}(r)$, the nonlinear electron shielding effects should be taken into account in the ion-ion interaction potential $\phi_{ii}(r)$.

As mentioned above, the differences of the pair distribution functions between the simulation and the theories originate from that the ion-ion and electron-ion pair distribution functions are calculated separately in the theories. Recently R. Ying and G. Kalman[10] perform the calculation of the ion-ion and bound electron-ion pair distribution functions self-consistently for a strongly coupled hydrogen plasma by a

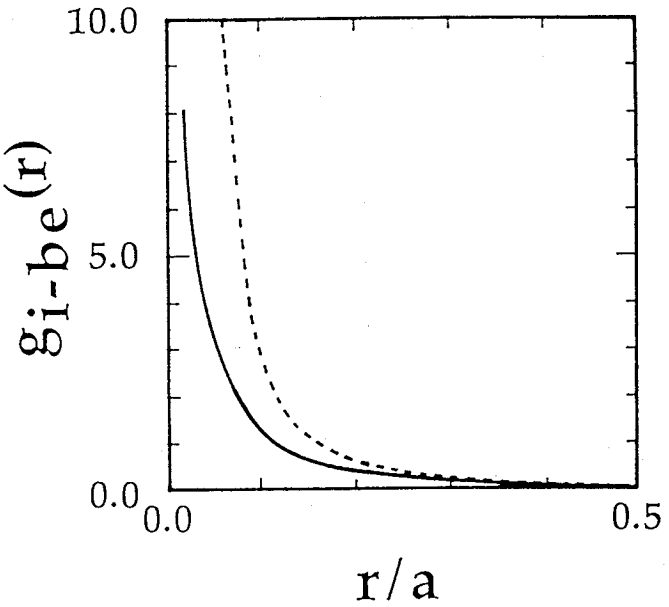

Fig. 3.4 The bound electron-ion pair distribution functions for the case of Z=6, Γ=1 and T=1keV. The two lines indicate the same as in Fig. 3.2. The distance r is normalized by the ion-sphere radius a.

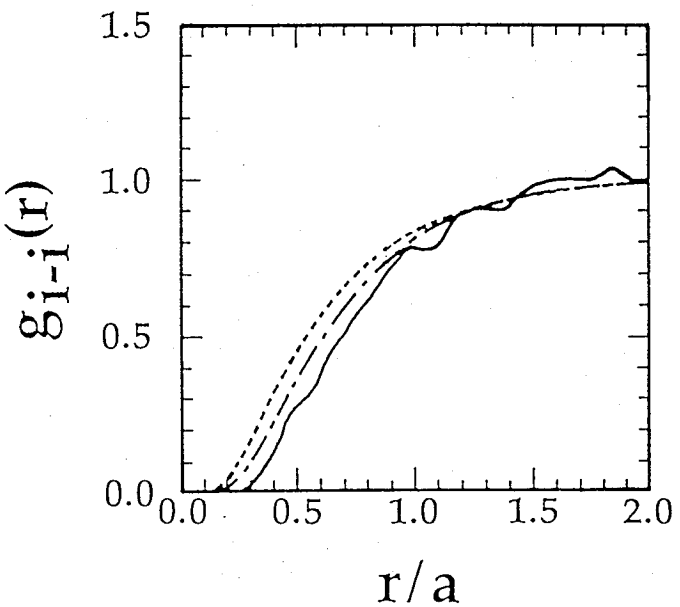

Fig. 3.5 The ion-ion pair distribution functions, the solid line represents that obtained by simulation, the dashed line represents that obtained from Eq. (3.23)~(3.26) and the solid-dashed line represents that obtained from Eq. (3.23)~(3.26) by replacing Z^* to Z. The distance r is normalized by the ion-sphere radius a.

newly developed atomic model based on T-F model. But in their model, the free electron pair distribution function is assumed to be independent on the distance r, i.e., $g_{fe\text{-}i}(r)=1$. This assumption is not always correct as our simulation shows. And ion-ion distribution function is roughly treated compared with our theoretical model. Note also that the quantum effects are not included in their model too.

The electron-electron symmetry effects on the pair distribution functions are estimated for the second case of Z=6, Γ=1 and T=1keV. The force arising from the symmetry effects, defined by Eq. (2.11), is proportional to the square of the plasma temperature, because the de Broglie wave length $\lambda\!\!\!^{-}_{ee}$ is proportional to inverse square root of the plasma temperature, and its width is proportional to $\lambda\!\!\!^{-}_{ee}{}^2$. In the second case the plasma temperature is relatively high. Figure 3.6 shows the ratio of the force arising from the symmetry effects to that arising from the quantum diffraction effects, defined by Eq. (2.10). The ratio $f^{(s)}(r)/f^{(d)}(r)$ is greater than unity for $r \lesssim 0.5a_e$, a_e is the electron sphere radius, $a_e=(3/4\pi n_e)^{1/3}$. The symmetry effects are thus important for the second case of Z=6, Γ=1 and T=1keV. Figure 3.7 shows the ion-ion pair distribution functions obtained by simulation, in which the solid line represents the result with the symmetry effects and the dashed line represents that without the symmetry effects. Both are almost the same for $r \lesssim 2a$. The electron-electron symmetry effects are not significant for the ion-ion pair distribution function.

Figure 3.8 shows the electron-electron pair distribution functions obtained by simulation, in which the solid line represents the result with the symmetry effects and the dashed line represents that without the symmetry effects. As expected, the electron-electron symmetry effects

reduce the value of the electron-electron pair distribution function greatly for the region of $r \lesssim 0.5a_e$. The Pauli principle prevents that two electrons approach each other.

Figures 3.9, 3.10 and 3.11 show the electron-ion pair distribution functions, the bound electron-ion pair distribution functions and the free electron-ion pair distribution functions obtained by simulation, in which the solid line represents the result with the symmetry effects and the dashed line represents that without the symmetry effects. As shown in Figs. 3.9 and 3.10, the electron-electron symmetry effects enhance the value of the electron-ion, especially bound electron-ion pair distribution functions. The reason of the enhancement is guessed as follows. By adding symmetry term to diffraction term, the free energy of the plasma increases compared with the case without symmetry term. Many electrons are attracted to an ion compared with the case without symmetry effects in order to decrease the free energy of the plasma. Note that for the case without symmetry effects, Z^* is estimated to be 5.73. For the case with symmetry effects, Z^* is estimated to be the value of 5.67, as mentioned above. It seems that the difference of Z^* is too small to observe the deference of ion-ion pair distribution functions between the two cases. For the case with symmetry effects, the number of electrons which locate within the distance $r \lesssim 0.2a$ from an ion can be estimated by

$$N = 4\pi n_e \int_0^{0.2a} r^2 g_{ei}(r)\, dr \quad . \quad (3.38)$$

The number N takes on value on roughly 0.1. The distance r_e between these electrons is roughly estimated as

$$r_e = \frac{0.2a}{\sqrt[3]{0.1}} \approx 0.8a_e \quad . \quad (3.39)$$

This value is sufficiently large to reduce the symmetry effects on the electron-electron pair distribution function as shown in Fig. 3.8. Therefore the values of Z^* for the cases of with and without symmetry effects do not contradict each other.

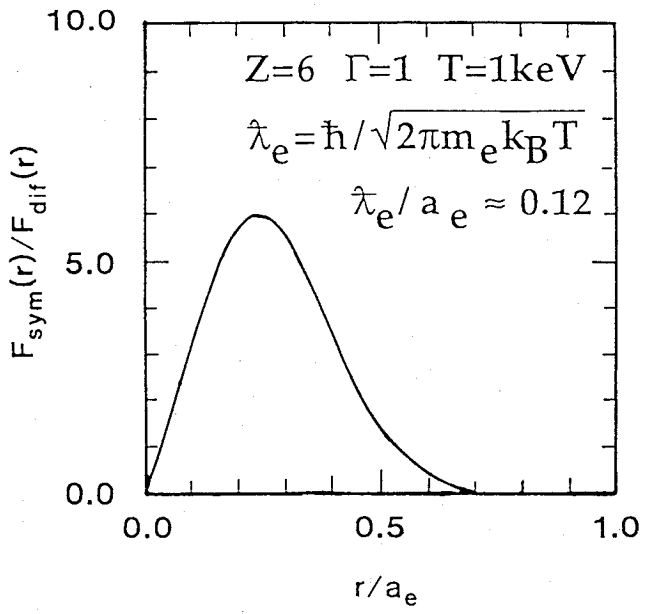

Fig. 3.6 The ratio of the force arising from the symmetry effects, defined by Eq. (2.11) and that arising from the quantum diffraction effects, defined by Eq. (2.10) for the case of Z=6, Γ=1 and T=1keV. The distance r is normalized by the electron-sphere radius a_e.

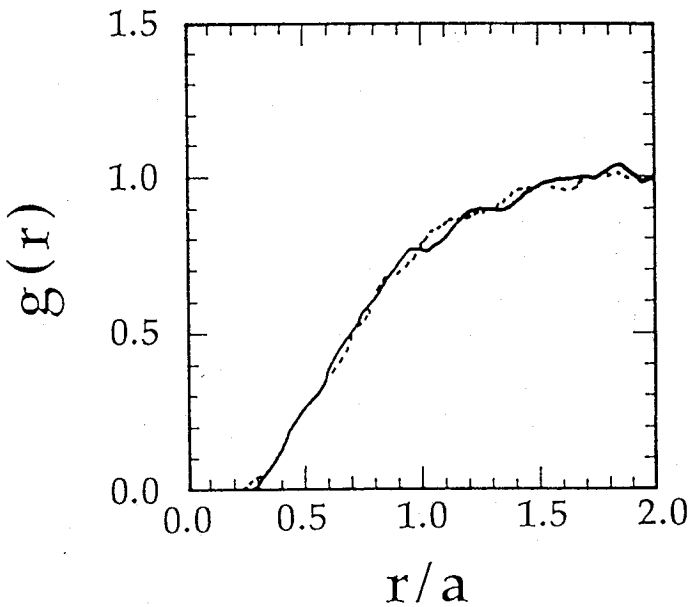

Fig. 3.7 The ion-ion pair distribution functions obtained by simulation, the solid line represents the result with the symmetry effects and dashed line represents the result without the symmetry effects for the case of Z=6, Γ=1 and T=1keV. The distance r is normalized by the ion-sphere radius a.

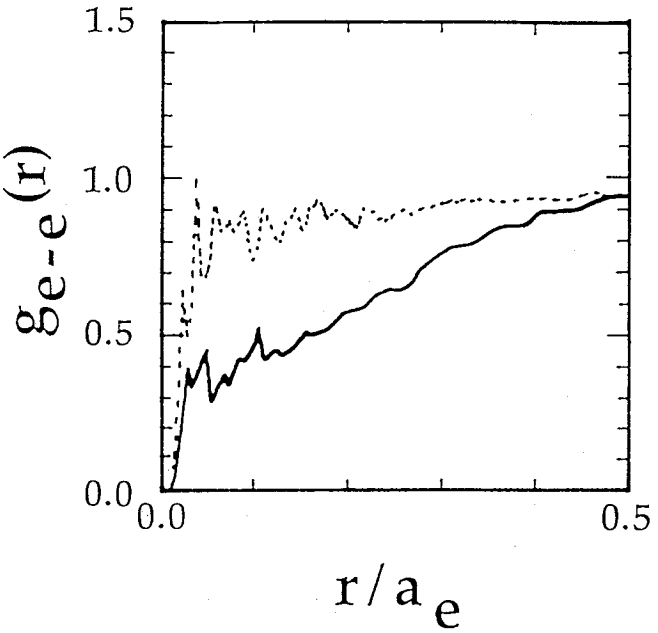

Fig. 3.8 The electron-electron pair distribution functions obtained by simulation, for the case of Z=6, Γ=1 and T=1keV. The two lines indicate the same as in Fig. 3.7. The distance r is normalized by the electron-sphere radius a_e.

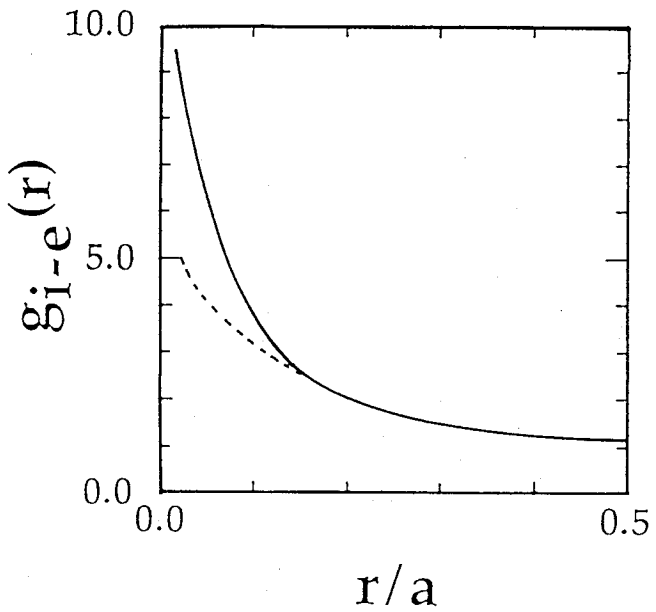

Fig. 3.9 The electron-ion pair distribution functions obtained by simulation, for the case of Z=6, Γ=1 and T=1keV. The two lines indicate the same as in Fig. 3.7. The distance r is normalized by the ion-sphere radius a.

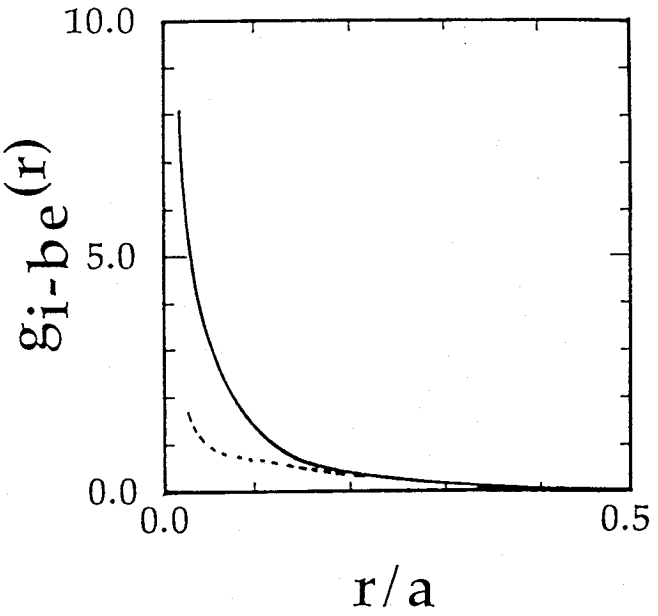

Fig. 3.10 The bound electron-ion pair distribution functions obtained by simulation, for the case of Z=6, Γ=1 and T=1keV. The two lines indicate the same as in Fig. 3.7. The distance r is normalized by the ion-sphere radius a.

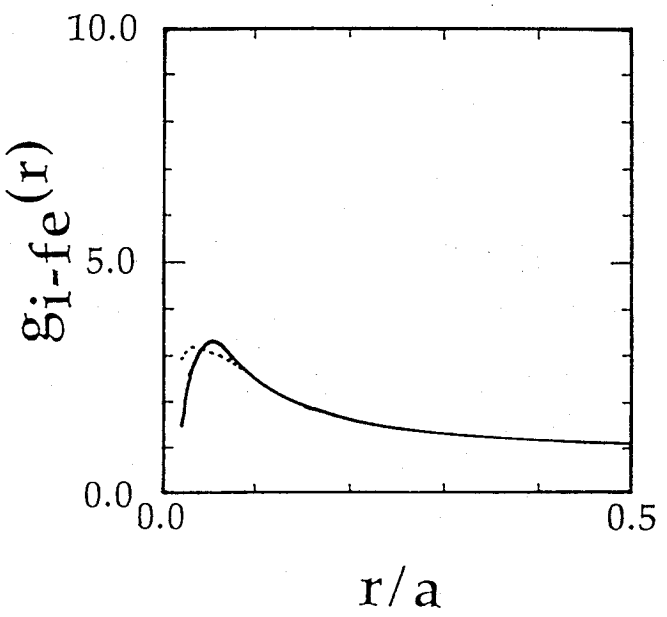

Fig. 3.11 The free electron-ion pair distribution functions obtained by simulation, for the case of Z=6, Γ=1 and T=1keV. The two lines indicate the same as in Fig. 3.7. The distance r is normalized by the ion-sphere radius a.

III - 4. REDUCTION IN BREMSSTRAHLUNG EMISSION FROM BINARY - IONIC - MIXTURE PLASMAS

First, I estimate the reduction in bremsstrahlung emission from a two-component strongly coupled plasma Z=6, Γ=1 and T=1keV using the pair distribution functions in Sec. III - 3. Figure 3.12 shows the reduction of bremsstrahlung emission coefficients obtained from Eqs. (3.12)-(3.19) as a function of the frequency. The dashed line represents the bremsstrahlung emission coefficients in which only the ion-ion correlation effects are included. The solid-dashed line represents the emission coefficients in which the ion-ion correlation and free electron shielding effects are included. The free electron shielding effects are estimated by replacing $g_{ei}(r)$ by $g_{fe\text{-}i}(r)$ in Eq. (3.13), where $g_{fe\text{-}i}(r)$ is the free electron-ion pair distribution function. The solid line represents the emission coefficients in which the ion-ion correlation and total electron shielding effects are included. R. Kawakami et al[2] calculate the reduction in bremsstrahlung emission from a two-component strongly coupled plasma Z=13, $n_i=8\times10^{21}cm^{-3}$ and T=1keV (Γ=0.787 and θ=123.8). Our results are in good agreement with their results qualitatively, for example the reduction rate for the low frequency near $\omega\sim\omega_{pe}$ and the frequency under which the emission is reduced although they calculate the ion-ion pair distribution function using the ion-ion interaction potential $\phi_{ii}(r)=Z^*eU(r)$ in HNC equation. The shielding effects in their ion-ion interaction potential is over-estimation as well in Eq. (3.26), because no ion-ion correlation effects are included as the same as in Eq. (3.26). As the result, the ion-ion pair distribution function obtained by their model is enhanced compared with the ion-ion pair distribution function obtained by our simulation. Because both of the ion-ion and electron-ion

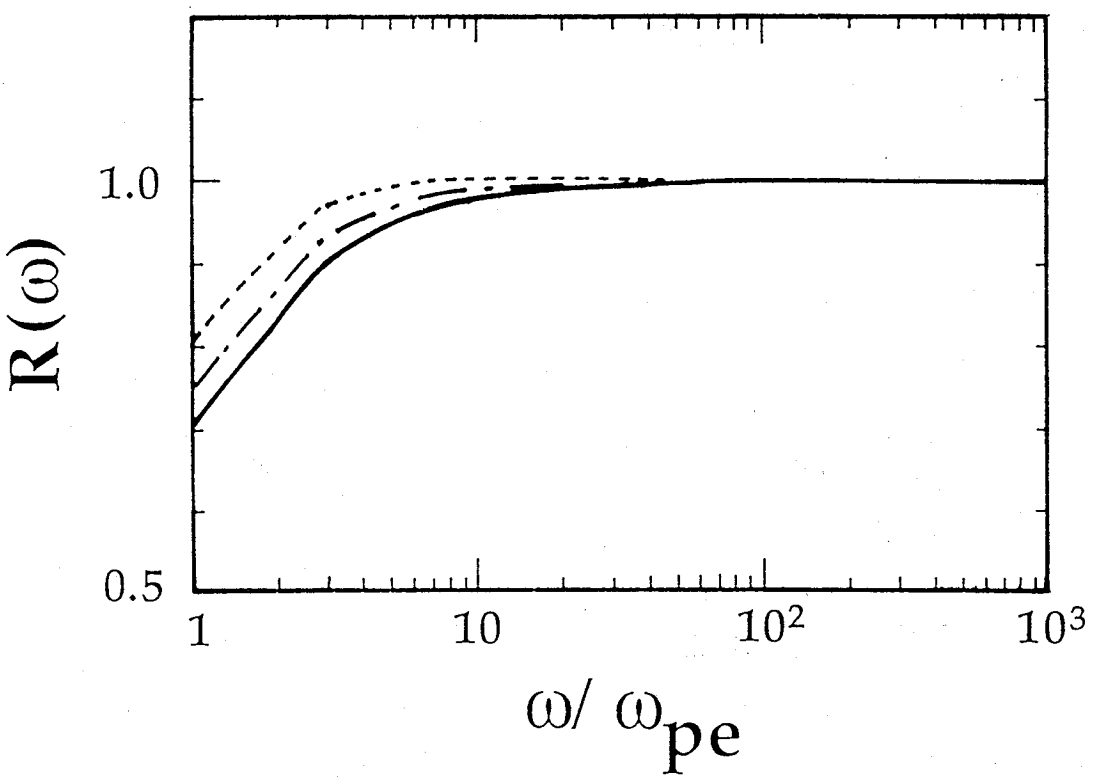

Fig. 3.12 The reduction of the bremsstrahlung emission coefficients as a function of the frequency for the case of Z=6, Γ=1 and T=1keV. The dashed line represents the bremsstrahlung emission coefficients which includes only the ion-ion correlation effects. The solid-dashed line represents that includes the ion-ion correlation and the free electron shielding effects. The solid line represents that includes the ion-ion correlation and the total electronic shielding effects. The frequency ω is normalized by the electron plasma frequency ω_{pe}.

pair distribution functions obtained by their model are enhanced compared with the pair distribution functions obtained by our simulation, the electron scattered by an ion feels almost the same charge for both case of our simulation and their model qualitatively.

Also estimated is the reduction in bremsstrahlung emission from a binary ionic mixture plasma Z_1=6, Z_2=1, n_1:n_2=1:1, Γ_1=1.0, Γ_2=0.0278 and Γ_{eff}=0.553, by simulation with symmetry effects. Here

$$\Gamma_1 = \frac{Z_1^2 e^2}{a_1 k_B T} \quad , \quad a_1 = \left(\frac{3}{4\pi n_1}\right)^{1/3} ,$$

$$\Gamma_2 = \frac{Z_2^2 e^2}{a_2 k_B T} \quad , \quad a_2 = \left(\frac{3}{4\pi n_2}\right)^{1/3} ,$$

$$\Gamma_{eff} = \frac{\langle Z^{5/3}\rangle \langle Z\rangle^{1/3} e^2}{a k_B T} \quad , \quad a = \left(\frac{3}{4\pi(n_1 + n_2)}\right)^{1/3} ,$$

. (3.40)

Simulation parameters are summarized in Table 3.2. Figure 3.13 shows the pair distribution functions, in which a) is the ion-ion and electron-ion distribution functions around the ion of Z_1=6, and the dashed line represents the ion of Z_2=1 distribution function around the ion of Z_1=6, and b) is the ion-ion and electron-ion distribution functions around the ion of Z_2=1. Figure 3.14 shows the electron-ion pair distribution functions around the ion of Z_1=6, the solid line, the dashed line and the solid dashed line represent the total electron, bound electron and free electron distribution functions, respectively. The effective ionization state of the carbon is estimated to be Z_1^*=5.77.

Table 3.2

Details of simulation. N_e is the number of electrons used in simulation. N_1 is the number of the first type of ions, corresponding to carbon, used in simulation. N_2 is the number of the second type of ions, corresponding to hydrogen, used in simulation. Δ is the size of one mesh in space. Δt is the time step in the numerical integration.

Z_1	6
Z_2	1
$n_1 : n_2$	1 : 1
Γ_{eff}	0.553
n_i(total, cm^{-3})	3.4×10^{24}
$n_e(cm^{-3})$	1.2×10^{25}
T(keV)	1.0
N_e	5600
N_1	800
N_2	800
Mesh	4X4X4
Δ/λ_{De}	2.645
$n_e \Delta^3$	87.5
$n_1 \Delta^3$	12.5
$\Delta t \omega_{pe}$	0.05
m_1 / m_e	600.0
m_2 / m_e	100.0

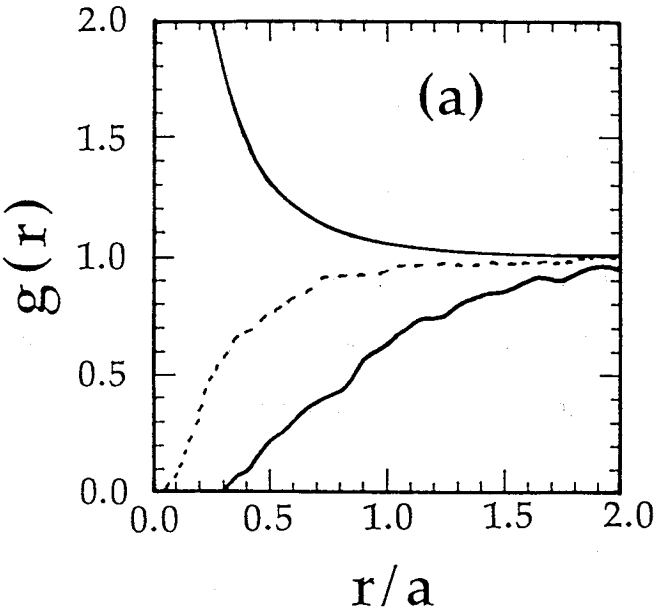

Fig. 3.13 a) The ion-ion and electron-ion pair distribution functions around the ion of Z_1=6, and the dashed line represents the ion of Z_2=1 distribution function around the ion of Z_1=6. The distance r is normalized by the ion-sphere radius a given by Eq. (3.40).

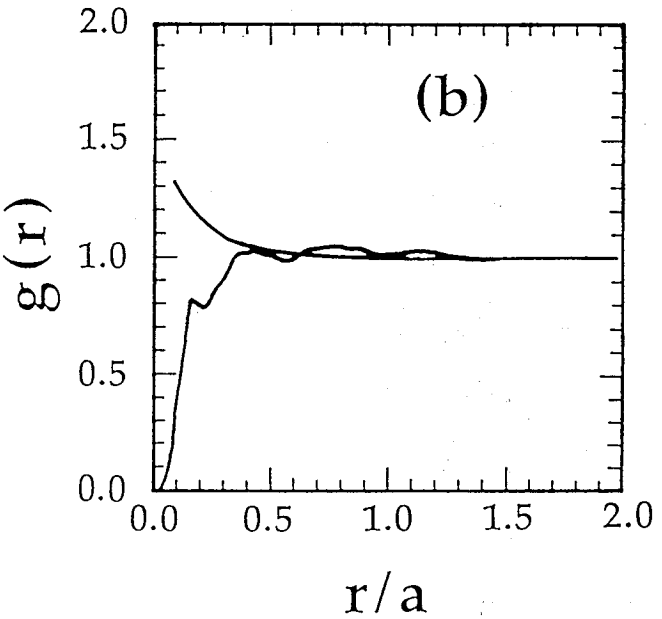

Fig. 3.13 b) The ion-ion and electron-ion distribution functions around the ion of Z_2=1. The distance r is normalized by the ion-sphere radius a given by Eq. (3.40).

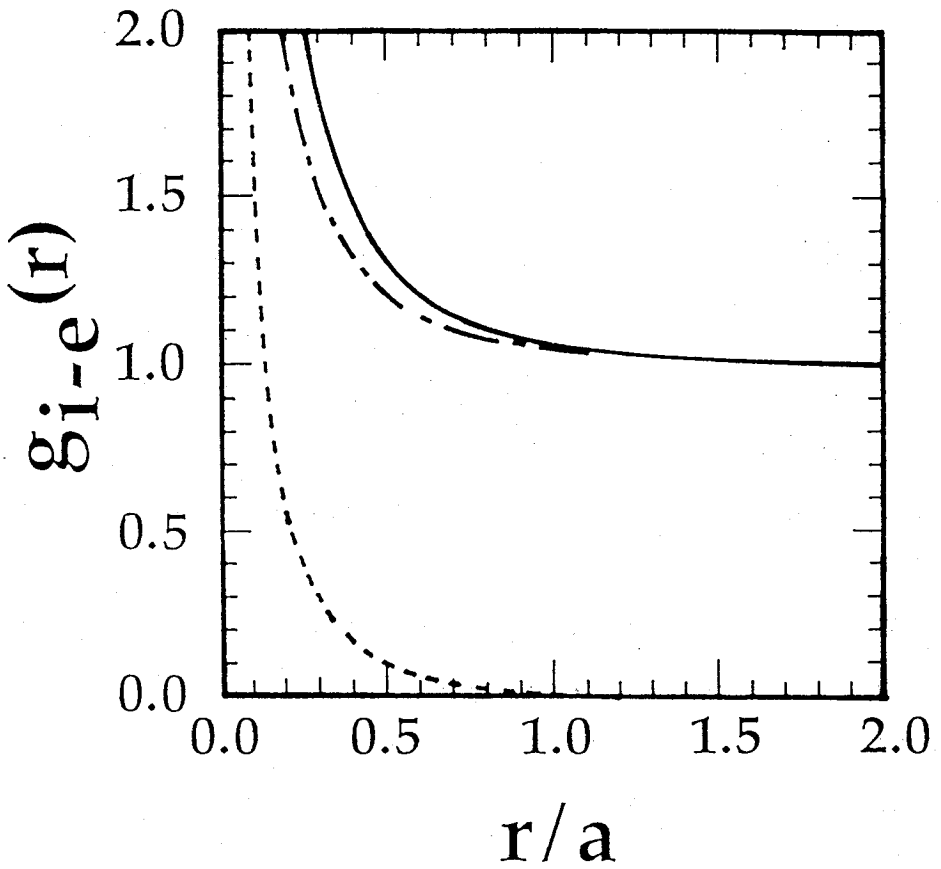

Fig. 3.14 The electron-ion pair distribution functions around the ion of Z_1=6, the solid line, the dashed line and the solid dashed line represent the total electron, bound electron and free electron distribution functions. The distance r is normalized by the ion-sphere radius a given by Eq. (3.40).

By using these pair distribution functions, estimated is the reduction in bremsstrahlung emission from a binary ionic mixture plasma as a function of the frequency. Figure 3.15 shows the reduction of the bremsstrahlung emission coefficients as a function of the frequency. The three lines indicate the same as mentioned above. As shown in Fig. 3.15, the dependence of the reduction on the frequency consists of roughly three parts. First for $\omega_{pe} \lesssim \omega \lesssim 5\ \omega_{pe}$, the ion-ion correlation and electronic shielding effects are comparable and the reduction rate at $\omega \sim \omega_{pe}$ is about 75%. Second for $5\omega_{pe} \lesssim \omega \lesssim 50\ \omega_{pe}$, the electronic shielding effects are dominant but the reduction rate is roughly 10%. Third for $50\omega_{pe} \lesssim \omega$, there is almost no reduction in bremsstrahlung, because high frequency emission originates in a very small impact parameter, and an electron feels the bare ion charge Ze.

Totsuji[3] has pointed out that when only ion-ion correlation effects are taken into account, the reduction from a binary ionic mixture plasma is approximated by a fictitious plasma of which the ion charge is given by

$$Z_{eff}^{\ 2} e^2 = \langle Z^{5/3} \rangle \langle Z \rangle^{1/3} e^2 \quad . \quad (3.41)$$

This is examined for the two-component plasma. For the plasma considered above Z_{eff} and Γ_{eff} take on value on 3.97 and 0.553, respectively. Simulation parameters are shown in Table 3.3. Note that in the simulation chosen is the ion charge Ze=4e instead of Ze=3.97e, and the effective Coulomb coupling constant for ions Γ=0.56, instead of Γ=0.553. In the calculation of Γ, Z=4 is used, instead of Z=3.97, a is the same value defined by Eq. (3.40) and T=1keV. The pair distribution functions are shown in Fig. 3.16 (a). Figure 3.16 (b) shows the electron-ion pair distribution functions, in which the three lines are the same as

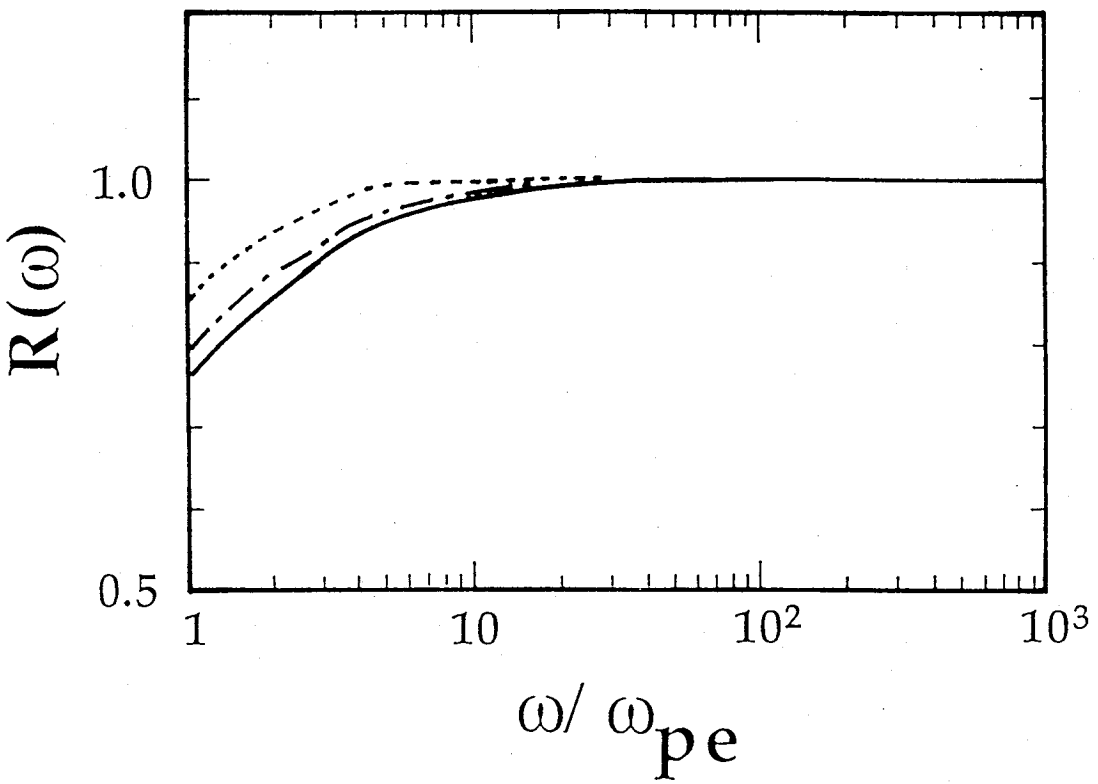

Fig. 3.15 The reduction of the bremsstrahlung emission coefficients as a function of the frequency for the case of the binary ionic mixture plasma. The three lines indicate the same as in Fig. 3.12. The frequency ω is normalized by the electron plasma frequency ω_{pe}.

those in Fig. 3.14. The reduction factor is shown in Fig. 3.17. In this plasma, Z^* takes on value on 3.86. In the case of the mixture plasma and the fictitious plasma, the reduction factors of both cases are in good agreement. The conclusion is that, if the binary ionic mixture plasma is almost fully ionized, the effective ion charge for bremsstrahlung can be approximated by Eq. (3.41), even if a two-component plasma.

Table 3.3

Details of simulation. N_e and N_i are the numbers of electrons and ions used in simulation respectively. Δ is the size of one mesh in space. Δt is the time step in the numerical integration.

Z	4
Γ	0.56
$n_i(cm^{-3})$	3.4×10^{24}
T(keV)	1.0
N_e	3200
N_i	800
Mesh	4X4X4
Δ/λ_{De}	2.425
$n_e \Delta^3$	50.0
$n_i \Delta^3$	12.5
$\Delta t \omega_{pe}$	0.05
m_i / m_e	400.0

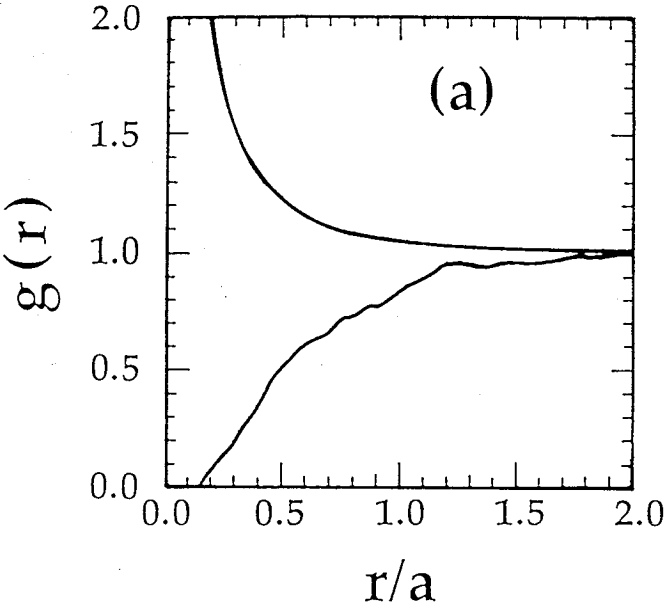

Fig. 3.16 a) The pair distribution functions for the case of the fictitious plasma of Z=4, Γ=0.56 and T=1keV. The distance r is normalized by the ion-sphere radius a given by Eq. (3.40).

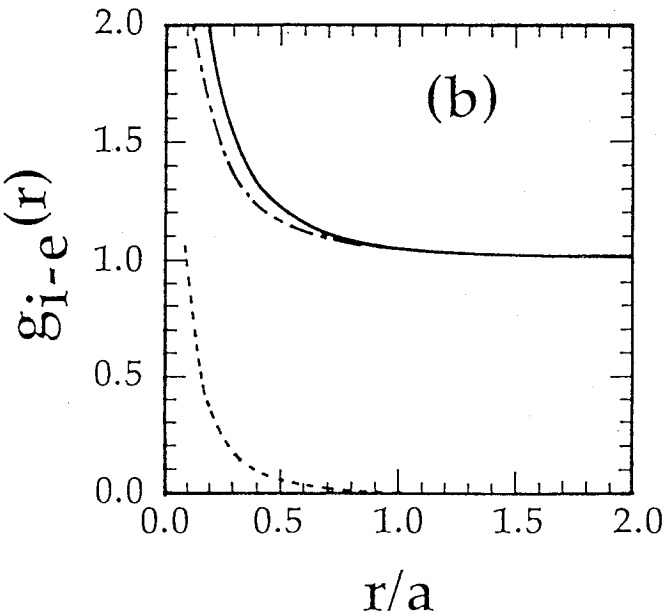

Fig. 3.16 b) The electron-ion pair distribution functions for the case of the fictitious plasma of Z=4, Γ=0.56 and T=1keV. The three lines indicate the same as in Fig. 3.3. The distance r is normalized by the ion-sphere radius a given by Eq. (3.40).

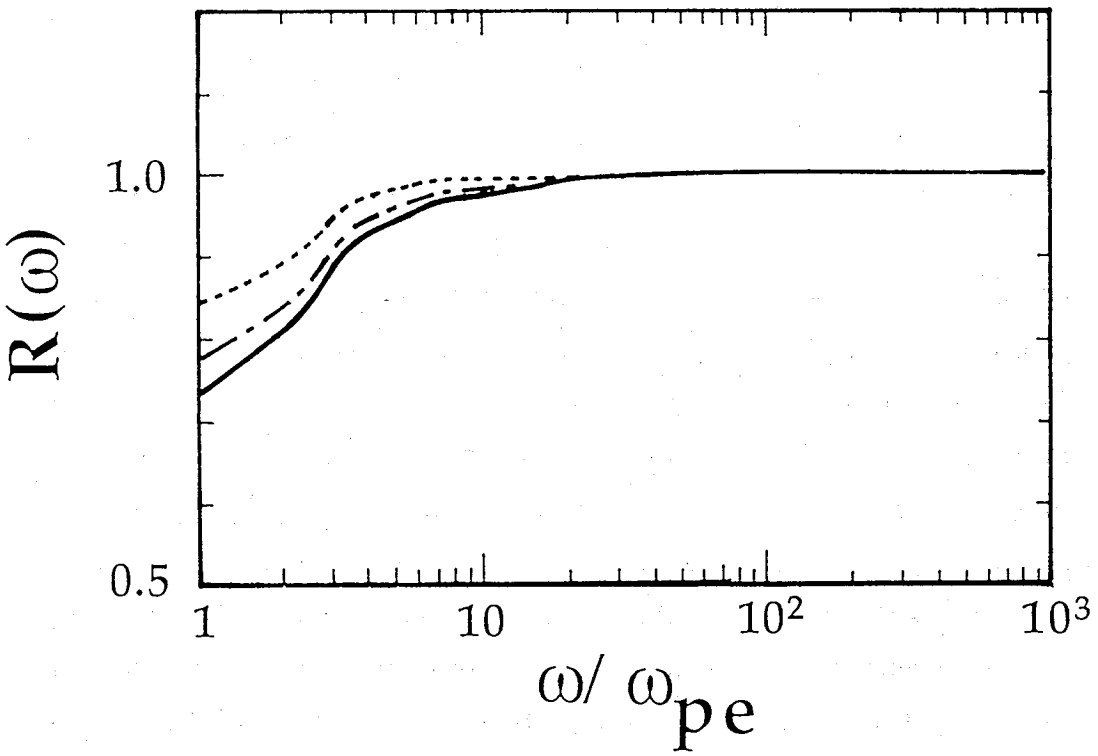

Fig. 3.17 The reduction of the bremsstrahlung emission coefficients as a function of the frequency for the case of the fictitious plasma of Z=4, Γ=0.56 and T=1keV. The three lines indicate the same as in Fig. 3.12.The frequency ω is normalized by the electron plasma frequency ω_{pe}.

III - 5. SUMMARY

The formulation of the calculation of the bremsstrahlung coefficients from a two-component binary ionic mixture plasma has been introduced on the basis of dipole emission model. The pair distribution functions are related to the emission coefficients.

The pair distribution functions obtained by using "SCOPE" are compared with analytical solutions for the cases of the weakly coupled and strongly coupled plasmas. For the weakly coupled plasma, the simulation results are in good agreements with R.P.A. theory. For the strongly coupled plasma, The differences in the pair distribution functions between the simulations and analytical models are not negligible. The differences originate in that in the previous theories the ion-ion and electron-ion pair distribution functions are calculated separately, the electron shielding effects are taken into as a linear response shielding and there is no quantum effects. The electron-electron symmetry effects are found to reduce the value of the electron-electron pair distribution function and enhance the value of the electron-ion pair distribution function, especially for bound electrons.

The reduction in the bremsstrahlung is estimated for the case of two-component strongly coupled plasma Z=6, Γ=1 and T=1keV, and compared with the results by R. Kawakami et al[2]. Our results are in good agreements with their results qualitatively.

The pair distribution functions are observed for the cases of the binary ionic mixture plasma, and estimated the reduction of the bremsstrahlung. The dependence of the reduction on the frequency consists of roughly three parts. First, the ion-ion correlation effects and electronic shielding effects are comparable for $\omega_{pe} \lesssim \omega \lesssim 5\omega_{pe}$ and the

reduction rate at $\omega \sim \omega_{pe}$ is about 75%, the electronic shielding effects are dominant but the reduction rate is roughly 10% for $5\omega_{pe} \lesssim \omega \lesssim 50\omega_{pe}$ and no reduction for $50\omega_{pe} \lesssim \omega$.

The reduction in the bremsstrahlung emission for a binary mixture plasma is concluded to be approximated by that for a single ion plasma of which ion has a fictitious averaged charge, even for the two-component plasma.

REFERENCES OF CHAPTER III

1). S. Ichimaru, S. Mitake, S. Tanaka and Xin-Zhong Yan, Phys. Rev. A, **32,** 1768 (1985).

2). R. Kawakami, K. Mima, H. Totsuji and Y. Yokoyama, Phys. Rev. A, **38,** 3618 (1988).

3). H. Totsuji, Memoirs of the School of Engineering, Okayama University, **21,** 45 (1986).

4). H. Furukawa and K. Nishihara, Phys. Rev. A, **42,** 3532 (1990).

5). H. Totsuji, Phys. Rev. A, **32,** 3005 (1985).

6). C. Deutsch, Phys. Lett. **60A,** 317 (1977).

7). V. B. Berestetskii, E. M. Lifshitz and L. P. Pitaevskii, Relativistic Quantum Theory (Pergamon, Oxford, 1971), Pt. 1, Sec. 45.

8). N.H. March and M.P. Tosi, Atomic Dynamics in Liquids, (John Wiley & Sons, 1976), pp 41-44.

9). S. Ichimaru, Basic Principles of Plasma Physics, (W. A. Benjamin, Reading, MA, 1973), Chap. 9 and Appendix.

10). R. Ying and G. Kalman, Phys. Rev. A, **40,** 3927 (1989).

IV. Application of "SCOPE" to Laser-Produced Hot, Dense Plasmas II

~ Self-diffusion and electric conductivity ~

With the use of "SCOPE", the velocity auto-correlation functions (V.A.F.) and the auto-correlation functions of the total microscopic electric current of laser-produced hot, dense plasmas are calculated. The self-diffusion coefficients and electric conductivities are then estimated. The dependence of the self-diffusion coefficients on the Coulomb coupling constant Γ is obtained. For the plasmas, $Z=6$, $\theta=5$, the normalized self-diffusion coefficients of electrons are proportional to $\Gamma^{-0.55}$ for the range of $0.5 \lesssim \Gamma \lesssim 3$, and roughly 0.1 times Spitzer-Härm value (Ref. 1). The normalized self-diffusion coefficients of ions are proportional to $\Gamma^{-0.69}$ for the range $0.5 \lesssim \Gamma \lesssim 2$. For the range $\Gamma \gtrsim 2$, the electric shielding effects on the self-diffusion coefficients of ions become strong. The normalized electric conductivities obtained by simulations are proportional to $\Gamma^{-0.52}$ and that of theoretical model are proportional to $\Gamma^{-1.32}$ for the range of $0.5 \lesssim \Gamma \lesssim 3$. The difference is attributed to the dynamical effects and the treatment of electron degeneracy.

IV - 1. INTRODUCTION

In laser-produced hot, dense plasmas, it is expected that the self-diffusion coefficients are smaller than that in the ideal plasma. To estimate the self-diffusion coefficients quantitatively, the knowledge of the time dependent interparticle correlations is necessary.

The self-diffusion coefficients are related to the velocity auto-correlation functions (V.A.F.)[2,3]. It is very difficult to calculate the velocity auto-correlation functions by statistical model[2], but it is not so difficult to calculate the velocity auto-correlation functions by simulation[3]. The velocity auto-correlation functions of the two-component nondegenerate plasmas are calculated by simulations, and estimated are the self-diffusion coefficients as a function of the Coulomb coupling constant for ions Γ. In the section IV - 2, described are the velocity auto-correlation functions and the self-diffusion coefficients.

The electric conductivities are related to the auto-correlation functions of the total microscopic electric current[2,3]. The auto-correlation functions of the total microscopic electric current of the two-component nondegenerate plasmas are calculated by simulations, and estimated are the electric conductivities. In the section IV - 3, described are the auto-correlation functions of the total microscopic electric current and the electric conductivities.

The section IV - 4 is devoted to summary.

IV - 2. VELOCITY AUTO-CORRELATION FUNCTIONS AND SELF-DIFFUSION COEFFICIENTS

The self-diffusion of both ions and electrons has been studied by computing the corresponding normalized velocity auto-correlation function (V.A.F.) defined as

$$Z_\alpha(t) = \frac{\langle \mathbf{v}_\alpha(t) \bullet \mathbf{v}_\alpha(0) \rangle}{\langle |\mathbf{v}_\alpha(0)|^2 \rangle} \quad , \quad (4.1)$$

where $v_\alpha(t)$ is the velocity at time t of an ion or an electron. The self-diffusion coefficient can be related to the velocity auto-correlation function as follows[4]. A particle in a plasma receives the friction force and the random force due to the internal particle-particle collisions. The equation of motion in one-dimension can be written as

$$m\,\dot{u}(t) = -\,m\,\nu\,u(t) + f(t) \quad , \quad (4.2)$$

where u is the velocity of a particle, ν is the collision frequency and f(t) is the random force. By using the Fourier transform of Eq. (4.2), the Fourier component of u is written as

$$\hat{u}(\omega) = \mu(\omega)\,\hat{f}(\omega) \quad , \quad (4.3)$$

where $\mu(\omega)$ is the complex mobility given by

$$\mu(\omega) = \frac{1}{m}\,\frac{1}{i\,\omega + \nu} \quad . \quad (4.4)$$

With the aid of Eq. (4.3), the power spectra of u(t) is given as

$$I_u(\omega) = I_f(\omega)\left|\mu(\omega)\right|^2 \quad . \quad (4.5)$$

Using the equipartition of energy, the power spectrum of f(t), $I_f(\omega)$, is given by

$$I_f(\omega) = m\,\nu\,k_B T\,/\,\pi \quad . \quad (4.6)$$

By Wiener-Khinchin's theorem, the power spectrum is related to the auto-correlation function as

$$I_u(\omega) = \frac{1}{2\pi}\int_{-\infty}^{\infty} dt \left\langle u(t)\,u(0)\right\rangle \exp(-i\,\omega t) \quad . \quad (4.7)$$

Using Eqs. (4.4)-(4.6), $I_u(\omega)$ can be written by

$$I_u(\omega) = \frac{k_B T}{2\pi m}\left(\frac{1}{i\,\omega+\nu} + \frac{1}{-i\,\omega+\nu}\right) \quad . \quad (4.8)$$

By Eqs. (4.7) and (4.8), the following equation can be derived.

$$\left\langle u(t)\,u(0)\right\rangle = \frac{k_B T}{2\pi m}\int_{-\infty}^{\infty} d\omega\left(\frac{1}{i\,\omega+\nu} + \frac{1}{-i\,\omega+\nu}\right)\exp(i\,\omega t) \quad . \quad (4.9)$$

By integrating Eq. (4.9) at the half circle of which radius is infinite on the half plane of imaginary part of $\omega > 0$, the following equation can be obtained.

$$\left\langle u(t)\,u(0)\right\rangle = \frac{k_B T}{2\pi}\int_{-\infty-i\varepsilon}^{\infty-i\varepsilon} d\omega\,\mu(\omega)\exp(i\,\omega t) \quad . \quad (4.10)$$

Eq. (4.10) is equal to the equation as follows.

$$\mu(\omega) = \frac{1}{k_B T}\int_{0}^{\infty} dt \left\langle u(t)\,u(0)\right\rangle \exp(-i\,\omega t) \quad . \quad (4.11)$$

With the aid of Einstein's law, the self-diffusion is related to velocity auto-correlation function as

$$D = \int_0^\infty dt \langle u(t)\, u(0) \rangle \quad . \quad (4.12)$$

For the case of 3-dimension, Eq. (4.12) can be rewritten as

$$D_\alpha = \frac{k_B T}{m_\alpha} \int_0^\infty dt\, Z_\alpha(t) \quad . \quad (4.13)$$

In the Spitzer-Härm's theory[1] the electron-ion collision frequency is given by

$$\nu_{ei} = \frac{4\sqrt{2\pi}}{3} \frac{Z^2 e^4 n_i}{m_e{}^2 v^3} \ln\left(n_e \lambda_{De}{}^3\right) \quad , \quad (4.14)$$

where v is the velocity of an electron. Assumed is that the self-diffusion coefficients of the electrons can be written as

$$D_e = \left\langle \frac{v^2}{3\nu_{ei}} \right\rangle \quad , \quad (4.15)$$

where < > means the average by Maxwellian. Eq. (4.15) can be rewritten as

$$D_e = \frac{12\pi^{3/2}}{\sqrt{2}\, Z} \frac{n_e \lambda_{De}{}^3}{\ln\left(n_e \lambda_{De}{}^3\right)} \frac{\omega_{pe} \lambda_{De}{}^2}{3} \left\langle \frac{x^5}{\Psi(x)} \right\rangle \quad , \quad (4.16)$$

where

$$x = v / v_{Te} \quad , \quad (4.17)$$

and

$$\Psi(x) = \frac{2}{\sqrt{\pi}} \int_0^x dt\, t^{1/2} \exp(-t) \quad . \quad (4.18)$$

When $x_{max} = 3.0$, $< x^5 / \Psi(x) > \sim 30$. In the same way, the self diffusion coefficients of the ions can be written as

$$D_i = \frac{12\pi^{3/2}}{\sqrt{2}} \frac{n_i \lambda_{Di}^{\ 3}}{\ln(n_i \lambda_{Di}^{\ 3})} \frac{\omega_{pi} \lambda_{Di}^{\ 2}}{3} \left\langle \frac{x^5}{\Psi(x)} \right\rangle \quad , \quad (4.19)$$

for the case of ideal plasmas.

Figure 4.1 shows the normalized velocity auto-correlation functions which are obtained by simulation for Z=6, Γ=1 and θ=5. The horizontal axis represents the time normalized by ω_{pe}^{-1}, where $\omega_{pe}=(4\pi n_e e^2/m_e)^{1/2}$. Note that the mass ratio of ion to electron in this simulation is 600 because this simulation requires the long time even if the mass ratio mentioned above. However, as shown in Eqs. (4.16) and (4.19), for the case of ideal plasmas the normalized self-diffusion coefficients are independent of the mass of an electron or an ion. For the case of strongly coupled plasmas, the mass dependence of the normalized self-diffusion coefficients is probably weak. As shown in Fig 4.1, at the time t~0 the V.A.F. decreases proportional to t^2 and at the long time scale V.A.F. decreases exponentially.

The self-diffusion coefficients are estimated according to the Eq. (4.13) as a function of Γ with Z=6 and θ=5. The parameters are summarized in Table 4.1. Figure 4.2 shows the self-diffusion coefficients normalized by $\omega_{p\alpha}\lambda_{D\alpha}^{\ 2}$, where α means electron or ion and $\lambda_{Di}=(k_BT/4\pi Z^2 n_i e^2)^{1/2}$. The horizontal axis represents the Coulomb coupling constant for ions Γ. The open triangle means the self-diffusion coefficients of electron and the open circle means the self-diffusion coefficients of ion. The dashed lines show the Γ dependence of the self-diffusion coefficients of electron and ion. As shown in Fig. 4.2 the

normalized self-diffusion coefficients of both electron and ion obey the power law of Γ for the range of $0.5 \lesssim \Gamma \lesssim 3$ except that of ions at $\Gamma=3$. It seems that for the range of $3 \lesssim \Gamma$ the electron shielding effects are stronger than that for the range of $\Gamma \lesssim 3$. By the least square method the normalized self-diffusion coefficients are interpolated as

$$D_e / \omega_{pe} \lambda_{De}^2 = 16.42 \Gamma^{-0.55} \quad , \quad (4.20)$$

$$D_i / \omega_{pi} \lambda_{Di}^2 = 5.781 \Gamma^{-0.69} \quad , \quad (4.21)$$

In Fig. 4.2, the solid line means the self-diffusion coefficients of electrons obtained by Eq. (4.16) when $x_{max}=3.0$. Note that for the range of $\Gamma \gtrsim 2$, Eq. (4.16) is meaningless because $\ln(n_e \lambda_{De}^3)$ is negative. As shown in Fig. 4.2, in the strongly coupled plasmas the self-diffusion coefficients of electrons are almost 0.1 times of that of Spitzer-Härm's theory because of strongly coupled effects. In Spitzer-Härm's theory, if $\ln(n_e \lambda_{De}^3)$ is neglected, the normalized self-diffusion coefficients of electron are proportional to $\Gamma^{-3/2}$ because of the relationship of $n_e \lambda_{De}^3$ and $\Gamma^{-3/2}$. Because of strong coupling effects, the Γ dependence of the self-diffusion coefficients of electron is different from that of Spitzer-Härm's theory.

Table 4.1

Details of simulation parameters. N_e and N_i are the numbers of electrons and ions used in the simulations respectively. Δ is the size of one mesh in space. Δt is the time step in the numerical integration. For almost all simulations in this table, Z=6, θ=5, N_e=600, N_i=100, $\Delta t\omega_{pe}$=0.05, mesh=8x8x8, the mesh size of P-P area is 6x6x6 and the mass ratio of an ion to electron is 600.

Γ	0.5	1.0	2.0	3.0
n_i(cm-3)	2.14×10^{25}	2.67×10^{24}	3.34×10^{23}	9.91×10^{22}
T(keV)	4.65	1.16	0.290	0.129
Δ/λ_{De}	0.468	0.661	0.935	1.145
D_e^*	24.02	16.9	10.4	9.47
D_i^*	9.42	5.64	3.64	5.11

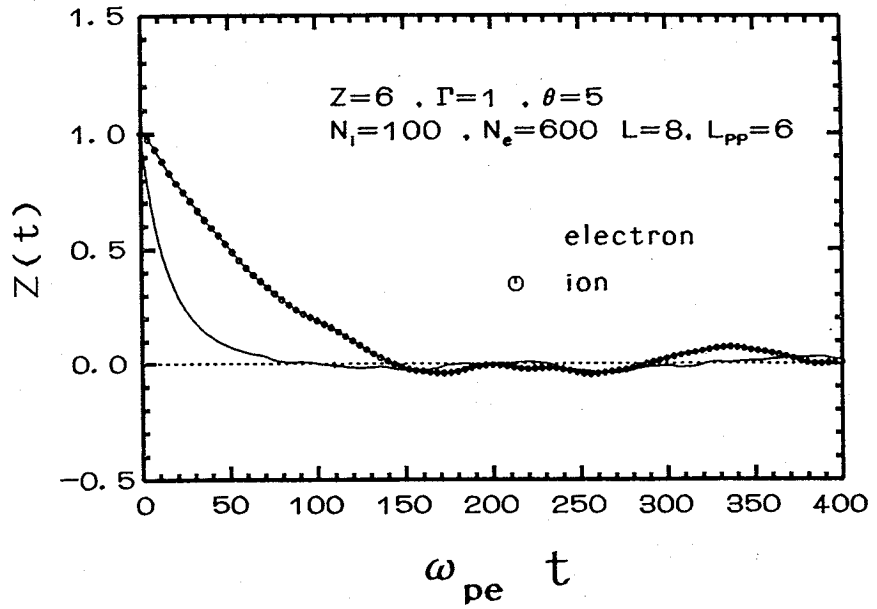

Fig. 4.1 The normalized velocity auto-correlation functions of the plasma Z=6, Γ=1 and θ=5. The horizontal axis represents the time normalized by ω_{pe}^{-1}.

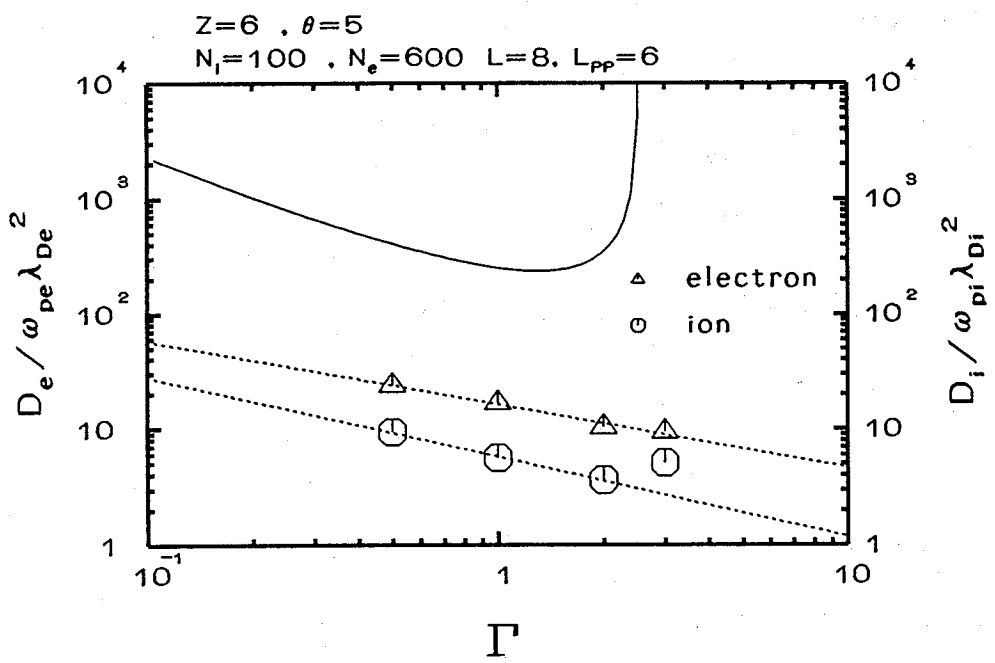

Fig. 4.2 The self-diffusion coefficients normalized by $\omega_{p\alpha}\lambda_{D\alpha}^{2}$, where α means electron or ion. The horizontal axis represents the Coulomb coupling constant for ions Γ.

IV - 3. AUTO CORRELATION FUNCTION OF TOTAL ELECTRIC CURRENT AND ELECTRIC CONDUCTIVITY

The electric conductivity has been studied by computing the corresponding normalized auto-correlation function of the total microscopic electric current defined as[2,3]

$$J(t) = \frac{\langle \mathbf{j}(t) \bullet \mathbf{j}(0) \rangle}{\langle |\mathbf{j}(0)|^2 \rangle} \quad , \quad (4.22)$$

where

$$\mathbf{j}(t) = \sum_{\alpha} \sum_{i}^{N_\alpha} Z_\alpha \, \mathbf{v}_{i\alpha}(t) \quad . \quad (4.23)$$

The frequency-dependent (AC) conductivity can be related to J(ω) as

$$\sigma(\omega) = \frac{\omega_p{}^2}{4\pi} J(\omega) \quad , \quad (4.24)$$

where

$$J(\omega) = \int_0^\infty dt \, J(t) \exp(-i\omega t) \quad , \quad (4.25)$$

and

$$\omega_p{}^2 = \omega_{pe}{}^2 + \omega_{pi}{}^2 \quad . \quad (4.26)$$

Especially for the case of ω=0, Eq. (4.24) means the frequency independent (DC) conductivity. And σ is normalized as follows.

$$\sigma^* = \sigma / \omega_{pe} \quad . \quad (4.27)$$

The DC conductivity can be also estimated by statistical model[5]. The

electric resistivity ρ stemming from scattering of the electric current by the random potential fields produced by the ions is expressed as

$$\rho = 4\left(\frac{2\pi}{3}\right)^{1/2} \frac{\Gamma^{3/2}}{Z^{3/2}} \frac{1}{\omega_{pe}} L_E \quad , \quad (4.28)$$

L_E is the generalized Coulomb logarithm defined by[5]

$$L_E = \frac{3\sqrt{\pi}\,\theta^{3/2}}{4} \int_0^\infty \frac{dk}{k} f(k/2) \frac{S_{ii}(k)}{|\varepsilon_e(k)|^2} \quad , \quad (4.29)$$

where f is the Fermi distribution function defined by Eq. (3.15), S_{ii} is the ion structure factor defined by Eq. (3.9) and ε_e is the electric dielectric function defined by

$$\varepsilon_e(k) = 1 + (1 - G_{ee}(k)) \frac{4me^2}{\pi\hbar^2 k^3} \int_0^\infty dq\, q\, f(q) \ln\left|\frac{2q + k}{2q - k}\right| \quad , \quad (4.30)$$

where G_{ee} is the electron-electron local field correction function[6] and discussed in Chap. VI in detail. Using the relation of σ to ρ

$$\sigma = 1/\rho \quad , \quad (4.31)$$

the conductivity is obtained from Eqs. (4.28)-(4.31).

Figure 4.3 shows the auto-correlation functions of total electric current of the plasma Z=6, Γ=1 and θ=5. The horizontal axis represents the time normalized by ω_{pe}^{-1}. As shown in Fig 4.3, the auto-correlation function decreases exponentially at the same time scale as the velocity auto-correlation functions of electron. The electric current is dominant for the total electric current.

Figure 4.4 shows the frequency dependence of the electric conductivity of the plasma Z=6, Γ=1 and θ=5. The horizontal axis represents the frequency normalized by the electron plasma frequency ω_{pe}. The solid line represents the real part of the electric conductivity and the dashed line represents the imaginary part of the electric conductivity. As the frequency increases, the electric conductivity decreases rapidly. Note that the real part of the electric conductivity is finite and the imaginary part of the electric conductivity is zero at ω=0. This means that the plasma is good conductor against the DC current.

Estimated are the DC electric conductivity according to the Eq. (4.25) and the statistical model mentioned above as a function of Γ with Z=6 and θ=5. The parameters are summarized in table 4.2. Figure 4.5 shows the DC electric conductivities normalized by ω_{pe}. The horizontal axis represents the Coulomb coupling constant for ions Γ. The open circle means the DC electric conductivities obtained by the simulations and the open triangle means the DC electric conductivities obtained by the statistical model. The dashed lines show the Γ dependence of the DC electric conductivities obtained by the simulations and the statistical model. As shown in Fig. 4.5 the normalized DC electric conductivities obtained by the simulations and the statistical model obey the power law of Γ for the range of $0.5 \lesssim \Gamma \lesssim 3$. By the least square method the normalized DC electric conductivities are interpolated as

$$\sigma_s(0) / \omega_{pe} = 1.41 \Gamma^{-0.52} \quad , \quad (4.32)$$

$$\sigma_t(0) / \omega_{pe} = 1.40 \Gamma^{-1.32} \quad , \quad (4.33)$$

where the subscript s denotes the simulation results and t denotes the results

of statistical (theoretical) model. As shown in Fig. 4.5, the Γ dependence of normalized DC conductivities is quit different between simulations and theories. In this theoretical model it is assumed that the electrons are scattered by ions which have a static structure factor $S_{ii}(k)$, namely the dynamical effects are not included. And Eq. (4.29) is correct only the case of $\theta<1$. For this case, $\theta=5$.

Table 4.2

Details of simulation parameters. N_e and N_i are the numbers of electrons and ions used in the simulations respectively. Δ is the size of one mesh in space. Δt is the time step in the numerical integration. For almost all simulations in this table, Z=6, θ=5, N_e=600, N_i=100, $\Delta t\omega_{pe}$=0.05, mesh=8x8x8, the mesh size of P-P area is 6x6x6 and the mass ratio of ion to electron is 600.

Γ	0.5	1.0	2.0	3.0
n_i(cm-3)	2.14×10^{25}	2.67×10^{24}	3.34×10^{23}	9.91×10^{22}
T(keV)	4.65	1.16	0.290	0.129
Δ/λ_{De}	0.468	0.661	0.935	1.145
σ_s^*	2.27	1.14	1.06	0.816
σ_t^*	3.49	1.41	0.564	0.330

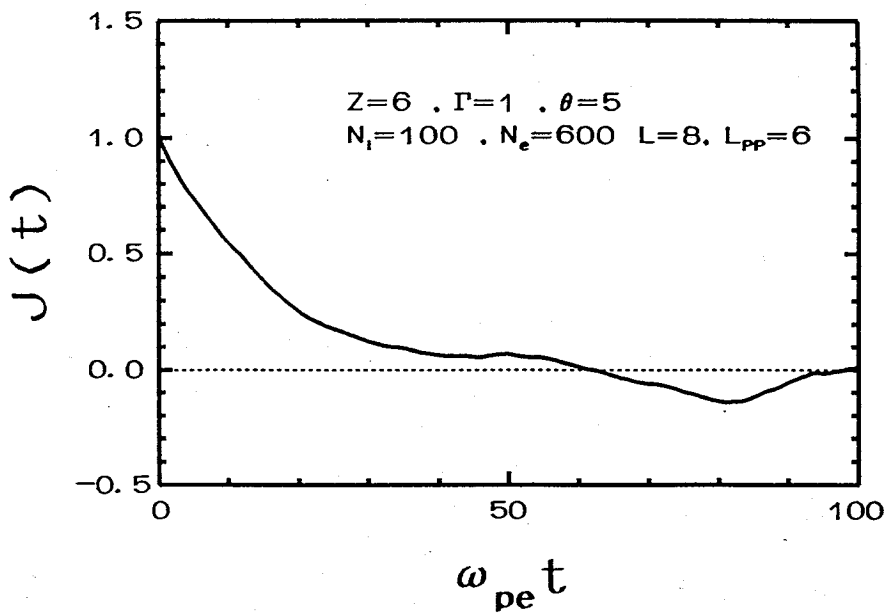

Fig. 4.3 The normalized auto-correlation functions of total electric current of the plasma Z=6, Γ=1 and θ=5. The horizontal axis represents the time normalized by ω_{pe}^{-1}.

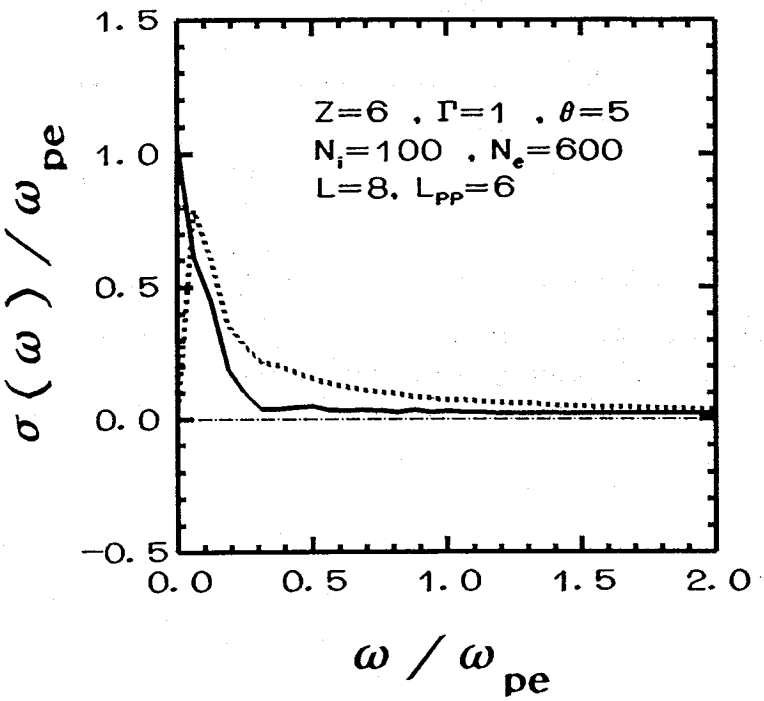

Fig. 4.4 The AC electric conductivities normalized by ω_{pe} of the plasma Z=6, Γ=1 and θ=5. The horizontal axis represents the frequency normalized by ω_{pe}.

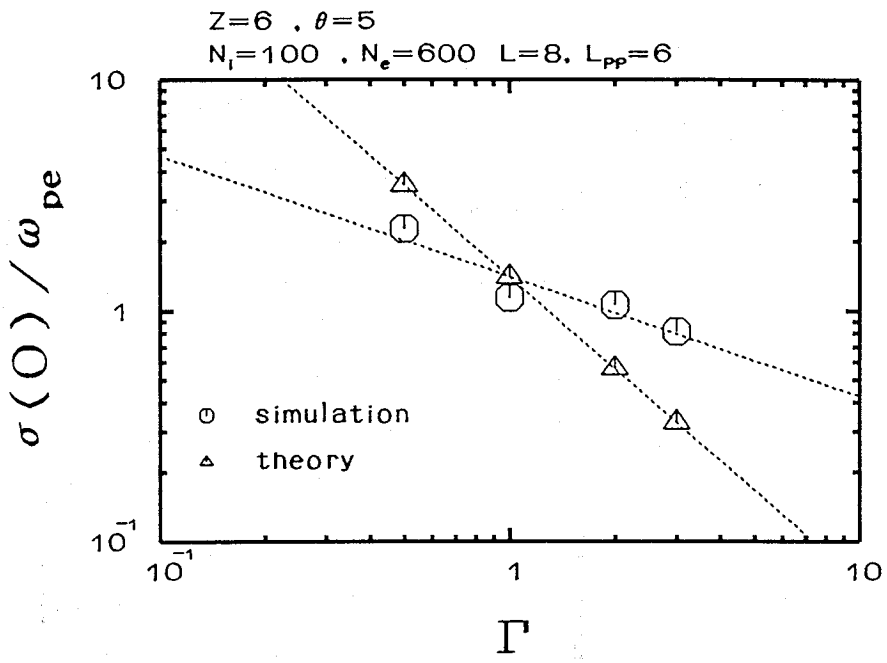

Fig. 4.5 The DC electric conductivities normalized by ω_{pe}. The horizontal axis represents the Coulomb coupling constant for ions Γ. The open circle means the DC electric conductivities obtained by simulations and the open triangle means the DC electric conductivities obtained by statistical model.

IV - 4. SUMMARY

With the use of "SCOPE", the velocity auto-correlation functions (V.A.F.) and auto-correlation functions of total electric current of laser-produced hot, dense plasmas are calculated. The self-diffusion coefficients and the electric conductivities are estimated. The dependence of the self-diffusion coefficients on the Coulomb coupling constant Γ is obtained. For $Z=6$, $\theta=5$, the normalized self-diffusion coefficients of electron are proportional to $\Gamma^{-0.55}$ for the range of $0.5 \lesssim \Gamma \lesssim 3$, and are roughly 0.1 times of that obtained by Spitzer-Härm theory. The normalized self-diffusion coefficients of ion are proportional to $\Gamma^{-0.69}$ for the range of $0.5 \lesssim \Gamma \lesssim 2$. For the range of $\Gamma \gtrsim 2$, the electric shielding effects on the self-diffusion coefficients of ions become strong. The normalized electric conductivities obtained by simulations are proportional to $\Gamma^{-0.52}$ for the range of $0.5 \lesssim \Gamma \lesssim 3$ and its value agrees with that obtained by theoretical model at $\Gamma \sim 1$.

REFERENCES OF CHAPTER IV

1). L. Spitzer and R. Härm, Phys. Rev., **89,** 977 (1953).

2). L. Sjögren, J. P. Hansen and E. L. Pollock, Phys. Rev. A, **24,** 1544 (1981).

3). J. P. Hansen and I. R. McDonald, Phys. Rev. A, **23,** 2041 (1981).

4). 岩波講座, 現代物理学の基礎, 第2版, 5, " 統計物理学 ", pp 219-226, 岩波書店

5). S. Ichimaru and S. Tanaka, Phys. Rev. A **32,** 1790 (1985).

6). S. Ichimaru, S. Mitake, S. Tanaka and Xin-Zhong Yan, Phys. Rev. A **32,** 1768 (1985).

V. Atomic Model for Laser-Produced Hot, Dense Plasmas in the Density Functional Theory

Within the framework of the Density Functional Theory (DFT), the atomic model based on the spherical cell model is developed (Ref. 1, 2). Calculated are the pair distribution functions, and the effective potential acting on an electron and an ion, by solving numerically a set of the coupled modified Poisson - HNC - Schrödinger equations for a range of parameters which are interested in laser fusion. The results are compared with other theoretical models (Ref. 3, 4).

V - 1. INTRODUCTION

For highly compressed plasmas, for an example, the plasma of six hundred times of solid density which has been recently made with the use of a deuterated polystyrene shell target[5] at ILE, the thermal de Broglie wavelength defined by Eq. (2.8) and the electron sphere radius defined by $a_e=(3/4\pi n_e)^{1/3}$ are comparable. It is very important for laser fusion to calculate various thermodynamics functions of plasmas in such a region. In order to investigate such highly compressed plasmas, the quantum effects should be taken into account through the Schrödinger equation, and many body effects are also important because of high density.

To calculate the pair distribution functions and the effective potentials acting on an electron and an ion, an atomic model has been made within the framework of DFT. In the next section, described are the outline of the atomic model.

V - 2. OUTLINE OF ATOMIC MODEL

The spherical cell model[1,2] (SCM) due to Perrot and Dharma-wardana is improved to obtain my atomic model. By the SCM, it is possible to determine various effective pair potentials, pair distribution functions, bound states, and the effective charge of ions $Z^*=Z-N_{be}$, with N_{be} a mean number of bound electrons per ion in a self-consistent manner. In the SCM, the system size should be large enough to represent a physically relevant part of the plasma.

The outline of the calculation is as follows.

1). Using modified T-F model[4], the initial potential of the Schrödinger equation is obtained.

2). Using the initial potential, the Schrödinger equation is solved and the initial electron-ion pair distribution function is calculated.

3). Solving OCP HNC equations, obtained are the initial ion-ion and electron-electron pair distribution functions.

4). Using the pair distribution functions, calculated are the effective potentials.

5). Using the effective potentials calculated are the pair distribution functions.

6). I repeat 4) and 5) until the iteration is converge.

In Fig. 5.1, the schematic diagram of the present atomic model is illustrated.

electron-ion

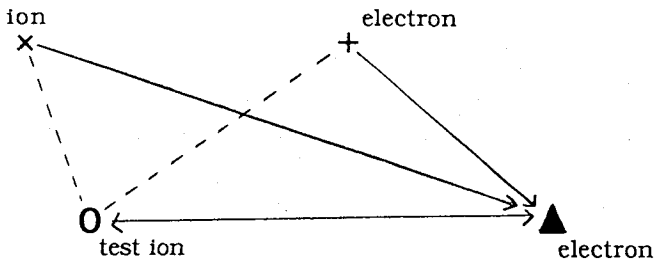

electron-electron

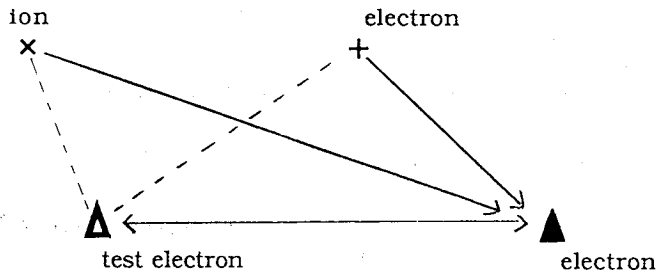

ion-ion

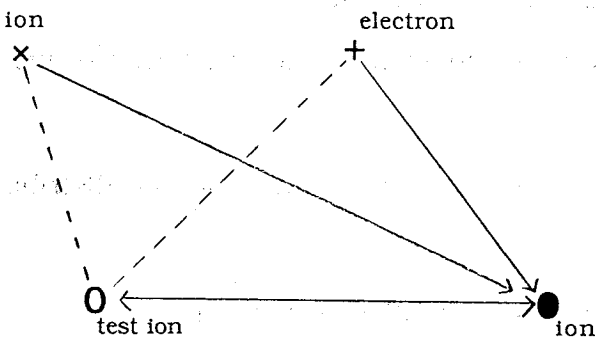

Fig. 5.1 The schematic diagram of the present atomic model.
x and + are the ions and electrons around the test particle.
The allows means the potentials V_{ee}, V_{ei}, V_{ii}.

And the dashed lines are the correlation taking into account.

V - 3. SCHRÖDINGER EQUATION IN HOT, DENSE PLASMAS

The one-electron Schrödinger equation is expressed in atomic unit as

$$\left[-\frac{1}{2}\nabla^2 + V_{ei}(r)\right]\psi(\mathbf{r}) = E\,\psi(\mathbf{r}) \quad , \qquad (5.1)$$

where $V_{ei}(r)$ is the effective potential acting on an electron contributed from a test ion, $\Psi(\mathbf{r})$ is the eigenfunction and E is the eigenvalue. Note that in atomic unit, $\hbar$=e=m_e=1, namely the potential and the eigenvalues are normalized by two times of Rydberg energy (13.6 eV), the distance r is normalized by the Bohr radius defined by

$$a_B = \frac{\hbar^2}{m_e e^2} \quad . \qquad (5.2)$$

Since the effective potential $V_{ei}(r)$ is spherically symmetric, $\Psi(\mathbf{r})$ is expanded into the spherical harmonics $Y_{lm}(\theta,\phi)$ as

$$\psi(\mathbf{r}) = \sum_{l,\,m} R_l(r) Y_{lm}(\theta, \phi) \quad , \qquad (5.3)$$

where l and m are the azimuthal and magnetic quantum numbers, respectively. Writing the radial part $R_{vl}(r)=\chi_{vl}(r)/r$, obtained is

$$-\frac{1}{2}\frac{d^2\chi_{vl}}{dr^2} + \left\{V_{ei}(r) + \frac{l(l+1)}{2r^2}\right\}\chi_{vl} = E\chi_{vl} \quad . \qquad (5.4)$$

Note that the number v means the principal number when the eigenvalue E is negative and means the wave number when the eigenvalue E is positive. To solve this equation, it is transformed into an eigenvalue problem with

appropriate boundary conditions and applied are the finite difference method and shooting method.

V - 3 - 1. WAVE FUNCTIONS FOR BOUND STATES

An electronic state with E<0 is obtained according to the following procedures[6].

1). Find the turning point(s) satisfying the condition,

$$E - \left\{ V_{ei}(r) + \frac{l(l+1)}{2r^2} \right\} = 0 \quad . \quad (5.5)$$

2). Find approximate solution of Eq. (5.4) near r=0,

$$\chi_{nl} \approx r^{l+1} \quad . \quad (5.6)$$

3). Find asymptotic form of χ_{nl} for r->∞,

$$\chi_{nl} \approx \exp(-\sqrt{|2E|}) \quad . \quad (5.7)$$

After the above three procedures for a test value E (<0), Eq. (5.4) is solved numerically for $0<r\leq r_t$ by starting with Eq. (5.6) (this is called inner solution) and $r_t \leq r \leq r_{max}$ by starting with Eq. (5.7) (this is called outer solution), where r_t is the turning point given by Eq. (5.5). And assumed is that at $r=r_t$, $(\chi_{nl}, \chi_{nl}') = (\chi_{nl}^{in}, \chi_{nl}'^{in})$ for the inner solution $= (\chi_{nl}^{out}, \chi_{nl}'^{out})$ for the outer solution, where the dash denotes the derivative with respect to r. These values are functions of the energy eigenvalue E.

The wave functions mentioned above should be normalized as follows.

$$\int_0^{r_{max}} |\chi_{nl}|^2 dr = 1 \quad . \quad (5.8)$$

V - 3 - 2. WAVE FUNCTIONS FOR FREE (SCATTERING) STATES

The wave function for a given E (>0) is obtained according to the following procedures[6].

1). Expand the wave function into a series of partial waves

$$\Psi_k(\mathbf{r}) = \sum_{l=0}^{\infty} (2l+1)\, i^l R_{kl}(r)\, P_l(\cos\theta) \quad . \quad (5.9)$$

where $P_l(\cos\theta)$ is Legendre polynomial and k is the wavenumber.

2). Find the outer solution defined in $r>r_{max}$ by assuming the asymptotic solution as

$$\Psi_k(\mathbf{r}) \xrightarrow[r\to\infty]{} e^{i\mathbf{k}\cdot\mathbf{r}} \quad , \quad (5.10)$$

and by using the following relation

$$e^{i\mathbf{k}\cdot\mathbf{r}} = \sum_{l=0}^{\infty} (2l+1)\, i^l j_l(kr)\, P_l(\cos\theta) \quad , \quad (5.11)$$

where j_l is the spherical Bessel function, and found is the outer solution as

$$R_{kl}(r) \xrightarrow[r\to\infty]{} \frac{\sin\left(kr - \frac{\pi}{2}l + \delta_l(k)\right)}{kr} \quad , \quad (5.12)$$

where $\delta_l(k)$ is the phase shift. Note that the relation

$$j_l(z) \xrightarrow[r\to\infty]{} \frac{\sin\left(z - \frac{\pi}{2}l\right)}{z} \quad . \quad (5.13)$$

3). Find the inner solution by integrating Eq. (5.4) with the starting form of

$$R_{kl}(r)\,(=R_{kl}(r)^{in}) = A\frac{\chi_{kl}(r)}{r} \quad . \qquad (5.14)$$

4). Smooth connection of the inner solution and outer solution at $r=r_{max}$, and determined are A and $\delta_l(k)$.

The free state wave functions should also satisfy the normalization condition Eq. (5.8).

V - 3 - 3. ELECTRON NUMBER DENSITY AROUND A TEST ION

The elementary quantum theory tells us that the local electron density around a test ion can be written as

$$n_{ei}(r) = \bar{n}_e + n_b(r) + \Delta n_f(r) \quad , \qquad (5.15)$$

with

$$n_b(r) = \sum_{n,l}(2l+1)\left|R_{nl}(r)Y_{l,0}(\theta,\phi)\right|^2 f(E_{n,l}) \quad , \qquad (5.16)$$

and

$$\Delta n_f(r) = \frac{1}{\pi^2}\int_0^\infty dk\,k^2 f(k)\sum_l(2l+1)\left[R_{kl}{}^2(r) - R_{kl}{}^{(0)^2}(r)\right] \quad , \qquad (5.17)$$

where $\bar{n}_e=<Z>\bar{n}_i$ is the average electron number density, $n_b(r)$ is the bound electron number density and $\Delta n_f(r)$ is the displaced free electron number density in atomic unit. Since the magnetic effects are not included in this model, in the spherical harmonics Y_{lm} the magnetic number m is always zero and the factor $2l+1$ originates in the summation about the magnetic number m. Note that in atomic unit the number densities are normalized by a_B^{-3}, namely

$$\bar{n}_e^{\,a.u} = \bar{n}_e^{\,cgs}\, a_B^{\,3} \quad . \quad (5.18)$$

In Eq. (5.17) the $R_{kl}(0)$ is the solution of Eq. (5.4) when $V_{ei}(r)=0$, and are compensate R_{kl} in the asymptotic region and rapid convergence of l-sum.

The self-consistency of whole calculation can be tested by the finite-temperature version of Friedel sum rule[1,2]

$$Z = N_{be} + \frac{2}{\pi}\int_0^\infty f(k)dk \sum_l (2l+1)\frac{d\delta_l(k)}{dk} \quad . \quad (5.19)$$

An integration by parts gives, with the convention $\delta_l(0)=0$,

$$Z - N_{be} = \frac{2}{\pi k_B T}\int_0^\infty k\, f(k)\,[1-f(k)] \sum_l (2l+1)\delta_l(k)dk \quad . \quad (5.20)$$

The r_{max} should be determined satisfying the condition of Eq. (5.19) or Eq. (5.20).

The total electron-ion pair distribution function is given by

$$g_{ei}(r) = n_{ei}(r) \,/\, \bar{n}_e \quad . \quad (5.21)$$

The bound electron-ion pair distribution function is given by

$$g_{be-i}(r) = n_b(r) \,/\, \bar{n}_e \quad . \quad (5.22)$$

And the free electron-ion pair distribution function is given by

$$g_{fe-i}(r) = n_f(r) \,/\, \bar{n}_e \quad , \quad (5.23)$$

where

$$n_f(r) = \bar{n}_e + \Delta n_f(r) \quad . \quad (5.24)$$

The electron-ion pair correlation function $h_{ei}(r)$ is related to the total electron-ion pair distribution function as

$$h_{ei}(r) = g_{ei}(r) - 1 \quad . \quad (5.25)$$

V - 4. EFFECTIVE POTENTIAL AND HYPERNETTED-CHAIN APPROXIMATION

The effective potentials $V_{ei}(r)$, $V_{ii}(r)$ and $V_{ee}(r)$ are determined as follows[7].

$$-\beta V_{ei}(r) = \beta\frac{Ze^2}{r} + h_{ei}(r) - c_{ei}(r) \quad , \quad (5.26)$$

$$-\beta V_{ii}(r) = -\beta\frac{Z^2e^2}{r} + h_{ii}(r) - c_{ii}(r) \quad , \quad (5.27)$$

$$-\beta V_{ee}(r) = -\beta\frac{e^2}{r} + h_{ee}(r) - c_{ee}(r) \quad , \quad (5.28)$$

where $\beta=1/k_BT$, $h_{\mu\nu}$ is the pair correlation function, $c_{\mu\nu}$ is the direct correlation function and the suffix $\mu\nu$ denotes μ-type particle around ν-type particle. Within the hypernetted-chain (HNC) approximation, $h_{\mu\nu}$ and $c_{\mu\nu}$ satisfy the Ornstein-Zernik relation for a multi-component plasma

$$\hat{h}_{\mu\nu}(k) - \hat{c}_{\mu\nu}(k) = \sum_{\gamma} \bar{n}_{\gamma}\, \hat{c}_{\mu\gamma}(k)\, \hat{h}_{\gamma\nu}(k) \quad , \quad (5.29)$$

where the hat mark means the Fourier-transform. For entirely classical electron and ion systems Eq. (5.29) is applicable, however, in the quantum region Eq. (5.29) is not applicable. According to Chihara's analysis of metallic hydrogen[7,8], the e-i part of Eq. (5.29) is given by

$$-\beta\frac{\bar{n}_e}{\chi_e{}^0(k)}\,\hat{h}_{ei}(k) - \hat{c}_{ei}(k) = \sum_{\gamma} \bar{n}_{\gamma}\, \hat{c}_{e\gamma}(k)\, \hat{h}_{\gamma i}(k) \quad , \quad (5.30)$$

where $\chi_e{}^0(k)$ is the Fourier-transform of non-interacting density response

function of the homogeneous electron gas defined by

$$\chi_e^{(0)}(k) = -\frac{\bar{n}_e}{k_B T}\frac{3\theta}{4K}\int_0^\infty dx \frac{x}{1+\exp\{(x^2-M)/\theta\}} \ln\left|\frac{2x+K}{2x-K}\right|^2 \quad , \quad (5.31)$$

where

$$K = \frac{k}{(3\pi^2\bar{n}_e)^{1/3}} \quad . \quad (5.32)$$

The dimensionless chemical potential M in Eqs. (5.31) is to be determined through a numerical solution of the equation

$$\frac{1}{3} = \int_0^\infty dx \frac{x^2}{1+\exp\{(x^2-M)/\theta\}} \quad . \quad (5.33)$$

In the same way, the ion-electron part should be change. Chihara calls it a "quantal-hypernetted-chain" (QHNC) approximation. In the classical limit[9], $\chi_e^0(k) \sim -\beta n_e$ and Eq. (5.30) reduces Eq. (5.29).

The ion-ion pair correlation function $h_{ii}(r)$ is related to the ion-ion pair distribution function $g_{ii}(r)$ as

$$h_{ii}(r) = g_{ii}(r) - 1 \quad . \quad (5.34)$$

The ion-ion pair distribution function $g_{ii}(r)$ is calculated using $V_{ii}(r)$ as

$$g_{ii}(r) = \exp\{-\beta V_{ii}(r)\} \quad . \quad (5.35)$$

In the same way, $h_{ee}(r)$ is related to $g_{ee}(r)$ as

$$h_{ee}(r) = g_{ee}(r) - 1 \quad . \quad (5.36)$$

The electron-electron pair distribution function $g_{ee}(r)$ is calculated using $V_{ee}(r)$ as

$$g_{ee}(r) = n_{ee}(r) / \bar{n}_e \quad , \quad (5.37)$$

$$n_{ee}(r) = \int \frac{2d\mathbf{k}}{(2\pi)^3} f_{ee}(k) \quad , \quad (5.38)$$

and

$$f_{ee}(k) = \frac{1}{1 + \exp \dfrac{(\hbar k)^2 / 2m + V_{ee}(r) - \mu}{k_B T}} \quad , \quad (5.39)$$

where μ is chemical potential.

V - 5. RESULTS AND DISCUSSIONS

The pair distribution functions are obtained by the atomic model. For the first case, the parameters are Z=1, r_s=1 and T=25eV (Γ=1.088, θ=0.4989 and n_i=1.611x10^{24} cm^{-3}). r_s is defined as

$$r_s = \frac{a_e}{a_B} \quad . \quad (5.40)$$

Figure 5.2 shows the electron-electron pair distribution functions. The horizontal axis represents the distance normalized by the electron sphere radius a_e. The solid line shows the electron-electron pair distribution function obtained by presented model using the classical HNC equation, and the dashed line shows that by S. Ichimaru et al[3] by the approximation of classical electron one component plasma. The solid line is enhanced compared with the dashed line, because in the Ichimaru model the degeneracy effects and ion correlation effects are not included.

Figure 5.3 shows the ion-ion pair distribution functions. The horizontal axis represents the distance normalized by the ion sphere radius a. The solid line shows the ion-ion pair distribution function obtained by presented model using the classical HNC equation, the solid-dashed line shows that by Eqs. (3.23)-(3.26) (by the approximation of ion one component plasma with linear electron shielding), and the dashed line shows that by the approximation of ion one component plasma with no electric shielding. As shown in Fig. 5.3, it becomes easy to close the ions each other compared with the case of no electric shielding, but the linear response shielding is slightly over-estimation.

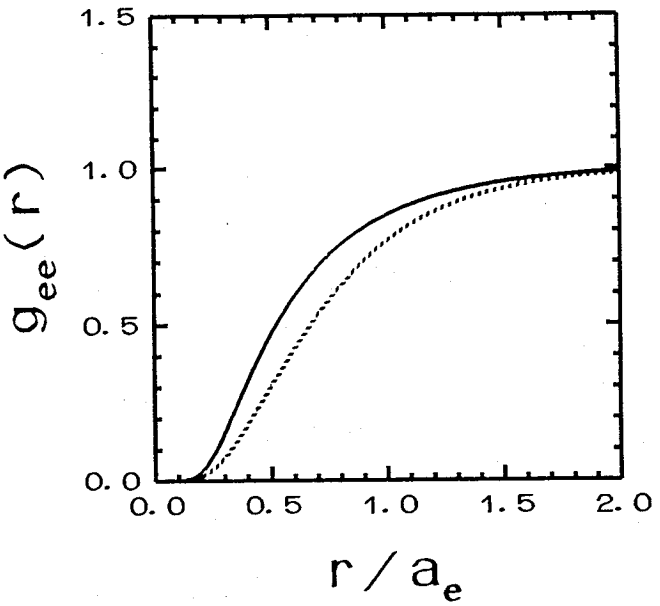

Fig. 5.2 The electron-electron pair distribution functions for the case of Z=1, r_s=1,T=25eV. The horizontal axis represents the distance normalized by the electron sphere radius a_e. The solid line shows that obtained by using the classical HNC , and the dashed line shows that by classical electron OCP.

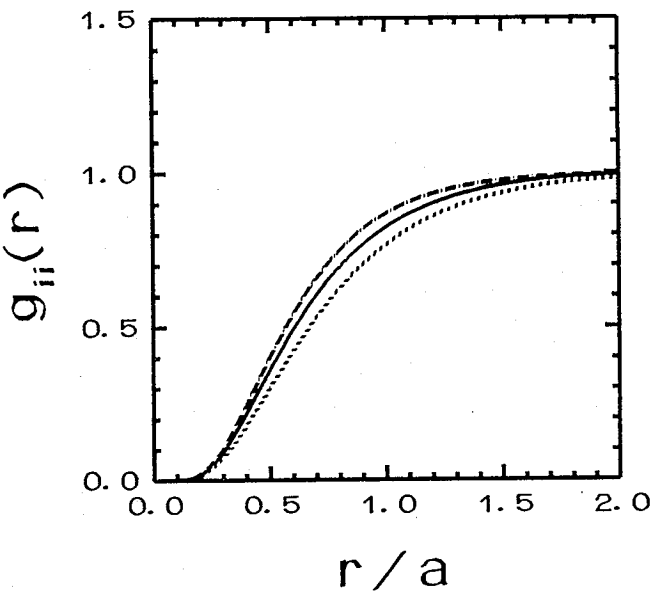

Fig. 5.3 The ion-ion pair distribution functions for the case of Z=1, r_s=1, T=25eV. The horizontal axis represents the distance normalized by the ion sphere radius a_e.

The solid line shows the ion-ion pair distribution function obtained by presented model using the classical HNC equation, the solid-dashed line shows that by Eqs. (3.23)-(3.26) , and the dashed line shows that by the approximation of ion one component plasma with no electric shielding.

Figure 5.4 shows the electron-ion pair distribution functions. The horizontal axis represents the distance normalized by the ion sphere radius a. The solid line shows the electron-ion pair distribution function obtained by presented model using the classical HNC equation, and the dashed line shows the result of Eqs. (3.27)-(3.30) with replacing Z^* by Z. As shown in Fig. 5.4, the solid line is reduced compared with the dashed line because of the quantum diffraction effects in the Schrödinger equation and the value at r=0 is finite. Note that for the first case there is no bound state, namely $Z^*=1$, because of the pressure ionization effects.

For the second case, the parameters are Z=1, $r_s=2$ and T=25eV ($\Gamma=0.5442$, $\theta=1.996$ and $n_i=2.014\times10^{23}$ cm^{-3}). Figure 5.5 represents the electron-electron pair distribution functions. The horizontal axis represents the distance normalized by the electron sphere radius a_e. The solid line shows the electron-electron pair distribution function obtained using the QHNC equation, the solid-dashed line shows that obtained using the classical HNC equation and the dashed line shows obtained by the classical electron one component plasma. Because of the quantum diffraction effects in the QHNC equation, it becomes easy to close the electrons each other compared with that the case of the classical HNC equation.

Figure 5.6 represents the ion-ion pair distribution functions. The horizontal axis and the three types of lines mean as same as in Fig. 5.3. Note that there is almost no difference between the ion-ion pair distribution function with QHNC equation and that with classical HNC equation. Because Γ is smaller than that of the first case, the solid-dashed line becomes close to the solid line compared with the first case.

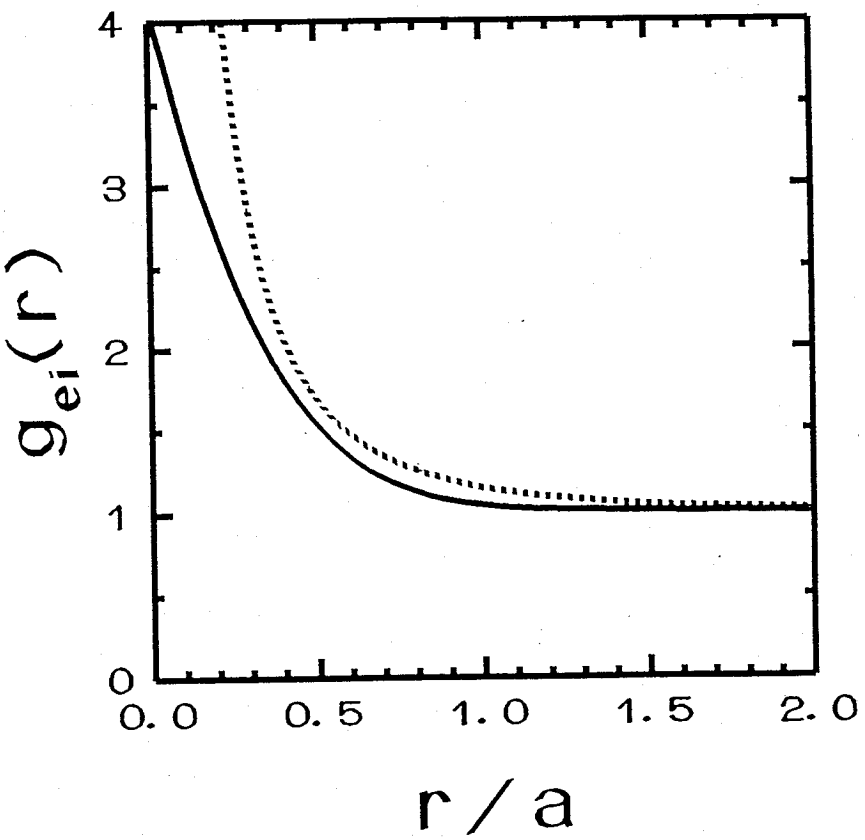

Fig. 5.4 The electron-ion pair distribution functions for the case of Z=1, r_s=1, T=25eV. The horizontal axis represents the distance normalized by the ion sphere radius a_e. The solid line represents the result of the present model in which the classical HNC is used, and the dashed line represents the result of the modified T-F.

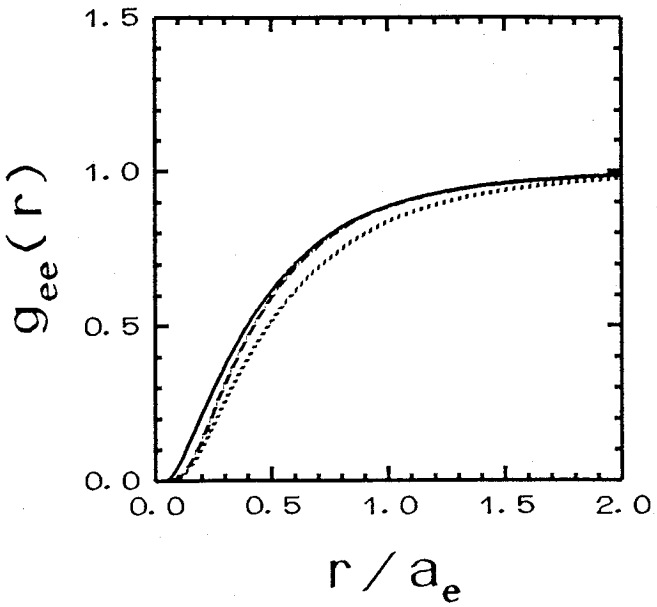

Fig. 5.5 The electron-electron pair distribution functions for the case of Z=1, r_s=2,T=25eV. The horizontal axis and three types of lines represent the same as in Fig. 5.2.

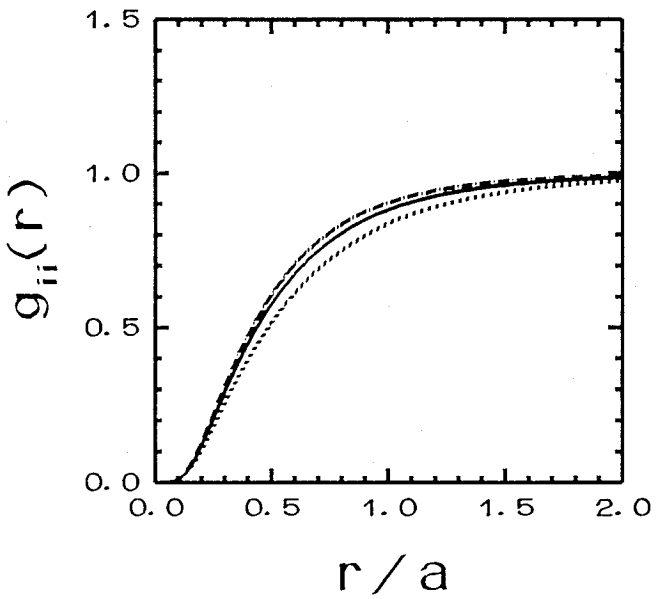

Fig. 5.6 The ion-ion pair distribution functions for the case of Z=1, r_s=2, T=25eV. The horizontal axis and three types of lines represent the same as in Fig. 5.3.

Figure 5.7 represents the electron-ion pair distribution functions using the classical HNC equation. The solid line represents the total electron-ion pair distribution function, the solid-dashed line represents the free electron-ion pair distribution function, and the dashed line represents the bound electron-ion pair distribution function. Because of the low electron number density compared with the first case, the pressure ionization effects become weak, therefore the bound state exists. Note that only 1s state exists for the second case. The effective ionization state Z^* is estimated to be approximately 0.762 and the energy of the 1s state is calculated to be about -5.89×10^{-2} in atomic unit.

Figure 5.8 represents the electron-ion pair distribution functions using the QHNC equation. Three types of lines represent the same as in Fig 5.7. The values of the electron-ion pair distribution functions are reduced compared with using classical HNC equation because of the quantum diffraction effects in the QHNC equation. The effective ionization state Z^* is estimated to be approximately 0.773 and the energy of the 1s state is calculated to be about -1.304×10^{-4} in atomic unit.

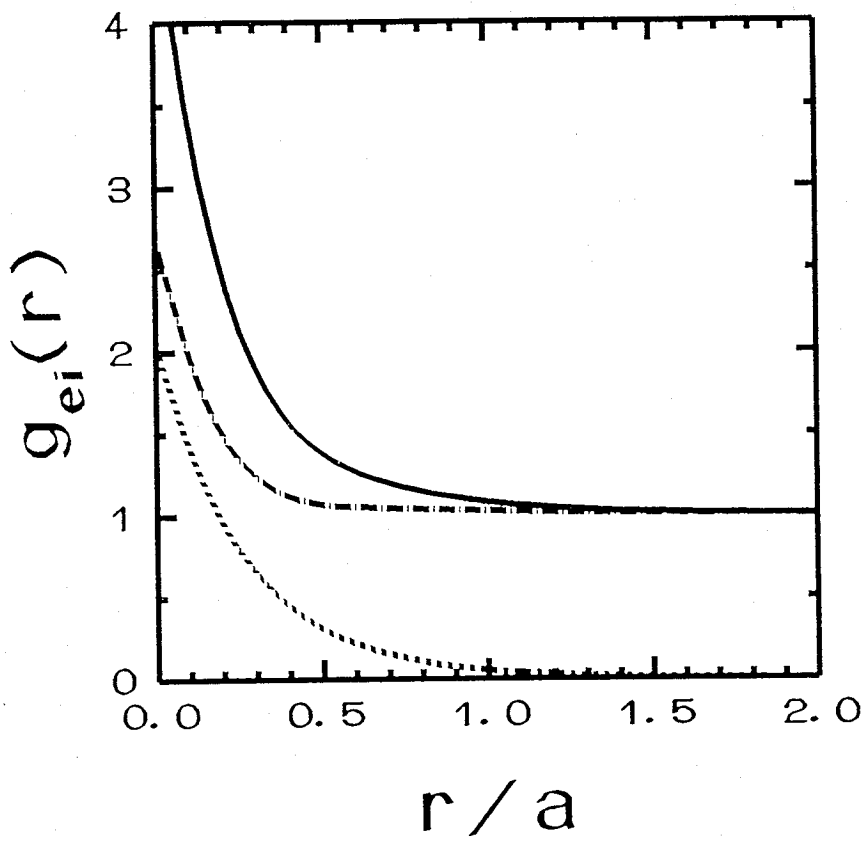

Fig. 5.7 The electron-ion pair distribution functions using the classical HNC.
The solid line represents that of the total electron, the solid-dashed line represents that of the free electron, and the dashed line represents that of the bound electron.

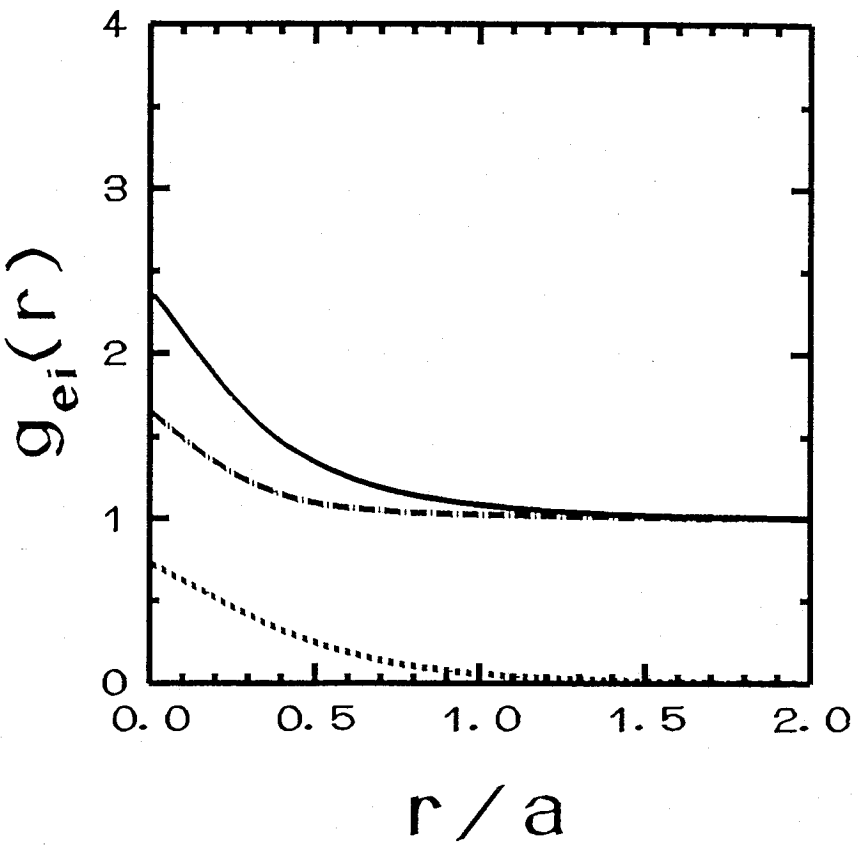

Fig. 5.8 The electron-ion pair distribution functions using the QHNC. The three types of lines represent the same as in Fig. 5.7.

V - 6. SUMMARY

The spherical cell model (SCM) due to Perrot and Dharma-wardana is improved in the calculation of the electron-electron correlation by extending from the Debye-Hückel model to the HNC framework with taking the degeneracy effect into account. Calculated are the pair distribution functions, the effective potential acting on an electron and an ion, by solving numerically a set of the coupled modified Poisson - HNC - Schrödinger equations for a range of parameters which are interested in laser fusion.

The differences appeared in the various pair distribution functions between the improved SCM and the previous works are summarized as follows. The electron-electron pair distribution function is slightly large in the region $r<1.5a_e$ compared with that by S. Ichimaru et al, because in the Ichimaru model the degeneracy effects and ion correlation effects are not included. On the other hand, the electron linear response shielding in the calculation of the ion-ion pair distribution function is found to be slightly over-estimated. The electron-ion pair distribution function is very small near the origin, $r<0.2a$, compared with that by the modified T-F model, because the quantum diffraction effects are automatically included in the Schrödinger equation. The value of the e-i pair distribution function at r=0 is finite in the improved SCM model.

The ionization states for the two cases, $n_i=1.6\times10^{24}\,cm^{-3}$ ($r_s=1$), T=25eV and $n_i=2\times10^{23}\,cm^{-3}$ ($r_s=2$), T=25eV, are compared. For the first case , $r_s=1$, there is no bound state, namely $Z^*=1$, because of the pressure ionization effects. For the second case because of the relatively low number density

compared with the first case, the pressure ionization effects become weak, therefore the bound state (1s state) exists. The effective ionization state Z^* using the HNC equation is estimated to be approximately 0.762 and the energy of the 1s state is calculated to be about - 5.89×10^{-2} in atomic unit.

The differences of quantal HNC and the classical HNC appears in the pair distribution functions, especially, the electron-ion pair distribution function. The e-i pair distribution function by QHNC is small near the origin because of the quantum diffraction effects.

REFERENCES OF CHAPTER V

1). F. Perrot, Phys. Rev. A **25,** 489 (1982).

2). M. W. C. Dharma-wardana and F. Perrot, Phys. Rev. A **26,** 2096 (1982).

3). S. Ichimaru, S. Mitake, S. Tanaka and Xin-Zhong Yan, Phys. Rev. A **32,** 1768 (1985).

4). R. Kawakami, K. Mima, H. Totsuji and Y. Yokoyama, Phys. Rev. A **38,** 3618 (1988).

5). S. Nakai, Bull. Am. Phys. Soc, **34,** 2040 (1989).

6). For example; L. I. Schiff, "Quantum Mechanics, Third Edition" (McGraw Hill, Inc., 1968).

7). F. Perrot, Y. Furutani and M. W. C. Dharma-wardana, Phys. Rev. A **41,** 1096 (1990).

8). J. Chihara, Phys. Rev. A **33,** 2575 (1986).

9). A. K. Fetter and J. D. Walecka, "Quantum Theory of Many-Particle Systems" (McGraw Hill, New York, 1971).

VI. Application of Atomic Model to Laser-Produced Hot, Dense Plasmas I

~ Stopping power of charged particles in laser-produced hot, dense plasmas ~

With the use of the atomic model, the stopping power of the charged particles is estimated. The stopping power can be calculated using the dielectric function $\varepsilon(k,\omega)$. The dielectric function $\varepsilon(k,\omega)$ of a highly compressed plasma can be calculated using the local field correction theory (Ref. 1). In the dielectric function $\varepsilon(k,\omega)$ obtained by presented model, the strong coupling effects, the electric shielding effects, Fermi degeneracy effects and quantum diffraction effects are included. The stopping numbers obtained by presented model are compared with those by some other theoretical models. In Ref. 1 the electron-ion local field correction function $G_{ei}(k,\omega)$ is assumed to be zero because it is very difficult to calculate electron-ion local field correction function in their frame work. The static electron-ion local field correction function $G_{ei}(k,\omega)$ is estimated using the atomic model mentioned the previous chapter in this paper. The stopping power obtained by presented model is about 1.05 times greater than that obtained by Xin-Zhong Yan et al (Ref. 2) for the plasma $Z=1$, $r_s=1$ and $T=25eV$.

VI - 1. INTRODUCTION

Recently the various physical values can be observed by using the charged particles made by fusion reaction experimentally. The energy spectra of the charged particle made by fusion reaction should be estimated correctly in order to obtain the correct physical values which characterize the highly compressed fusion plasmas experimentally. The charged particles lose the energy by collisions. The loss rate of the particle energy per unit length is called stopping power. The correct stopping power is required for the estimation of the plasma self-heating by the charged particles and the product of the mass density ρ and the core radius R[3,4].

The stopping power can be calculated using the dielectric function $\varepsilon(k,\omega)$. In the next section, connected are the stopping power and the dielectric function $\varepsilon(k,\omega)$. The dielectric function $\varepsilon(k,\omega)$ of such a highly compressed plasma can be calculated using the local field correction (LFC) theory[1]. In the section VI - 3, surveyed is the local field correction theory. In Ref. 1 the electron-ion local field correction function $G_{ei}(k,\omega)$ is assumed to be zero because it is very difficult to calculate the electron-ion local field correction function in their frame work. The static electron-ion local field correction function $G_{ei}(k,\omega)$ is estimated using the atomic model. In the section VI - 4, derived are the static local field correction functions especially the static electron-ion local field correction function $G_{ei}(k,\omega)$. In the section VI - 5, described are the high and low velocity limit of the stopping number and the ion effects on the stopping number. In the section VI - 6, described

are the effects of the local field correction functions on stopping number. And my results are compared with the results obtained by the model in Ref. 1, 2. In the section V - 7, I summarize this chapter.

VI - 2. FORMULATION OF STOPPING POWER

First, described is the formulation of stopping power in hot, dense plasmas. A charged particle is assumed moving with the constant velocity in a hot, dense plasma. The external charge density ρ_{ext} is given by

$$\rho_{ext}(\mathbf{r}, t) = q_0 \delta(\mathbf{r} - \mathbf{v}t) \quad , \quad (6.1)$$

where q_0 is the charge of the test particle and δ is delta function. And the Fourier component of $\rho_{ext}(\mathbf{r},t)$ is given by

$$\hat{\rho}_{ext}(\mathbf{k}, \omega) = 2\pi q_0 \delta(\omega - \mathbf{k} \bullet \mathbf{v}) \quad . \quad (6.2)$$

The dielectric function $\varepsilon(\mathbf{k},\omega)$ is related to the charge density as

$$\hat{\rho}_{ext}(\mathbf{k}, \omega) + \hat{\rho}_{ind}(\mathbf{k}, \omega) = \frac{\hat{\rho}_{ext}(\mathbf{k}, \omega)}{\varepsilon(\mathbf{k}, \omega)} \quad , \quad (6.3)$$

where $\hat{\rho}_{ind}(\mathbf{k},\omega)$ is the induced charge density in the plasma. From Eq. (6.2) and (6.3), $\hat{\rho}_{ind}(\mathbf{k},\omega)$ is calculated as

$$\hat{\rho}_{ind}(\mathbf{k}, \omega) = -2\pi q_0 \left(1 - \frac{1}{\varepsilon(\mathbf{k}, \omega)}\right) \delta(\omega - \mathbf{k} \bullet \mathbf{v}) \quad . \quad (6.4)$$

The induced potential ϕ_{ind} is given by Poisson equation and Eq. (6.4) as

$$\hat{\phi}_{ind}(\mathbf{k}, \omega) = -\frac{8\pi^2 q_0}{k^2} \left(1 - \frac{1}{\varepsilon(\mathbf{k}, \omega)}\right) \delta(\omega - \mathbf{k} \bullet \mathbf{v}) \quad . \quad (6.5)$$

Using Eq. (6.5) the induced electric field $E_{ind}(\mathbf{r},t)$ is given as

$$\mathbf{E}_{ind}(\mathbf{r},t) = \frac{1}{(2\pi)^3}\int d\mathbf{k}\, i\mathbf{k}\,\frac{4\pi q_0}{k^2}\left(1-\frac{1}{\varepsilon(\mathbf{k},\mathbf{k}\cdot\mathbf{v})}\right)\exp\{i\,\mathbf{k}\cdot(\mathbf{r}-\mathbf{v}t)\} \quad . \quad (6.6)$$

The force which the charged particle feels is described as

$$\mathbf{F} = q_0\mathbf{E}_{ind}(\mathbf{r},t)$$
$$= \frac{1}{(2\pi)^3}\int d\mathbf{k}\, i\mathbf{k}\,\frac{4\pi q_0^{\,2}}{k^2}\left(1-\frac{1}{\varepsilon(\mathbf{k},\mathbf{k}\cdot\mathbf{v})}\right) \quad . \quad (6.7)$$

The stopping power is obtained with the aid of Eq. (6.7) as

$$\frac{dw}{ds} = \frac{Z_0^{\,2}e^2}{2\pi^2 v}\int d\mathbf{k}\;\frac{\mathbf{k}\cdot\mathbf{v}}{k^2}\;\mathrm{Im}\,\frac{1}{\varepsilon(\mathbf{k},\mathbf{k}\cdot\mathbf{v})} \quad , \quad (6.8)$$

where Z_0 is the atomic number of the charged particle. If the dielectric function ε is given, the stopping power can be obtained.

The non-dimensional value L is introduced as follows.

$$\frac{dw}{ds} = -\frac{4\pi\bar{n}_e Z_0^{\,2}e^4}{m_e v^2}L \quad . \quad (6.9)$$

This value L is called stopping number. Stopping number L is described as

$$L = -\frac{1}{(2\pi)^3}\frac{m_e v}{\bar{n}_e e^2}\int d\mathbf{k}\;\frac{\mathbf{k}\cdot\mathbf{v}}{k^2}\;\mathrm{Im}\,\frac{1}{\varepsilon(\mathbf{k},\mathbf{k}\cdot\mathbf{v})} \quad . \quad (6.10)$$

IV - 3. LOCAL FIELD CORRECTION THEOREM

The dielectric function $\varepsilon(k,\omega)$ in hot, dense plasmas can be calculated by the local field correction (LFC) theorem[1]. Assumed is a fictitious external potential field $V_\mu(r,t)$ which couples only to the density field $\rho_\mu(\mathbf{r},t)$ of the μ-species particles. By using $V_\mu(\mathbf{r},t)$ and $\rho_\mu(\mathbf{r},t)$ the density-density response functions $\chi_{\mu\nu}(k,\omega)$ between the μ and ν species particles is defined as follows.

$$\delta\hat{\rho}_\mu(\mathbf{k},\omega) = \sum_\nu \chi_{\mu\nu}(k,\omega)\hat{V}'_\nu(\mathbf{k},\omega) \quad , \quad (6.11)$$

where $\delta\hat{\rho}_\mu(\mathbf{k},\omega)$ is the Fourier component of the displacement of the density field $\rho_\mu(\mathbf{r},t)$ from the unperturbed values and $V_\mu(\mathbf{k},\omega)$ is the Fourier component of the fictitious external potential field $V_\mu(\mathbf{r},t)$. With the aid of Eq. (6.3), the dielectric function $\varepsilon(k,\omega)$ is given by

$$\frac{1}{\varepsilon(k,\omega)} = 1 + \upsilon(k)\sum_{\mu,\nu} Z_\mu Z_\nu \chi_{\mu\nu}(k,\omega) \quad , \quad (6.12)$$

where $\upsilon(k)=4\pi e^2/k^2$.

The effective potential $\phi_{\mu\nu}(k,\omega)$ on a μ-species particle produced by the density fluctuation $\delta\hat{\rho}_\nu(\mathbf{k},\omega)$ in the ν-species particles may be written as

$$\phi_{\mu\nu}(\mathbf{k},\omega) = Z_\mu Z_\nu \upsilon(k)\{1 - G_{\mu\nu}(k,\omega)\}\delta\hat{\rho}_\nu(\mathbf{k},\omega) \quad . \quad (6.13)$$

This potential generally differs from the bare Coulomb potential because of the microscopic correlation effects involved; the difference is here measured by

the dynamic LFC $G_{\mu\nu}(k,\omega)$. Using the free-particle polarizability function $\chi_\mu^{(0)}(k,\omega)$, a density response of the μ-species particles against a renormalized potential field $\hat{V}_\mu(\mathbf{k},\omega) + \Sigma_\nu \phi_{\mu\nu}(\mathbf{k},\omega)$ in the plasma is described as

$$\delta\hat{\rho}_\mu(\mathbf{k},\omega) = \chi_\mu^{(0)}(k,\omega)\left[\hat{V}_\mu(\mathbf{k},\omega) + v(k)\sum_\nu Z_\mu Z_\nu\{1 - G_{\mu\nu}(k,\omega)\}\delta\hat{\rho}_\nu(\mathbf{k},\omega)\right] \quad . \quad (6.14)$$

The function $\chi_\mu^{(0)}(k,\omega)$ is given by

$$\mathrm{Re}\left[\chi_\mu^{(0)}(k,\omega)\right] = -\frac{\bar{n}_\mu}{k_B T}\frac{3\Theta_\mu}{4K_\mu}\int_0^\infty dx \frac{x}{1+\exp\{(x^2 - M_\mu)/\Theta_\mu\}} \ln\left|\frac{(2K_\mu x + K_\mu^2)^2 - \Omega_\mu^2}{(2K_\mu x - K_\mu^2)^2 - \Omega_\mu^2}\right| \quad , \quad (6.15)$$

and

$$\mathrm{Im}\left[\chi_\mu^{(0)}(k,\omega)\right] = -\frac{\bar{n}_\mu}{k_B T}\frac{3\pi\Theta_\mu^2}{8K_\mu} \ln\left|\frac{1+\exp\left[-\frac{\{(\Omega_\mu + K_\mu^2)/2K_\mu\}^2 - M_\mu}{\Theta_\mu}\right]}{1+\exp\left[-\frac{\{(\Omega_\mu - K_\mu^2)/2K_\mu\}^2 - M_\mu}{\Theta_\mu}\right]}\right| \quad , \quad (6.16)$$

where

$$K_\mu = \frac{k}{(3\pi^2 n_\mu)^{1/3}} \quad , \quad \Omega_\mu = \frac{2m_\mu\omega}{\hbar(3\pi^2 n_\mu)^{2/3}} \quad , \quad \Theta_\mu = \frac{2m_\mu k_B T}{\hbar^2(3\pi^2 n_\mu)^{2/3}} \quad . \quad (6.17)$$

The dimensionless chemical potential M_μ in Eqs. (6.15) and (6.16) is to be determined through a numerical solution of the equation

$$\frac{1}{3} = \int_0^\infty dx \frac{x^2}{1+\exp\{(x^2 - M_\mu)/\Theta_\mu\}} \quad . \quad (6.18)$$

Expression for $\chi_{\mu\nu}(k,\omega)$ may be obtained through a comparison between Eqs. (6.11) and (6.14). For a two-component (electron and ion) plasma, $\chi_{\mu\nu}(k,\omega)$ is written as

$$\chi_{ee} = \chi_e^{(0)}\{1 - Z^2 \upsilon \chi_i^{(0)}(1 - G_{ii})\} / D \quad , \quad (6.19)$$

$$\chi_{ii} = \chi_i^{(0)}\{1 - \upsilon \chi_e^{(0)}(1 - G_{ee})\} / D \quad , \quad (6.20)$$

$$\chi_{ei} = - Z\upsilon \chi_e^{(0)} \chi_i^{(0)}(1 - G_{ei}) / D \quad , \quad (6.21)$$

$$\chi_{ie} = - Z\upsilon \chi_e^{(0)} \chi_i^{(0)}(1 - G_{ie}) / D \quad , \quad (6.22)$$

where

$$D = \{1 - \upsilon \chi_e^{(0)}(1 - G_{ee})\}\{1 - Z^2 \upsilon \chi_i^{(0)}(1 - G_{ii})\} - Z^2 \upsilon^2 \chi_e^{(0)} \chi_i^{(0)}(1 - G_{ei})(1 - G_{ie}) \quad . \quad (6.23)$$

The dielectric function, Eq. (6.12), takes the form

$$\frac{1}{\varepsilon} = 1 + \frac{\upsilon}{D}[\chi_e^{(0)} + Z^2 \chi_i^{(0)} + Z^2 \upsilon \chi_e^{(0)} \chi_i^{(0)}(G_{ee} + G_{ii} - G_{ei} - G_{ie})] \quad . \quad (6.24)$$

In the same way, for a binary-ionic-mixture (BIM) plasma, the $\chi_{\mu\nu}(k,\omega)$ is written as

$$\upsilon D \chi_{ee} = \chi_e\{1 - \chi_1(1 - G_{11})\}\{1 - \chi_2(1 - G_{22})\} - \chi_e \chi_1 \chi_2 (1 - G_{12})(1 - G_{21}) \quad , \quad (6.25)$$

$$- Z_1 \upsilon D \chi_{e1} = \chi_e \chi_1 \chi_2 (1 - G_{e2})(1 - G_{21}) + \chi_e \chi_1 (1 - G_{e1})\{1 - \chi_2(1 - G_{22})\} \quad , \quad (6.26)$$

$$- Z_2 \upsilon D \chi_{e2} = \chi_e \chi_1 \chi_2 (1 - G_{e1})(1 - G_{12}) + \chi_e \chi_2 (1 - G_{e3})\{1 - \chi_1(1 - G_{11})\} \quad , \quad (6.27)$$

$$- Z_1 \upsilon D \chi_{1e} = \chi_e \chi_1 \chi_2 (1 - G_{2e})(1 - G_{12}) + \chi_e \chi_1 (1 - G_{1e})\{1 - \chi_2(1 - G_{22})\} \quad , \quad (6.28)$$

$$Z_1^2 \upsilon D \chi_{11} = \chi_1\{1 - \chi_e(1 - G_{ee})\}\{1 - \chi_2(1 - G_{22})\} - \chi_e \chi_1 \chi_2 (1 - G_{e2})(1 - G_{2e}) \quad , \quad (6.29)$$

$$Z_1 Z_2 \upsilon D\chi_{12} = \chi_e\chi_1\chi_2(1-G_{e2})(1-G_{1e}) + \chi_1\chi_2(1-G_{12})\{1-\chi_e(1-G_{\infty})\} \quad , \quad (6.30)$$

$$-Z_2 \upsilon D\chi_{2e} = \chi_e\chi_1\chi_2(1-G_{1e})(1-G_{21}) + \chi_e\chi_2(1-G_{2e})\{1-\chi_1(1-G_{11})\} \quad , \quad (6.31)$$

$$Z_2 Z_1 \upsilon D\chi_{21} = \chi_e\chi_1\chi_2(1-G_{2e})(1-G_{e1}) + \chi_1\chi_2(1-G_{21})\{1-\chi_e(1-G_{\infty})\} \quad , \quad (6.32)$$

$$Z_2^{\,2} \upsilon D\chi_{22} = \chi_2\{1-\chi_e(1-G_{\infty})\}\{1-\chi_1(1-G_{11})\} - \chi_e\chi_1\chi_2(1-G_{e1})(1-G_{1e}) \quad , \quad (6.33)$$

where

$$\begin{aligned} D = {} & \{1-\chi_e(1-G_{\infty})\}\{1-\chi_1(1-G_{11})\}\{1-\chi_2(1-G_{22})\} \\ & - \chi_e\chi_1\chi_2(1-G_{e1})(1-G_{12})(1-G_{2e}) \\ & - \chi_e\chi_1\chi_2(1-G_{1e})(1-G_{21})(1-G_{e2}) \\ & - \chi_e\chi_2(1-G_{e2})(1-G_{2e})\{1-\chi_1(1-G_{11})\} \\ & - \chi_1\chi_2(1-G_{12})(1-G_{21})\{1-\chi_e(1-G_{\infty})\} \\ & - \chi_e\chi_1(1-G_{e1})(1-G_{1e})\{1-\chi_2(1-G_{22})\} \end{aligned} \quad , \quad (6.34)$$

and

$$\chi_e = \upsilon\chi_e^{(0)} \quad , \quad \chi_1 = Z_1^{\,2}\upsilon\chi_1^{(0)} \quad , \quad \chi_2 = Z_2^{\,2}\upsilon\chi_2^{(0)} \quad , \quad (6.35)$$

where the suffix 1, 2 means the species of ions.

As mentioned above, if $G_{\mu\nu}(k,\omega)$ are given I can obtain the dielectric function $\varepsilon(k,\omega)$. In the next section, the static local field correction functions $G_{\mu\nu}(k,0)$ are derived.

VI - 4. DERIVATION OF STATIC LOCAL FIELD CORRECTION FUNCTIONS

In this section the static local field correction functions[1] are derived for a two-component plasma (TCP, ie, electrons and ions) and a binary-ionic-mixture plasma (BIM, ie, electrons and two species of ions) using HNC approximation and Eqs. (6.13) and (6.14).

For a two-component plasma, the Fourier components of the electron-electron effective potential and the electron-ion effective potential are given with the aid of Eqs. (5.21), (5.23) and (5.24) as

$$\beta \hat{V}_{ee}(k) = \beta \upsilon(k) - \bar{n}_i c_{ei}(k) h_{ie}(k) - \bar{n}_e c_{ee}(k) h_{ee}(k) \quad , \quad (6.36)$$

$$\beta \hat{V}_{ei}(k) = -\beta Z \upsilon(k) - n_i c_{ei}(k) h_{ii}(k) - n_e c_{ee}(k) h_{ei}(k) \quad . \quad (6.37)$$

As the same way, with the use of Eqs. (6.13) and (6.14) the effective potentials mentioned above can be written as follows.

$$\beta \hat{V}_{ee}(k) = \beta \upsilon(k) + \beta \upsilon(k) \{ - Z (1 - G_{ei}(k)) \bar{n}_i h_{ie}(k) + (1 - G_{ee}(k)) \bar{n}_e h_{ee}(k) \} \quad , \quad (6.38)$$

$$\beta \hat{V}_{ei}(k) = -\beta Z \upsilon(k) + \beta \upsilon(k) \{ - Z (1 - G_{ei}(k)) \bar{n}_i h_{ii}(k) + (1 - G_{ee}(k)) \bar{n}_e h_{ei}(k) \} \quad . \quad (6.39)$$

Using Eqs. (6.36)-(6.39), two equations can be introduced as follows.

$$\beta \upsilon(k) \{ - Z (1 - G_{ei}(k)) \bar{n}_i h_{ie}(k) + (1 - G_{ee}(k)) \bar{n}_e h_{ee}(k) \} = - \bar{n}_i c_{ei}(k) h_{ie}(k) - \bar{n}_e c_{ee}(k) h_{ee}(k) \quad , \quad (6.40)$$

$$\beta v(k)\{-Z(1-G_{ei}(k))\bar{n}_i h_{ii}(k) + (1-G_{ee}(k))\bar{n}_e h_{ei}(k)\} = -\bar{n}_i c_{ei}(k) h_{ii}(k) - \bar{n}_e c_{ee}(k) h_{ei}(k) \quad . \quad (6.41)$$

Solving Eqs. (6.40) and (6.41) about G_{ee} and G_{ei}, G_{ee} and G_{ei} are obtained as follows.

$$G_{ee}(k) = 1 + \frac{1}{\beta v(k)} c_{ee}(k) \quad , \quad (6.42)$$

$$G_{ei}(k) = 1 - \frac{1}{\beta Z v(k)} c_{ei}(k) \quad . \quad (6.43)$$

As the same way, G_{ii} and G_{ie} are given as follows.

$$G_{ii}(k) = 1 + \frac{1}{\beta Z^2 v(k)} c_{ii}(k) \quad , \quad (6.44)$$

$$G_{ie}(k) = 1 - \frac{1}{\beta Z v(k)} c_{ie}(k) \quad . \quad (6.45)$$

To author's knowledge, this is the first calculation of the electron-ion local field correction function in plasmas.

Let's demonstrate that in the specific cases the local field correction functions mentioned above conclude the form of Eqs. (32), (44a)-(44c) in Ref. 1. For the case of electron OCP, Ornstein-Zernik relation is written as

$$h_{ee}(k) = c_{ee}(k) + \bar{n}_e c_{ee}(k) h_{ee}(k) \quad . \quad (6.46)$$

By putting Eq. (6.46) into Eq. (6.42), obtained is

$$G_{ee}(k) = 1 + \frac{1}{\beta v(k)} \frac{h_{ee}(k)}{1 + \bar{n}_e h_{ee}(k)} \quad . \quad (6.47)$$

And the structure factor $S_{ee}(k)$ is defined as

$$S_{ee}(k) = 1 + \bar{n}_e h_{ee}(k) \quad . \quad (6.48)$$

Putting Eq. (6.48) into Eq. (6.47), obtained is

$$G_{ee}(k) = 1 + \frac{1}{\beta \bar{n}_e \upsilon(k)} \left(1 - \frac{1}{S_{ee}(k)} \right) \quad . \quad (6.49)$$

Eq. (6.49) is equal to Eq (32) in Ref. 1. As the same way, $G_{ii}(k)$ is calculated as

$$G_{ii}(k) = 1 + \frac{1}{\beta \bar{n}_i Z^2 \upsilon(k)} \left(1 - \frac{1}{S_{ii}(k)} \right) \quad . \quad (6.50)$$

Eq. (6.50) is equal to Eq (44b) in Ref. 1 except the first term of the right hand side. The term $1/\varepsilon_e(k)$ originates in an assumption of the linear response shielding.

If the linear response shielding is assumed, the electron-ion direct correlation function $c_{ei}(k)$ is reduced to $\beta Z \upsilon(k)$[5]. Therefore G_{ei} is zero.

For a binary-ionic-mixture plasma, the local field correction functions can be obtained as follows.

$$G_{ee}(k) = 1 + \frac{1}{\beta \upsilon(k)} c_{ee}(k) \quad , \quad (6.51)$$

$$G_{e1}(k) = 1 - \frac{1}{\beta Z_1 \upsilon(k)} c_{e1}(k) \quad , \quad (6.52)$$

$$G_{e2}(k) = 1 - \frac{1}{\beta Z_2 \upsilon(k)} c_{e2}(k) \quad , \quad (6.53)$$

$$G_{11}(k) = 1 + \frac{1}{\beta Z_1^{\,2} \upsilon(k)} c_{11}(k) \quad , \quad (6.54)$$

$$G_{12}(k) = 1 + \frac{1}{\beta Z_1 Z_2 \upsilon(k)} c_{12}(k) \quad , \quad (6.55)$$

$$G_{22}(k) = 1 + \frac{1}{\beta Z_2^{\,2} \upsilon(k)} c_{22}(k) \quad , \quad (6.56)$$

$$G_{1e}(k) = G_{e1}(k) \quad , \quad (6.57)$$

$$G_{2e}(k) = G_{e2}(k) \quad , \quad (6.58)$$

$$G_{21}(k) = G_{12}(k) \quad . \quad (6.59)$$

VI - 5 . HIGH AND LOW VELOCITY LIMIT AND ION EFFECTS ON STOPPING NUMBER

In the high velocity limit the stopping number of the form of Eq. (6.10) approaches the Bethe-Bloch formula[6-8]

$$L_B = \ln\left(\frac{1.123\, m_e v^2}{\hbar\omega_{pe}}\right) \quad . \quad (6.60)$$

Figure 6.1 shows the stopping numbers of the plasma, Z=1, n_i=3.0X10^{25}cm^{-3}, T=0.3keV. The horizontal axis represents the velocity normalized by the electron thermal velocity. The solid line represents the stopping numbers obtained by the formula mentioned in the previous sections with $G_{\mu\nu}$=0, and the solid-dashed line represents the stopping numbers of the Bethe-Bloch formula. As shown in Fig. 6.1, at high velocity region the solid line approaches the dashed line. At the region of $v \lesssim 0.8 v_{Te}$, L_B is negative and becomes meaningless. Thus the stopping number can be calculated at the low velocity.

In Fig. 6.1, the dashed line represents the stopping number obtained by electron OCP with G_{ee}=0. As shown in Fig. 6.1, at the region of $v \lesssim 0.2 v_{Te}$ the dashed line is quit different from the solid line. This difference originates in the ion effects on the stopping number. At very low velocity the contribution of ions to the stopping number is dominant because of the heavy mass of ions.

As shown in Fig. 6.1, the stopping number obtained by presented formula decreases proportionally to v^3. This fact can be explained as follows. For the small velocity ($v \lesssim v_{Te}$), the dielectric function $\varepsilon(k, \mathbf{k}\cdot\mathbf{v})$ can be expanded keeping the parameter $(\hbar k/2m_e)/v$ to only first order[9]. The imaginary part

of the dielectric function is found to be

$$\mathrm{Im}\,\varepsilon(\mathbf{k}, \mathbf{k}\bullet\mathbf{v}) = \mathbf{k}\bullet\mathbf{v}\,\frac{2m_e^2 e^2}{(\hbar k)^3}\left\{\exp\left(\frac{\hbar^2 k^2}{8 m_e k_B T} - \alpha\right) + 1\right\}^{-1} \quad , \quad (6.61)$$

The result for the real part is

$$\mathrm{Re}\,\varepsilon(\mathbf{k}, \mathbf{k}\bullet\mathbf{v}) = 1 + \frac{k_e^2}{k^2}\frac{\partial}{\partial\alpha}\ln I_{1/2}(\alpha) \quad , \quad (6.62)$$

where k_e is the Debye wavenumber defined by $k_e=\lambda_{De}^{-1}$. The function $I_{1/2}(\alpha)$ is the standard Fermi integral

$$I_{1/2}(\alpha) = \int_0^\infty dx \frac{x^{1/2}}{e^{x-\alpha}+1} \quad , \quad (6.63)$$

where $\alpha=\mu/k_BT$, μ is chemical potential. Using Eqs. (6.61) and (6.62), it is obtained that $\mathrm{Im}(1/\varepsilon)$ is proportional to v and L is proportional to v^3 for $v \approx 0$.

Figure 6.2 shows the value of $L \times (v_F/v)^3$. The solid line represents that obtained by TCP with $G_{\mu\nu}=0$, the dashed line represents that obtained by electron OCP with $G_{ee}=0$. Both of the two case, $L \times (v_F/v)^3$ approaches a constant value at $v \approx 0$. The value of $L \times (v_F/v)^3$ at the low velocity limit $=C(\Gamma,\theta)$ can be also calculated as[2]

$$C(\Gamma,\theta) = -\frac{\hbar^3}{2e^2 m^2}\int_0^\infty dk\, k\left\{\frac{\partial}{\partial v}\,\mathrm{Im}\,\frac{1}{\varepsilon(\mathbf{k}, \mathbf{k}\bullet\mathbf{v})}\right\}_{v=0} \quad . \quad (6.64)$$

When ε in Eq. (6.64) is given by Eqs. (6.61) and (6.62), Eq. (6.64) takes the

form[2]

$$C(\Gamma,\theta)=\int_0^\infty dk\,\frac{k^3}{(k^2+\kappa^2)}\left\{\exp\left(\frac{\hbar^2k^2}{8m_ek_BT}-\alpha\right)+1\right\}^{-1} \quad , \quad (6.65)$$

where

$$\kappa^2=k_e^{\,2}\frac{d}{d\alpha}\ln I_{1/2}(\alpha) \quad . \quad (6.66)$$

For a TCP, this expression may be extended as

$$C(\Gamma,\theta)=\int_0^\infty dk\,\frac{k^3}{(k^2+\kappa^2)}\left[\left\{\exp\left(\frac{\hbar^2k^2}{8m_ek_BT}-\alpha_e\right)+1\right\}^{-1}+Z^2\left(\frac{m_i}{m_e}\right)^2\left\{\exp\left(\frac{\hbar^2k^2}{8m_ik_BT}-\alpha_i\right)+1\right\}^{-1}\right] \quad , \quad (6.67)$$

where $\alpha_i=\mu_i/k_BT$, μ_i is chemical potential of ion and

$$\kappa^2=k_e^{\,2}\left\{\frac{d}{d\alpha_e}\ln I_{1/2}(\alpha_e)+Z\frac{d}{d\alpha_i}\ln I_{1/2}(\alpha_i)\right\} \quad . \quad (6.68)$$

Found are the values of $C \approx 0.649$ for electron OCP and $C \approx 2.54\times10^2$ for TCP. And observed are the values of $L\times(v_F/v)^3$ at $v=3\times10^{-3}v_F$ is 0.665 for electron OCP and is 2.46×10^2 for TCP. There are in very good agreements.

Figure 6.3 shows the stopping numbers, the solid line represents the stopping number of carbon and deuteron mixture plasma of $n_C=n_D=3.0\times10^{25}cm^{-3}$, T=0.3keV, and the dashed line represents that of deuteron plasma of $n_D=3.0\times10^{25}cm^{-3}$, T=0.3keV. Note that the stopping power is proportional to $\bar{n}_eL$. As shown in Fig. 6.3 at the low velocity region the effect due to the carbon is dominant for the case of carbon and deuteron mixture plasma. This fact is explained as follows. Assumed is a test particle of the charge Z_0e moving with a constant velocity v in a plasma of the charge Ze,

electron number density $\bar{n}_e$. When the collision cross-section is given by $\sigma=\pi r^2$, where $r=2Z_0Ze^2/m_ev^2$, the stopping power is written as

$$\frac{dW}{ds} \approx - \frac{4\pi \bar{n}_e Z_0^{\,2} Z^2 e^4}{m_e v^2} \quad . \quad (6.69)$$

As the definition of L, Eq. (6.9), L includes the term Z^2. Therefore the effects of deuteron cannot appear for the case of carbon and deuteron mixture plasma.

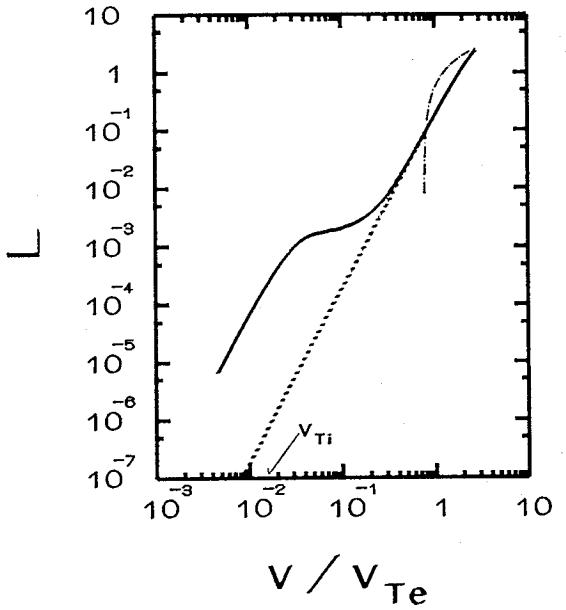

Fig. 6.1 The stopping number of the plasma Z=1, n_i=3.0X10^{25} and T=0.3keV.

The horizontal axis represents the velocity normalized by the electron thermal velocity. The solid line represents the stopping numbers obtained by the formula mentioned in the previous sections with $G_{\mu\nu}$=0, the dashed line represents the stopping number obtained by electron OCP with G_{ee}=0 and the solid-dashed line represents the stopping numbers of the Bethe-Bloch formula.

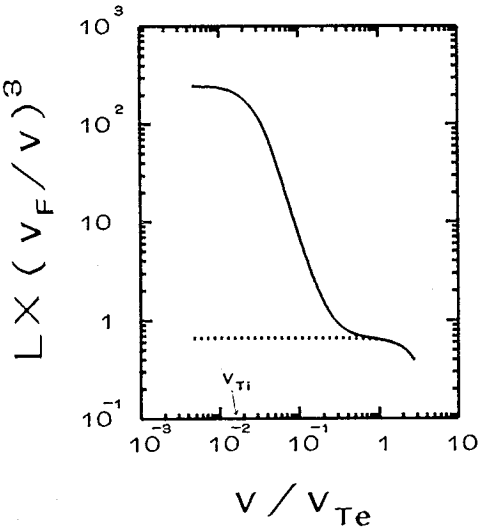

Fig. 6.2 The value of L X $(v_F/v)^3$ of the plasma Z=1, n_i=3.0X10^{25} and T=0.3keV.

The solid line represents that obtained by TCP with $G_{\mu\nu}$=0, the dashed line represents that obtained by electron OCP with G_{ee}=0.

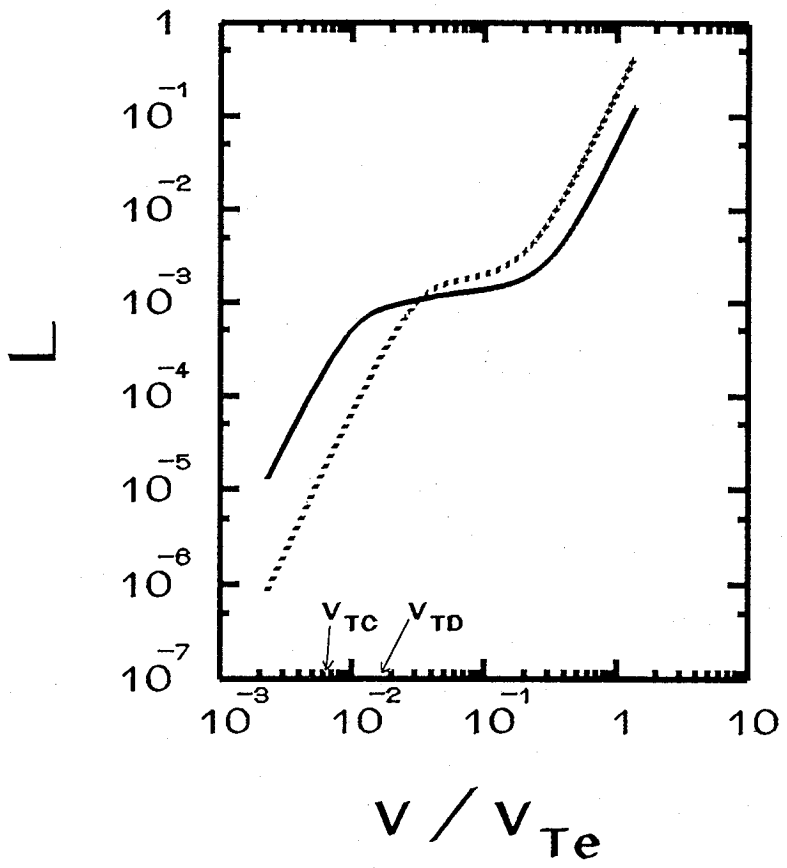

Fig. 6.3 The stopping numbers. The solid line represents the stopping number of carbon and deuteron mixture plasma of $n_C=n_D=3.0\times10^{25}cm^{-3}$, T=0.3keV, and the dashed line represents the stopping number of deuteron plasma of $n_D=3.0\times10^{25}cm^{-3}$, T=0.3keV.

VI - 6. LOCAL FIELD CORRECTION EFFECTS ON STOPPING NUMBER

For the plasma Z=1, r_s=1 and T=25eV, the static local field correction functions are calculated with the use of the atomic model using the classical HNC equation and the stopping numbers are estimated. Figure 6.4 shows the local field correction functions. The horizontal axis represents the wavenumber normalized by a_e^{-1}. The solid line represents the electron-ion static local field correction function, the solid-dashed line represents the electron-electron static local field correction function and the dashed line represents the ion-ion static local field correction function. As shown in Fig. 6.4, the electron-electron and ion-ion static local field correction functions over the value of unity at the range of $10 \lesssim ka_e \lesssim 20$, and approach to unity for large wavenumber. The electron-ion static local field correction function simply increases as wavenumber k increases and approaches to unity for large wave number.

The static local field correction functions are compared with that obtained by S. Ichimaru et all. Figure 6.5 shows the electron-electron static local field correction functions, the solid line represents that by the presented model and the dashed line represents that by Eq. (32) in Ref. 1. The difference originates in the degeneracy effects and ion correlation effects. Figure 6.6 shows the ion-ion static local field correction functions, the solid line represents that by presented model and the dashed line represents that by Eq. (44b) in Ref. 1. The difference between two results is smaller than that of the electron-electron static local field correction functions.

The stopping numbers are calculated by the presented model and

compared with that obtained by Xin-Zhong Yan et al[2]. Figure 6.7 shows the stopping numbers normalized by that obtained by R.P.A., i.e. $G_{\mu\nu}$=0. The solid line represents the stopping number obtained by the presented model, the solid-dashed line represents that obtained by the presented model replacing G_{ei} to 0 and the dashed line represents that obtained by Xin-Zhong Yan et al[2]. As shown in Fig. 6.7, at the velocity $v \sim v_{Te}$, all of the three stopping numbers have a peak value because of the effects of G_{ee}, and at $v \sim 0.01 v_{Te}$ ($\sim v_{Ti}$), the effects of G_{ii} are found. For the velocity of $v_{Ti} \lesssim v \lesssim 0.1 v_{Te}$, because of the effects of G_{ei} the stopping number is enhanced compared with that without the effects of G_{ei}. The stopping number obtained by the presented model is about 1.05 times greater than that obtained by the model in Ref. 2 for the plasma Z=1, r_s=1 and T=25eV. This fact can be explained as follows. For the case without G_{ei} and G_{ie}, the dielectric function $\varepsilon(k,\omega)$ is written by Eq. (6.23) and (6.24) as

$$\varepsilon(\mathbf{k}, \omega) = 1 - \frac{\chi_e}{1 + \chi_e G_{ee}} - \frac{\chi_i}{1 + \chi_i G_{ii}} \quad , \quad (6.70)$$

where

$$\chi_\mu = Z_\mu^{\,2} \upsilon(k) \chi_\mu^{(0)}(\mathbf{k}, \omega) \quad . \quad (6.71)$$

Eq. (6.70) means that the dielectric function $\varepsilon(k,\omega)$ can be expressed by the summation of the effects contributed vacuum, electron and ion. For the case with G_{ei} and G_{ie}, the dielectric function $\varepsilon(k,\omega)$ is written by Eq. (6.23) and (6.24) as

$$\varepsilon(\mathbf{k},\omega) = 1 - \frac{\chi_e}{1+\chi_e G_{ee}} - \frac{\chi_i}{1+\chi_i G_{ii}} - \varepsilon_{e-i}(\mathbf{k},\omega) \quad , \quad (6.72)$$

where

$$\varepsilon_{e-i}(\mathbf{k},\omega) = \left[\left\{ \frac{\chi_e}{1+\chi_e G_{ee}} + \frac{\chi_i}{1+\chi_i G_{ii}} \right\} \frac{\chi_e \chi_i G_{ei} G_{ie}}{(1+\chi_e G_{ee})(1+\chi_i G_{ii}) - \chi_e \chi_i G_{ei} G_{ie}} \right.$$

$$\left. - \frac{\chi_e \chi_i (G_{ei} + G_{ie})}{(1+\chi_e G_{ee})(1+\chi_i G_{ii}) - \chi_e \chi_i G_{ei} G_{ie}} \right] \quad . \quad (6.73)$$

I call $\varepsilon_{e\text{-}i}$ as the electron-ion mixture term. The term $\varepsilon_{e\text{-}i}$ expresses the coupling rate of electron and ion. For small k and large k, the $\varepsilon_{e\text{-}i}$ reduces to zero. The main region of k integral at $v=\alpha v_{Te}$ will be given by $ka_e \lesssim \alpha(9\pi/4)^{1/3}\theta^{1/2}$. Namely for high velocity and low velocity, the effects of $\varepsilon_{e\text{-}i}$ on the stopping number become very weak. The effects of $\varepsilon_{e\text{-}i}$ on the stopping number appear for the intermediate velocity. In this meaning G_{ei} implies the electron-ion strong coupling effect.

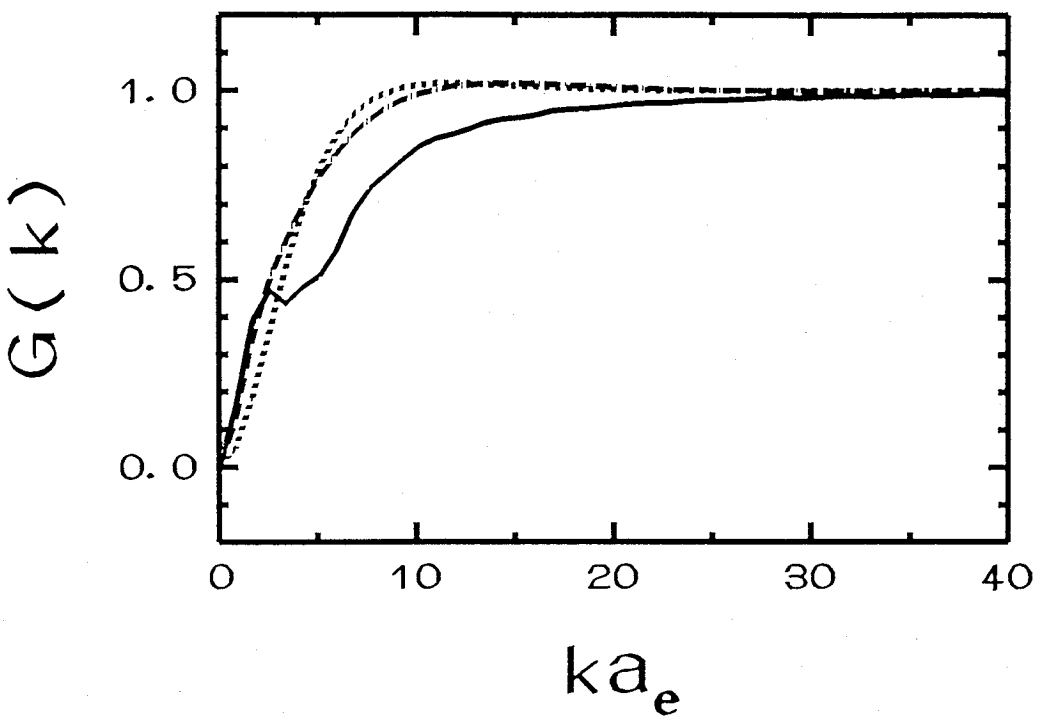

Fig. 6.4 The local field correction functions. The horizontal axis represents the wavenumber normalized by a_e^{-1}. The solid line represents the electron-ion static local field correction function, the solid-dashed line represents the electron-electron static local field correction function and the dashed line represents the ion-ion static local field correction function.

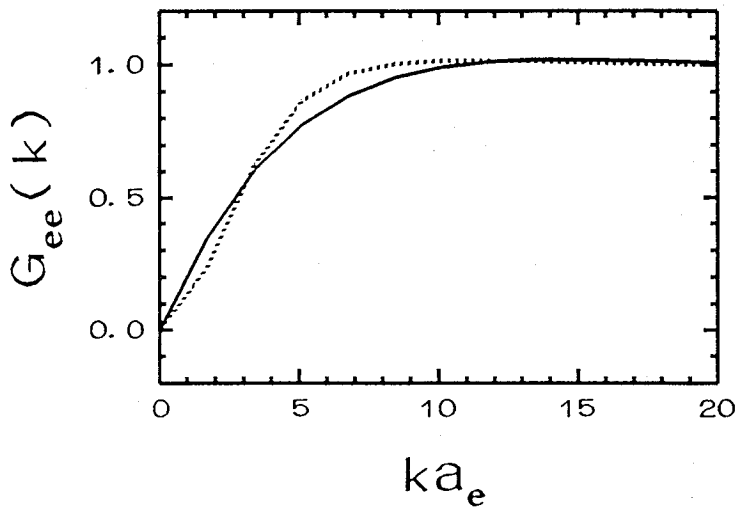

Fig. 6.5 The electron-electron static local field correction functions, the solid line represents that by presented model and the dashed line represents that by Eq. (32) in Ref. 1.

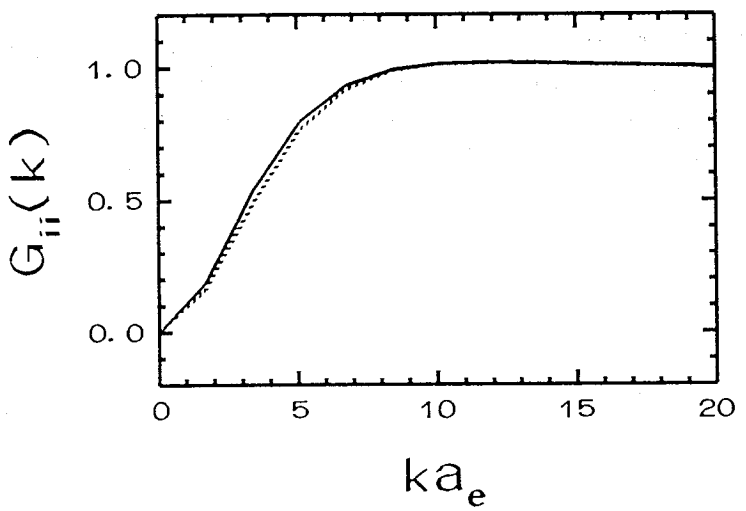

Fig. 6.6 The ion-ion static local field correction functions, the solid line represents that by presented model and the dashed line represents that by Eq. (32) in Ref. 1.

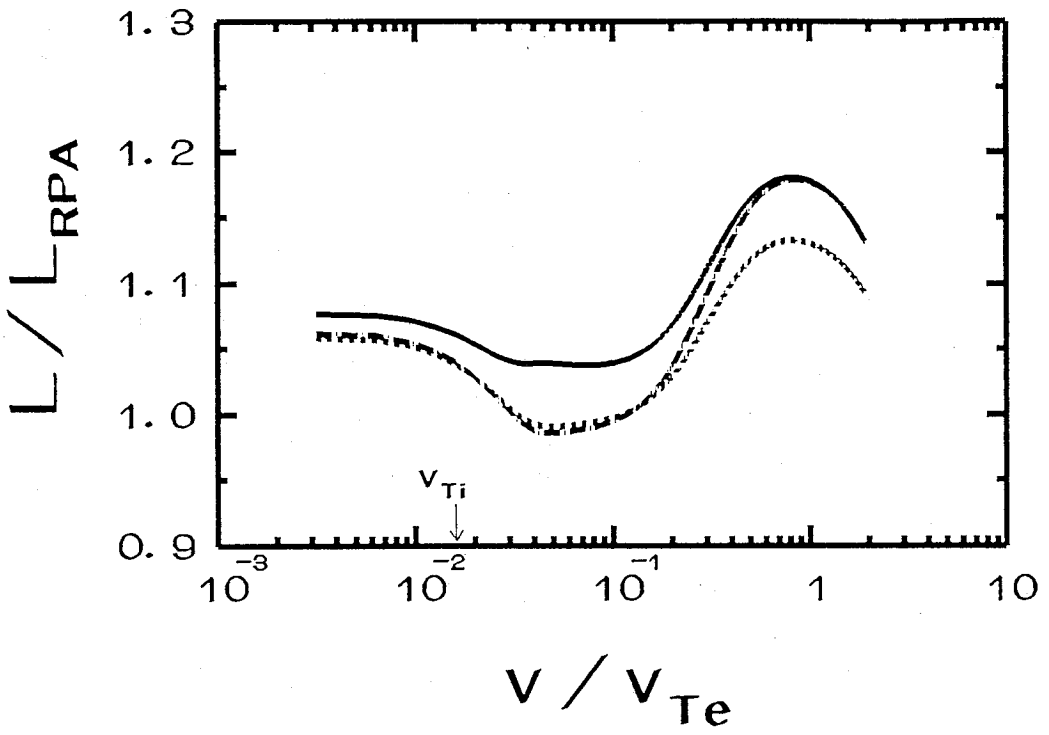

Fig. 6.7 The stopping numbers normalized by the stopping number obtained by R.P.A.,i.e. $G_{\mu\nu}=0$. The solid line represents the stopping number obtained by presented model, the solid-dashed line represents the stopping number obtained by presented model replacing G_d to 0 and dashed line represents the stopping number obtained by Xin-Zhong Yan et al.

VI - 7. SUMMARY

With the use of the atomic model developed, the stopping power of charged particles in a hot, dense plasma is estimated. The stopping power is obtained from the dielectric function of a highly compressed plasma $\varepsilon(k,\omega)$ which is calculated using the local field correction theory. The static electron-ion local field correction function $G_{ei}(k)$ is estimated for the first time by using the atomic model developed in Chap. V. It was difficult to calculate G_{ei} in Ichimaru's frame work. The stopping power obtained by the presented model is about 1.05 times that obtained by the model of Xin-Zhong Yan et al for the plasma Z=1, r_s=1 and T=25eV. The inclusion of G_{ei} results in the enhancement of the stopping power for the test particle velocity of $v_{Ti} \lesssim v \lesssim 0.1 v_{Te}$.

REFERENCES OF CHAPTER VI

1). S. Ichimaru, S. Mitake, S. Tanaka and Xin-Zhong Yan, Phys. Rev. A, **32,** 1768 (1985).

2). Xin-Zhong Yan, S. Tanaka, S. Mitake and S. Ichimaru, Phys. Rev. A, **32,** 1785 (1985).

3). Y. Setsuhara, H. Azechi, N. Miyanaga, H. Furukawa, R. Ishizaki, K. Nishihara, M. Katayama, A. Nishiguchi, K. Mima, and S. Nakai, Laser and Particle Beams, **8,** 609 (1990).

4). Y. Setsuhara, H. Azechi, N. Miyanaga, H. Furukawa, K. Nishihara, A. Nishiguchi, K. Mima, and S. Nakai, to be submitted.

5). J. Chihara, Phys. Rev. A, **40,** 4507 (1989).

6). H. Bethe, Ann. Phys. (Leipzig) **5,** 325 (1930).

7). F. Bloch, Ann. Phys. (Leipzig) **16,** 285 (1933).

8). S. Ichimaru, PLASMA PHYSICS (Benjamin, California, Reading, Mass., 1986), pp125-131.

9). S. Skupsky, Phys. Rev. A **16,** 727 (1977).

VII. CONCLUSIONS

In a laser-produced hot, dense plasma, plasma density and temperature cover very wide domains. There exists a domain called a two-component strongly coupled plasma of which the Coulomb coupling constant for ions $\Gamma \sim 1 \sim 10$ and the electron degeneracy parameter $\theta \sim 0.1 \sim 10$. In the present paper, investigated are some basic properties of a two-component strongly coupled plasma.

I summarize the conclusions below.

Chapter II

(1) In order to simulate the two-component strongly coupled plasmas, 3-dimensional Particle-Particle Particle-Mesh (PPPM) Code "SCOPE" has been developed. In "SCOPE" the short-range forces are calculated by using a direct Particle-Particle (P-P) summation over the spatially localized forces and the long-range forces by Particle-Mesh (P-M) method. Some quantum effects are taken into account through the effective pair potential by an approximated way. In "SCOPE", the Poisson equation has been solved by the 4-th order finite difference method and the third order spline weighting method. By introducing the 4-th order finite difference and the third order spline weighting, the number of meshes required to obtain the accuracy within a error $\leq 1\%$, is reduced $(1/5)^3$ of the conventional P-M method. For the close interactions, especially electron-ion interactions, the small time increment $\Delta t'$ is estimated as satisfies the condition $\Delta t' << \tau$, where τ is the interaction time.

Initial positions are determined by Metropolis method and initial velocities are determined by Maxwellian.

Chapter III

(1) The formulation of the calculation of the bremsstrahlung emission coefficients from a two-component binary-ionic-mixture plasma has been introduced on the basis of dipole emission model. The pair distribution functions are related to the bremsstrahlung emission coefficients.

(2) The pair distribution functions obtained by using "SCOPE" are compared with analytical solutions for the cases of the weakly coupled and strongly coupled plasmas. For the weakly coupled plasma, the simulation results are in good agreements with R.P.A. theory. For the strongly coupled plasma, the differences in the pair distribution functions between the simulations and analytical models are not negligible. The differences originate in that in the previous theories the ion-ion and electron-ion pair distribution functions are calculated separately, the electron shielding effects are taken into as a linear response shielding and there is no quantum effects. The electron-electron symmetry effects are found to reduce the value of the electron-electron pair distribution function and enhance the value of the electron-ion pair distribution function, especially for bound electrons.

(3) The reduction in the bremsstrahlung emission is estimated for the case of two-component strongly coupled plasma of $Z=6$, $\Gamma=1$ and $T=1keV$, and compared with the results by R. Kawakami et al. Our results are good agreements with their results qualitatively.

(4) The pair distribution functions are observed for the cases of the binary ionic mixture plasma, and the reduction in the bremsstrahlung emission is

estimated. The dependence of the reduction on the frequency consists of roughly three parts. First, for $\omega_{pe} \lesssim \omega \lesssim 5\omega_{pe}$ the ion-ion correlation effects and electronic shielding effects are comparable and the reduction rate at $\omega \sim \omega_{pe}$ is about 75%, for $5\omega_{pe} \lesssim \omega \lesssim 50\omega_{pe}$ the electronic shielding effects are dominant but the reduction rate is roughly 10% and no reduction for $50\omega_{pe} \lesssim \omega$.

(5) The reduction in the bremsstrahlung emission for a binary mixture plasma is concluded to be approximated by that for a single ion plasma of which ion has a fictitious averaged charge, even for the two-component plasma.

Chapter IV

(1) With the use of "SCOPE", the velocity auto-correlation functions (V.A.F.) of laser-produced hot, dense plasmas are calculated. And the self-diffusion coefficients are estimated. The dependence of the self-diffusion coefficients on the Coulomb coupling constant Γ is obtained. For the plasmas, $Z=6$, $\theta=5$, the normalized self-diffusion coefficients of electrons are proportional to $\Gamma^{-0.55}$ for the range of $0.5 \lesssim \Gamma \lesssim 3$, and are roughly 0.1 times Spitzer-Härm value. The normalized self-diffusion coefficients of ions are proportional to $\Gamma^{-0.69}$ for the range of $0.5 \lesssim \Gamma \lesssim 2$. For the range of $\Gamma \gtrsim 2$, the electric shielding effects on the self-diffusion coefficients of ion become strong.

(2) With the use of "SCOPE", auto-correlation functions of total electric current of laser-produced hot, dense plasmas are calculated. And the electric conductivities are estimated. The dependence of the electric conductivities on

the Coulomb coupling constant Γ is obtained. The normalized electric conductivities obtained by simulations are proportional to $\Gamma^{-0.52}$ for the range of $0.5 \lesssim \Gamma \lesssim 3$ and its value agrees with that obtained by theoretical model at $\Gamma \sim 1$.

Chapter V

(1) The spherical cell model (SCM) due to Perrot and Dharma-wardana is improved in the calculation of the electron-electron correlation by extending from the Debye-Hückel model to the HNC framework with taking the degeneracy effect into account. Calculated are the pair distribution functions, the effective potential acting on an electron and an ion, by solving numerically a set of the coupled modified Poisson - HNC - Schrödinger equations for a range of parameters which are interested in laser fusion.

(2) The differences appeared in the various pair distribution functions between the improved SCM and the previous works are summarized as follows. The electron-electron pair distribution function is slightly large in the region $r \lesssim 1.5a_e$ compared with that by S. Ichimaru et al, because in the Ichimaru model the degeneracy effects and ion correlation effects are not included. On the other hand, the electron linear response shielding in the calculation of the ion-ion pair distribution function is found to be slightly over-estimated. The electron-ion pair distribution function is very small near the origin, $r \lesssim 0.2a$, compared with that by the modified T-F model, because the quantum diffraction effects are automatically included in the Schrödinger equation. The value of the e-i pair distribution function at r=0 is finite in the improved SCM model.

(3) The ionization states for the two cases, $n_i = 1.6 \times 10^{24}\,cm^{-3}$ ($r_s=1$), T=25eV

and $n_i=2X10^{23}\,cm^{-3}$ ($r_s=2$), T=25eV, are compared. For the first case , $r_s=1$, there is no bound state, namely $Z^*=1$, because of the pressure ionization effects. For the second case because of the relatively low number density compared with the first case, the pressure ionization effects become weak, therefore the bound state (1s state) exists. The effective ionization state Z* using the HNC equation is estimated to be approximately 0.762 and the energy of the 1s state is calculated to be about - $5.89X10^{-2}$ in atomic unit.

(4) The differences of quantal HNC and the classical HNC appears in the pair distribution functions, especially, the electron-ion pair distribution function. The e-i pair distribution function by QHNC is small near the origin because of the quantum diffraction effects.

Chapter VI

(1) With the use of the atomic model developed, the stopping power of charged particles in a hot, dense plasma is estimated. The stopping power is obtained from the dielectric function of a highly compressed plasma $\varepsilon(k,\omega)$ which is calculated using the local field correction theory. The static electron-ion local field correction function $G_{ei}(k)$ is estimated for the first time by using the atomic model developed in Chap. V. It was difficult to calculate G_{ei} in the framework of S. Ichimaru et al. The stopping power obtained by the presented model is about 1.05 times that obtained by the model of Xin-Zhong Yan et al for the plasma Z=1, $r_s=1$ and T=25eV. The inclusion of G_{ei} results in the enhancement of the stopping power for the test particle velocity of $v_{Ti}\lesssim v\lesssim 0.1v_{Te}$.

謝　辞

本研究の遂行に際し、終始懇篤なる御指導、御鞭撻を賜りました三間圀興教授、西原功修教授、中井貞雄教授に深厚なる謝意を表します。

あわせて、大学院在学中御指導、御教示を頂いた山中千代衛名誉教授、渡辺健二名誉教授、山中龍彦教授、石村勉教授、横山昌弘教授、青木亮三教授、三宅正宣教授、井沢靖和教授、権田俊一教授、加藤義章教授、望月孝晏元教授、今崎一夫元教授に謝意を表します。

また、御指導、御助言を頂いた山中正宣助教授、西川雅弘助教授、伊藤慶文助教授、北川米喜助教授、佐々木孝友助教授、桂正弘助教授、朝日一助教授、中塚正大助教授、中島信昭助教授、高部英明講師、畦地宏講師、乗松孝好講師、吉田国雄講師、実野孝久講師、田中和夫講師、西村博明講師に謝意を表します。

さらに、熱心な討論、激励を頂いた仁木秀明助手、中井光男助手、大道博行助手、宮永憲明助手、白神宏之助手、宮本修治助手、阪部周二助手、藤原閲夫助手に厚く感謝します。

最後に、日頃からお世話になったレーザー核融合研究センター理論グループの皆様、計算機管理室の皆様、日本電気グループの皆様に心からの感謝を申し上げます。

業績目録

主要論文

(1) " Reduction in bremsstrahlung emission from hot, dense binary- ionic-mixture plasmas "
H. Furukawa and K. Nishihara, Phys. Rev. A, **42**, 3532 (1990).

(2) " Secondary Nuclear Fusion Reactions as Evidence of Electron Degeneracy in Highly Compressed Fusion Fuel "
Y. Setsuhara, H. Azechi, N. Miyanaga, *H. Furukawa*, R. Ishizaki, K. Nishihara, M. Katayama, A. Nishiguchi, K. Mima, and S. Nakai, Laser and Particle Beams, **8**, 609 (1990).

(3) " Observation of Electron Degeneracy in Highly Compressed Plastic Hollow Shell Targets "
Y. Setsuhara, H. Azechi, N. Miyanaga, *H. Furukawa*, K. Nishihara, A. Nishiguchi, K. Mima, and S. Nakai,
to be submitted.

(4) " PARTICLE SIMULATIONS ON STATIC AND DYNAMIC PROPERTIES OF TWO COMPONENT HOT DENSE PLASMAS "
H. Furukawa, K. Nishihara, M. Kawaguchi, H. Sakagami, T. Hiramatsu and H. Yasui,
YAMADA CONFERENCE XXIV ~ Strongly Coupled Plasma Physics ~ , 1990, page 613.

(5) " High Accuracy Particle-Particle Particle-Mesh Code and Its Application to Laser-Produced Dense Plasma "
K. Nishihara, *H. Furukawa*, M. Kawaguchi and Y. Abe,
"Japanese Supercomputing", (eds. R. H. Mendez, S. A. Orszag, Springer-Verlag, New York, 1988), Volume 36, page 59.

(6) " Particle-Particle Particle-Mesh Simulation of Laser-produced Dense Plasma "
K. Nishihara, *H. Furukawa* and M. Kawaguchi, T. Hiramatsu and H. Sakagami,
"Laser Interaction with Matter", (eds. Guillermo Velarde, Emilio Minguez, J. Manuel Perlado, World Scientific, Singapore, 1989), Page 368.

国内学会発表

主著

(1) 燃料とプッシャーのMixingの粒子コードシミュレーション
日本物理学会　関西学院大学　１９８６年１０月

(2) レーザー高密度プラズマの物性
日本物理学会　名古屋工業大学　１９８７年３月

(3) 高精度強結合プラズマ粒子コードとそのレーザー高密度プラズマへの応用
～不純物の拡散と制動輻射損失～
日本物理学会　東北大学　１９８７年９月

(4) 二成分強結合プラズマの拡散係数
日本物理学会　広島大学　１９８８年９月

（5）二成分強結合プラズマの粒子コードシミュレーション

プラズマ核融合学会　　東京　　１９８８年１１月

（6）3d Particle-Particle Particle-Mesh Method for Two-Component Strongly-Coupled Plasma

日本物理学会　　大阪大学　　１９９０年３月

共著

（1）３次元粒子ー粒子、粒子ー格子コード(SCOPE)の性質

日本物理学会　　広島大学　　１９８８年９月

（2）核反応生成荷電粒子の高密度プラズマ中の輸送

日本物理学会　　東海大学　　１９８９年３月

（3）高密度プラズマ中における波動の粒子コードシミュレーション

日本物理学会　　東海大学　　１９８９年３月

（4）異なる高密度プラズマ間の接触ポテンシャルと表面張力

日本物理学会　　東海大学　　１９８９年３月

（5）極超短レーザーパルスと固体水素との相互作用

日本物理学会　　大阪大学　　１９９０年４月

（6）レーザー核融合プラズマの電子縮退を示す２次反応

プラズマ核融合学会　　長岡技術科学大学　　１９９０年３月

（7）シェルターゲットの超高密度爆縮 V　～電子縮退の観測～

日本物理学会　　大阪大学　　１９９０年４月

（8）極超短レーザーパルスと固体水素との相互作用 II

日本物理学会　　岐阜大学　　１９９０年１０月

（9）２次核融合反応を用いた、高密度爆縮プラズマにおける電子縮退の検証
日本物理学会　　岐阜大学　　１９９０年１０月

国内研究会発表

主著

（1）ＰＰＰＭコードによる高密度プラズマシミュレーション
レーザー爆縮プラズマの原子過程研究会
岡山大学　　１９８７年1月

（2）強結合プラズマシミュレーション　～基本的性質とイオン音波～
リアルプラズマにおける波動現象とソリトン的励起研究会
大阪大学　　１９８７年１０月

（3）強結合二成分古典プラズマのダイナミクスのシミュレーション
強結合プラズマ物理研究会
箱根　　１９８７年１１月

（4）レーザー生成高密度プラズマの基本的性質とミキシングの評価
レーザー爆縮プラズマの原子過程研究会
岡山大学　　１９８８年1月

共著

（1）レーリーテーラー不安定性における表面電位効果
リアルプラズマにおける波動現象とソリトン的励起研究会
静岡大学　　１９８６年１０月

国際会議

(1) 3-d Particle Simulation of Ultrashort High Intensity Laser Interaction with Solid Density Hydrogen Plasma ;
K. Nishihara, H. Yasui and *H. Furukawa*,
9-th International Workshop on Laser Interaction and Related Plasma Phenomena ,
Monterey, California, November 6-10, 1989.

(2) SUPERCOMPUTING IN LASER FUSION RESEARCH AT INSTITUTE OF LASER ENGINEERING ;
K. Nishihara, Y. - O. Fukuda, *H. Furukawa*, M. Kawaguchi, K. Mima, A. Nishiguchi, H. Sakagami and H. Takabe,
Int. Conf. on Supercomputing in Nuclear Applications ,
Mito, March 12-16, 1990.

正　誤　表

p25	3行目	田中實、山本良一、計算物理学と計算化学、pp15-21、海文堂。 ⇓ M. Tanaka and R. Yamamoto, published by Kaibundo (海文堂) 1988, pp15-21, in Japanese (計算物理学と計算化学).
p82	4行目	岩波講座, 現代物理学の基礎, 第2版, 5, " 統計物理学 ", pp 219-226, 岩波書店 ⇓ H. Yukawa, M. Toda and R. Kubo, published by Iwanami (岩波書店), 1978, pp 219-226, in Japanese (岩波講座, 現代物理学の基礎, 第2版, 5, " 統計物理学).
p139	5行目	西川雅弘教授を挿入
p139	7行目	西川雅弘助教授を削除